5-2023

Super p-sulfur cathodes for quasi-solid-state lithium-sulfur-batteries.

Milinda Bharatha Kalutara Koralalage
University of Louisville

SUPER P-SULFUR CATHODES FOR QUASI-SOLID-STATE
LITHIUM-SULFUR BATTERIES

By

Kalutara Koralalage Milinda Bharatha

B.S., University of Peradeniya, Sri Lanka, 2016

M.S., University of Louisville, USA, 2020

A Dissertation

Submitted to the Faculty of the

College of Art and Science at the University of Louisville

In Partial Fulfilment of the Requirement

for the Degree of

Doctor of Philosophy in Physics

Department of Physics and Astronomy

University of Louisville

Louisville, Kentucky

May 2023

SUPER P-SULFUR CATHODES FOR QUASI-SOLID-STATE LITHIUM-SULFUR BATTERIES

By

Milinda Bharatha, Kalutara Koralalage

B.S., University of Peradeniya, 2016

M.S., University of Louisville, 2020

A Dissertation Approved on

April 06, 2023

By the Following Dissertation Committee:

_____

Dr. Gamini Sumanasekera (Dissertation Director)

_____

Dr. Ming Yu

_____

Dr. Serban Smadici

_____

Dr. Badri Narayanan

DEDICATION

This dissertation is dedicated to

my father

Mr. Indra Brito Adikaram

my mother

Mrs. Gnana Kannangara

and my wife

Mrs. Dulani Deeshani

who have always given me constant love, strength, and encouragement towards
successful completion of my PhD

ACKNOWLEDGEMENTS

ABSTRACT

SUPER P-SULFUR CATHODES FOR QUASI-SOLID-STATE
LITHIUM-SULFUR BATTERIES

Milinda Bharatha Kalutara Koralalage

April 06, 2023

Lithium-Sulfur (Li-S) batteries have become a promising candidate to meet the current energy storage demand, with its natural abundance of materials, high theoretical capacity of 1672 mAhg^{-1}, high energy density of 2600 Whkg^{-1}, low cost and lower environmental impact. Sulfide based solid state electrolytes (SSEs) have received greater attention due to their higher ionic conductivity, compatible interface with sulfur-based cathodes, and lower grain boundary resistance. However, the interface between SSEs and cathodes has become a challenge in all solid-state Li-S batteries due to the rigidity of the participating surfaces. A hybrid electrolyte containing SSE coupled with a small amount of ionic liquid, was essential to improve the interface contact of the SSE with the electrodes.

Coating-based cathodes were successfully fabricated using water-based carboxymethyl cellulose (CMC) solution and Styrene butadiene rubber (SBR) as the binder with low sulfur loading (0.70 mgcm^{-2}) as well as high sulfur loading (4.0 mgcm^{-2}). Solid-state composite

powder-based cathodes pressed onto SSE (loading 4.0 mgcm^{-2}) with enhanced electronic and ionic conductivity were fabricated with Super P: Sulfur (SP:S) and SSE.

Ionic Liquids (IL) prepared using Lithium bis(trifluoromethyl sulfonyl)imide (LiTFSI) as salt, with premixed pyrrolidinium bis(trifluoromethyl sulfonyl)imide (PYR) as solvent and 1,3-dioxolane (DOL) as diluent were used to wet both SSE-electrode interfaces. The effect of IL dilution, co-solvent amount, LiTFSI concentration, C rate at which the batteries are tested and the effect of SSE inside the cathode, were systematically studied and optimized to develop a quasi-solid-state electrolyte Li-S battery (QSSLSB) with higher capacity retention and cyclability. LiTFSI (2M) dissolved in PYR:DOL(1:1) found to be optimum IL combination for low sulfur loading QSSLSBs reaching 500 mAh/g after 100 cycles while LiTFSI (3M) in PYR:DOL(1:3) was the optimum IL concentration for higher loading QSSLSBs reaching 400 mAh/g after 100 cycles.

This work reports promising results of QSSLSB based on novel $Li_6PS_5F_{0.5}Cl_{0.5}$ Li-argyrodite solid-state electrolyte (SSE) with minute amount of IL, Super P-Sulfur (SP:S) cathode, and Li-anode. It also offers a new insight into the intimate interfacial contacts between the SSE and carbon-sulfur cathodes, which will be critical for improved electrochemical performance of quasi-solid-state lithium-sulfur batteries with high sulfur loading in the future.

TABLE OF CONTENT

LIST OF TABLES

LIST OF FIGURES

CHAPTER 1

INTRODUCTION

1.1 Motivation

With the intent of expanding the driving range (distances after a complete recharge) of electric vehicles (EVs), better performing rechargeable batteries with higher energy densities than available Li-ion technology are essential. More than a quarter century old Li-ion battery technology uses graphite anodes and transition metal oxide cathodes with total energy density of around 250 Wh kg^{-1}[1,2]. The excessive cost and low specific energy density of the electrode materials used in Li-ion batteries are among the main challenges of developing battery packs with energy density comparable to gasoline[3,4]. Even though there is some room left to improve existing Li-ion technology, it will not be enough to meet future requirements and demands[5,6,7].

Instead, the battery innovation needs (i) materials-science breakthroughs, (ii) new electrolytes, (iii) new electrode architectures etc. to achieve safe, cost-effective, and sustaining energy storage systems. US Department of Energy (DOE) has set the goal of identifying new battery chemistry and cell technologies with the potential to reduce the cost of electric vehicle battery packs by more than half, to less than $100/kWh (ultimate goal is $60/kWh battery cell cost), increase range to 300 miles, and decrease charge time to 15 minutes or less by 2028 [8]. Furthermore in 2020 DOE Vehicle Technologies Office

(VTO) annual progress report claims that the goal of the Electric Drive Technologies (EDT) program is to develop an electric traction drive system at a cost of $6/kW for a 100-kW peak system by 2025. In addition, the EDT program has a 2025 power density target of 33 kW/L for a 100kW peak system. While achieving these targets will require transformational technology changes to current materials and processes, it is essential for enabling widespread electrification across all light-duty vehicle platforms[9].

According to DOE-VTO, specific energy density at cell level should be 350 Wh kg^{-1} at C/3 discharge rate. The C rate is defined as nC when the battery is fully discharged in 1/n hours. Other specifications provided can be found in Table 1.1.1.

Table 1.1.1 : Battery and Cell requirements as published by DOE-VTO[8]

Energy storage goals (By characteristics)	Peak Level	Cell Level
Cost @ 100K units/year (kWh = usable energy)	$100/kWh*	$75/kWh*
Peak specific discharge power (30s)	470 W/kg	700 W/kg
Peak specific regen power (10s)	200 W/kg	300 W/kg
Usable specific energy (C/3)	235 Wh/kg*	350 Wh/kg*
Calendar life	15 years	15 years
Deep discharge cycle life	1000 cycles	1000 cycles
Low temperature performance	>70% usable energy at C/3 discharge at -20 °C	>70% usable energy at C/3 discharge at -20 °C
	*Current commercial cells and packs not meeting the goal	

To accomplish these objectives, battery chemistries beyond Li-ion must be considered. An overview of the technologies and their likelihood to achieve the DOE-VTO cost goals are shown in Fig 1.1.1 extracted from the DOE-VTO annual progress report published in 2021.
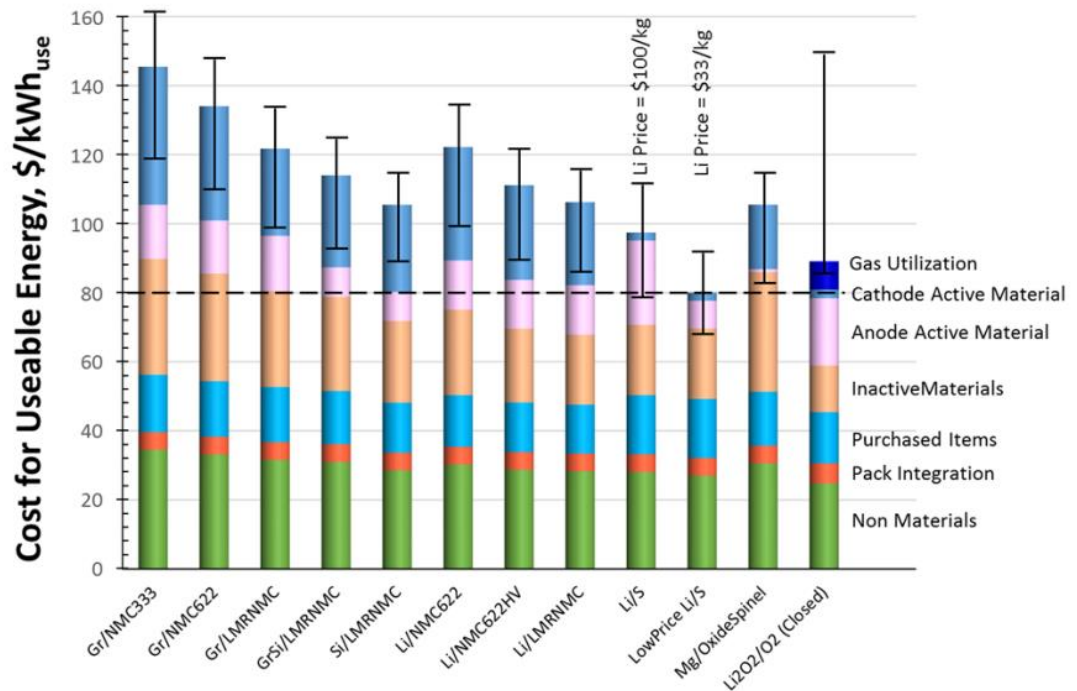
Figure 1.1.1: Estimated costs of cells in automotive battery packs with different combination of electrodes [8].

In Fig. 1.1.1 the packs are rated for 100 kWh Total (85 kWh Useable), 300 kW, 315 V, 168 cells, and produced at a plant volume of 100K packs/year. According to Fig. 1.1.1, Li-S battery chemistry demonstrates promise in terms of the cost per usable kilowatt hour compared to all other battery chemistries, due to the excellent theoretical energy density of sulfur cathode (2500 Wh kg^{-1} vs Lithium)[10,11,12]. However, the commercialization of Li-S technology is impeded by technical disputes such as poor cycle life, poor rate capabilities, self-discharging issues and unavailability of cost-effective safe liquid electrolytes with

good stability[13,14,15]. To address most of the liquid-electrolyte based challenges of the Li-S batteries, solid-state electrolytes have received the attention of the scientific community[16,17,18].

Most of today's research on solid-state Li-S batteries is focused on optimizing solid-state electrolytes (SSE), optimizing cathode materials, exploring the electrode-SSE interfaces and eventually constructing the solid-state battery[19,20] based on Li-metal anodes. There is an urgent need to develop the materials, battery chemistry, and technology necessary for the deployment of solid-state Li-S batteries with enhanced safety and greater energy density in mobile applications in particular, transportation which is the main motivation of this dissertation.

1.2 Rechargeable Li metal-based batteries.

1.2.1 Li-ion batteries.

A Li-ion battery is a type of rechargeable battery consist of a $LiCoO_2$ cathode and a carbon anode in which lithium ions move between the negative electrode and the positive electrode through an electrolyte during cycling. Upon charging the battery, the cathode becomes $Li_{1-x}CoO_2$ by delithiation and the anode converts to Li_xC_6. The practical capacity of $LiCoO_2$ anode has found to be 140 mAh g^{-1} which corresponds to $x \approx 0.5$ (i.e., ~50%) of its theoretical value (273 mAh/g)[21,22]. The high likelihood of thermal runaway triggered by overcharging and the excessive cost of Cobalt, have led to the exploration of other cathode materials for Li-ion cells with improved capacity and cycle life[23,24].
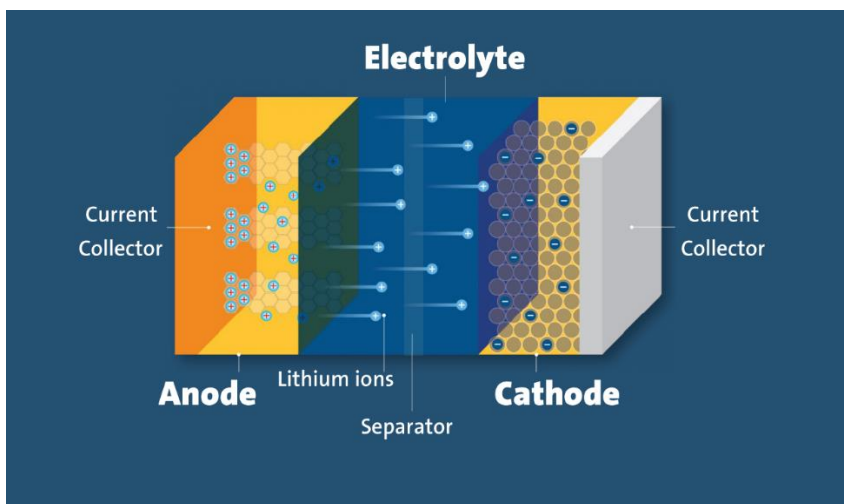
Figure 1.2.1.1: Components of a Li-ion battery [25]

Electrode materials of Li-ion batteries need to have wide stacking capability range, so that maximum lithium can be extracted and reinserted during lithiation and delithiation to maximize the energy density. Moreover, the electrode material needs to have better transport properties for Li-ion, providing high power capability. Carbon in the form of graphite has been the basis of anode material in Li-ion batteries thus, the required properties need to be pursued in novel cathode materials[26,27].

Various materials such as $LiNi_{0.8}Co_{0.15}Al_{0.05}O_2$ (NCA), $LiFePO_4$ (LFP), $LiMnO_4$, etc. have been studied as substitute materials for $LiCoO_2$ cathode material[28,29,30]. Regardless of higher practical capacity (180 $mAhg^{-1}$) of NCA cathode, its thermal volatility on delithiation compromises the safety of Li-ion cells. In contrast spinal $LiMn_2O_4$ and $LiFePO_4$ are significantly steadier but have less capacity of 100-150 mAh g^{-1} above 3 V. Recently developed manganese-based cathodes using Li_2MnO_3 and electrochemically active $LiMO_2$ (M=Mn, Ni, Co) have indicated that, it can lower the material expense while excess lithium raises the specific capacity to 250 mAh g^{-1} between 4.6 V and 2.5 V. Though,

their practical capacity decreases substantially when cycled against graphite anodes thus these Li-ion cells made of Ni-Mn-Co oxides (NMC) suffer severe energy density loss in practical Li-ion cells[31,32]. Additionally, these cathode materials have higher operating potentials, and thus requires electrolytes that are stable at higher potentials. Novel electrolytes have been studied with higher oxidative stability such as sulfones, nitriles and fluorinated solvents. They, however, introduce new complications due to solid electrolyte interphase (SEI) formation[33].

1.2.2 Li-Air batteries

Theoretically, Li-air battery technology has the potential to reach gravimetric capacity of fossil fuel which is around 13000 $Whkg^{-1}$ when free oxygen is not considered in the calculations. If not, at the cell level, Li-Air batteries offer 3623 Wh kg^{-1} (when discharged to form Li_2O_2 at 3.1 V) or 5200 Wh kg^{-1} (when discharged to form Li_2O at 2.9 V). A Li-air battery is comprised of a Li metal anode and an O_2 cathode[34,35]. Typically, Oxygen is supplied from an external source. Currently, there are three main architectures anticipated for Li-Air batteries. These include varieties with (i) aqueous electrolyte, (ii) a fully aprotic liquid electrolyte and (iii) a hybrid structure with cathode submerged in aqueous electrolyte and anode immersed in aprotic electrolyte.
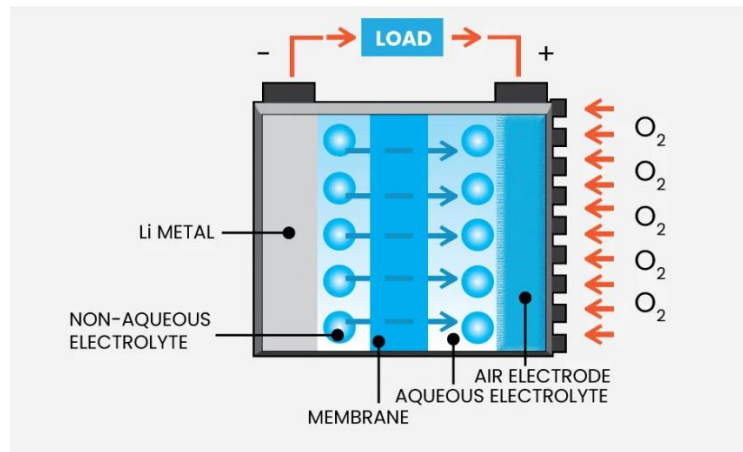
Figure 1.2.2.1: Components of Li-air battery [36]

Practical application of Li-Air Battery technology is restricted by low power output and poor cycle-ability. The non-aqueous electrolytes used in Li-Air batteries are volatile and insecure at high voltages, causing poor cyclability. It is found that, the supplied oxygen can crossover with the electrolyte influencing the overall functionality of the cell. This problem obviously mitigates the cycle life of Li-Air cell. Li_2O and Li_2O_2 depositions on the carbon cathode surface can clog the pores, limiting the oxygen flow, leading to poor capacity. Inefficient cathode structures and catalysis that can access the oxygen efficiently causes significant charge overpotentials[37,38].

1.2.3 Lithium-Sulfur (Li-S) batteries

Li-S battery technology has gained significant attention than any other battery technology due to its ability to invade the Li-ion battery technology with higher charge capacity (1672 $mAhg^{-1}$) and sufficient operating potential of 2.0 $V^{[39]}$. Furthermore, sulfur is an ample element on earth. Therefore, the material cost per kWh can be reduced compared to the other high energy density battery materials. Considering all these advantages, Li-S batteries

undoubtedly a promising candidate that can fulfill current energy demands, particularly in electric vehicle industry[40].
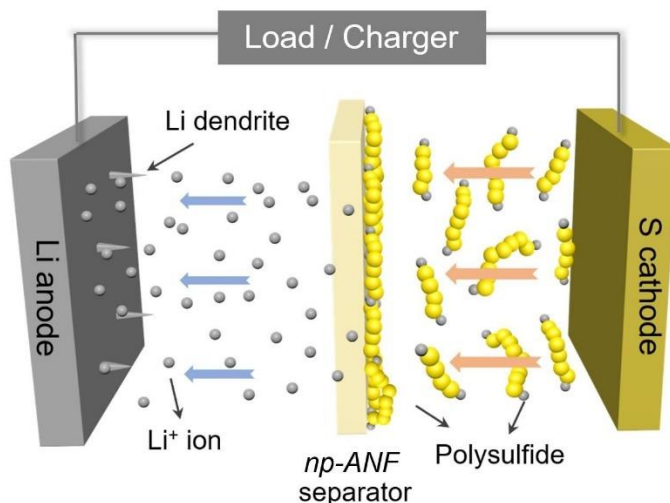
Figure 1.2.3.1: Components of liquid electrolyte Li-S battery [41]

Nevertheless, Li-S batteries are not yet ready for industrial applications mainly due to technical challenges[42,43]. Developing a Li-S battery with high capacity and durability requires resolving the issues related to the sulfur cathode, lithium metal anode and electrolytes. There are three main factors affecting the poor cyclability of sulfur cathode, i.e., (i) poor electrical conductivity of sulfur and polysulfides formed while discharging, (ii) dissolution of polysulfides in the liquid electrolyte during delithiation and lithiation and (iii) polysulfides shuttling between cathode and anode. During the discharge, sulfur first reduces to S_8^{-2} and forms Li_2S_6 and Li_2S_4 thereafter which can lead to active material inaccessible for further electrochemical reactions. The dissolved polysulfides can cause polysulfide shuttling. This phenomenon has been studied extensively and it is found that,

dissolved polysulfides can be reduced near the anode producing solid Li_2S_2 and Li_2S on the lithium metal causing blockage for Li ions[44].

To address these challenges related to the sulfur cathode, various liquid electrolytes have been explored. Among them, solvents, 1,2-Dimethoxyethane (DME) and 1,3-Dioxolane (DOL) based organic electrolytes stand out owing to their bulky anions which can essentially reduce polysulfide solubility. Dissolution of sulfur can increase the viscosity of the electrolyte thus less viscous electrolytes are carefully chosen. When employed with liquid electrolytes, Lithium metal anode alleviates the practical applicability of Li-S batteries due to the problems such as dendrite formation and fire hazard of lithium. Lithium anode is known to build up solid deposits (dendrites) upon charging the Li-S battery triggering cathode and anode short circuiting. To avoid these safety concerns , solid-state electrolytes are investigated. But they have problems such as interface mismatch at the electrode-SSE interfaces. Therefore, there is a vast demand for addressing these issues related both cathode, anode and electrolyte in order to develop high capacity and long-lasting solid-state Li-S batteries (SSLSB).

1.3 Solid-state electrolytes for Li-S batteries

Conventional liquid electrolytes employed in Li-S batteries have various shortcomings such as leakage, flammability, relatively poor chemical stability and narrow electrochemical windows [45]. Therefore, replacement of liquid electrolyte (LE) by solid-state electrolytes (SSE) has become essential for next generation energy storage. Benign characteristics such as better thermal, chemical and electrochemical stability and mechanical strength is almost achieved for most of the SSEs available in scientific arena.

9

SSEs act a vital role in transferring Li ions as well as the separator to prevent short circuit the electrodes. To satisfy above mentioned requirements SSEs employed in Li-S battery have intended to (i) possess high ionic conductivity and low electronic conductivity, (ii) have high Li-ion transference number, (iii) have permanent chemical stability with both anode and cathode materials, (iv) have low interfacial resistance with anode and cathode materials and (v) be nontoxic and environmentally friendly.
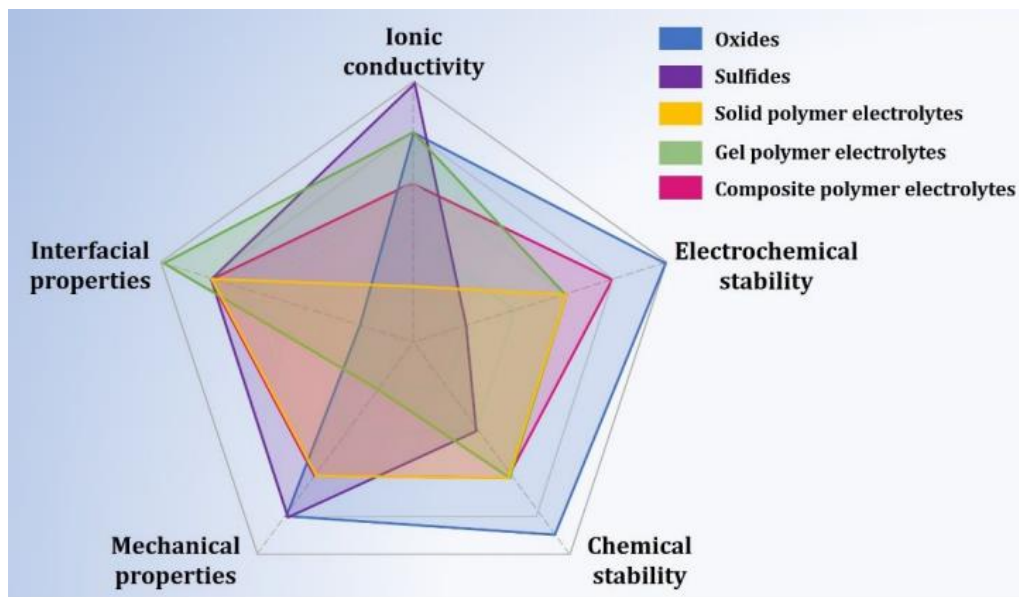
Figure 1.4.1: Comparison of different classes of SSEs used in Li-S battery[46]

There are many SSEs that have met these requirements. Table 1.4.1 shows different types of SSEs which have been employed with the Li-S batteries.

Table 1.4.1: Different types of SSEs[46]

Electrolyte Classification	Sub classification	Advantages	Disadvantages
Inorganic SSEs	Sulfides : $Li_2S-P_2S_5$, Li_6PS_5Cl, thio-LiSICON	High ionic conductivity Low grain boundary resistance	Moisture sensitive
	Oxides : NASICON, LIPON, Perovskite, garnet	High ionic conductivity Good thermal stability	High interfacial resistance
Organic SSEs	Solid polymer electrolytes	Low interfacial impedance Flexibility , stability with Li metal	Low ionic conductivity
	Gel polymer electrolytes	High ionic conductivity Low interfacial impedance	Low mechanical strength Poor thermal stability
Organic-inorganic hybrid SSE	Composite polymer electrolytes	High ionic conductivity Low interfacial impedance	Low mechanical strength Poor thermal stability

Inorganic solid-state electrolyte family contains sulfide-based electrolytes as well as oxide-based electrolytes. Inorganic SSEs have higher mechanical strength, thermal stability and wide electrochemical window. Even though their ionic conductivity varies depending on the material some of the sulfide-based SSEs have proven to accomplish higher ionic conductivities compared to organic liquid electrolytes ($\sim10^{-2}$ Scm^{-1})[47]. In addition to that, due to the compact structure sulfide-based SSEs prevent the polysulfide shuttle effect into great extent.

Solid-state polymer electrolytes are produced by dissolving lithium salt into a polymer host. They own numerous advantages such as higher energy density (due to their low density), good chemical stability, higher flexibility, high safety, easy preparation and low cost[48,49]. Poly(ethylene oxide) (PEO)-based electrolytes are the most commonly used electrolytes in Li-S battery among all of the solid-state polymer electrolytes. The ionic conductivities of solid-state polymer electrolytes at room temperature are not up to satisfactory level regardless of their flexibility and comparatively better interfacial performances with electrodes. Owing to this concern, polymer electrolytes with liquid additives known to be gel polymer electrolytes are recommended as a solution. Gel polymer electrolytes generally made by combining a small amount of organic solvents or ionic liquids (ILs) as plasticizer into a polymer matrix, is in an intermediate state between liquid electrolytes and solid-state polymer electrolytes. Li-ion drifts through the liquid component in gel polymer electrolytes, while the solid-state polymers structurally support the electrolytes and prevent the leakage of liquid[50]. A large amount of gel polymer electrolytes has been studied in solid-state Li-S battery, including poly(vinylidene difluoride) (PVDF), PEO, polyacrylonitrile (PAN), PMMA, etc.-based gels. The

introduction of plasticizers enhances the ionic conductivity of polymer electrolytes with the detriment of mechanical properties. Hence, composite polymer electrolytes with solid-state fillers are widely studied as another method to enhance the Li-ion conductivity of polymer electrolytes[51].

1.4 Challenges in Solid-state Li-S batteries

SSEs with ionic conductivity comparable to or even higher than that of liquid electrolytes have been developed and applied to solid-state Li-S batteries. Nonetheless, there is still enormous room for improvement of SSEs in SSLSB. Though inorganic SSEs like sulfides are gifted with high ionic conductivity, they are unstable to ambient atmosphere, while oxides got significant interfacial resistance with electrodes since their higher rigidity.

When rigid SSE is used in the battery, there is high chance to have a considerable mismatch at the interface with electrodes rising the interface resistance. Various different approaches have been experimented in the history to improve the SSE-cathode interface to have lower interfacial resistance to ion migration[52].(Fig 1.4.1).
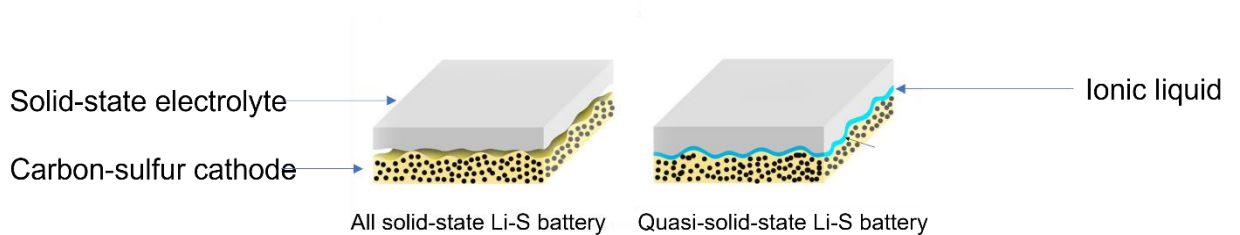
Figure 1.4.1: SSE-cathode interface of all-solid-sate Li-S battery and quasi-solid-state Li-S battery

On the other hand, designing a cathode perfectly matching to the selected SSE is one of the quite challenging parts in the SSLSB. Being electronically and ionic conductive is major requirement for the cathodes in liquid electrolyte Li-S batteries. SSLSB has no exceptions when considering the conductivity of the cathode. Even if the highest conductive SSE is utilized with the highest conductive cathode, still there is high chance of making a failed battery due to the interfacial resistance rising from interfacial contact of rigid surfaces. Furthermore, there can be side reactions which lead to battery failure. This emphasizes the importance of understanding and optimizing interfacial contacts at SSE-electrode interfaces. Yet, conductivity of the cathode is regarded as equally vital and will be further discussed in the chapter 2.

In summary, it is important to identify the design and the formulation of the cathode suitable for the SSE, understanding of the interfacial reactions and lowering the interfacial resistance between SSE and electrodes, in order to address major challenges in solid-state Li-S battery technology. In addition, there are several other critical challenges such as low sulfur mass loading in cathode (~0.3 mgcm^{-2}), large thickness of solid-state electrolyte, growth of lithium dendrite, and inability to charge faster etc. that prohibit the commercialization and application of solid-state Li-S batteries.

1.5 Proposed concepts for high performance quasi-solid-state Li-S batteries

1.5.1 Super P-Sulfur cathode (low sulfur loading)

High performance SSLSBs involve fast exchange of electrons and Li cations through the cathode. On the other hand, sulfur cathodes have an intrinsic drawback that elemental sulfur and the final discharge products both Li_2S_2 & Li_2S have poor electronic and ionic

conductivities,[53,54] leading to slow reaction kinetics of sulfur cathodes. Moreover, the volume change of cathode during the reaction can approach 80% due to the density difference between S and Li_2S [55-56]. The constant volume change will bring about the shedding of active materials and large internal stress, and ultimately result in capacity decay and poor cycle performance of the battery. Early researchers employed the mixtures of S and copper sulfide such as Cu_2S and CuS as active materials in the cathode.[57,58,59] Carbon materials [60,61,62,63] and conductive polymers[64] are also utilized to improve the electronic conductivity of sulfur cathode. Different types of sulfur cathodes have been developed for Li-S liquid electrolyte batteries whereas carbon-sulfur composite cathode stands out with the most effective outcomes due to their higher electronic conductivity[65].Various carbon-sulfur cathode designs can be found in literature developed from graphene, carbon nanotubes, acetylene carbon black etc.[66,67,68,69,70].

Traditionally, carbon black is only used as an extra conductive additive in the cathode. However, the low cost and high electrical conductivity of carbon black offer improvements for sulfur cathodes. After carbon black is mixed with sulfur particles or sulfur is evenly distributed in the carbon black clusters, the sulfur-carbon black composites can improve the sulfur utilization. Super P conductive carbon black (SP) was used as the conductive carbon additive for sulfur cathode in this research work, which has average pore volume of 0.14 cm^3g^{-1} and surface area of 62 m^2g^{-1} [71].
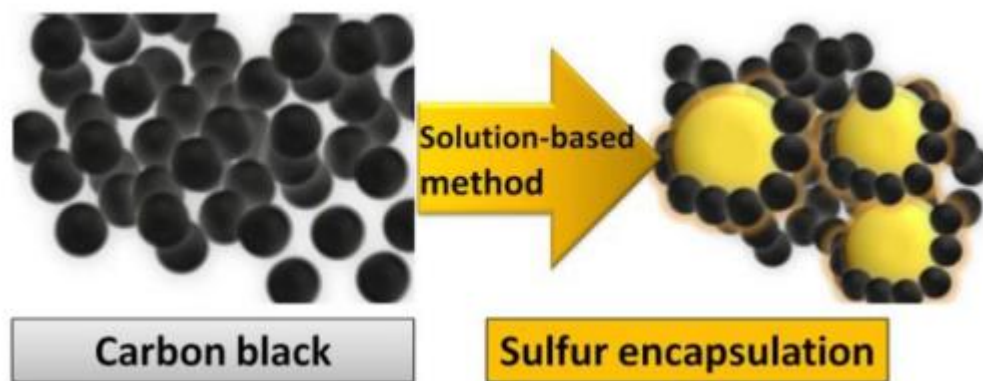
Figure 1.5.1: Mixing carbon black with sulfur to improve the electronic conductivity.

The binder is critical for fabricating battery electrodes. However, conventional binders such as Polytetrafluoroethylene (PTFE) or polyvinylidene fluoride (PVDF) are not effective for sulfur cathodes because of the dissolution of polysulfides [72]. Polyethylene oxide (PEO) is one of the earliest replacement binders that has been studied in Li-S batteries. Lacey et.al. [73] studied sulfur cathodes with different PEO binder contents prepared by two different methods, ball-milling and mechanical stirring. He et al.[74] utilized a water-soluble binder consisting of styrene butadiene rubber (SBR) and carboxymethyl cellulose (CMC) in sulfur electrodes. The SBR−CMC binder can not only act as an adhesion agent but also facilitate the dispersion of active materials, maintaining a uniform and electrochemically favorable structure in the sulfur electrode and leading to better cycling performance than that with the PVDF binder. Preliminary experiments of this work were based on the PVDF binder and due to unsuccessful results CMC-SBR was chosen due to its enhanced flexibility added into coatings.

In this study cathodes coated on Al foil, consisting of sulfur as the active material, Super P conductive carbon black, acetylene carbon black as conductive carbon additives, water

based carboxymethyl cellulose (CMC) solution combined with premixed styrene butadiene rubber (SBR) as the binder were developed. At the initial part of this study, batteries with low sulfur loading in the cathode were assembled using this formulation to optimize other parameters such as the ionic liquid amount etc. as discussed below.

1.5.2 Ionic Liquid optimization

Introducing a hybrid electrolyte consisting of SSE coupled with liquid electrolyte, polymer electrolyte or ionic liquid, was the proposed approach to address the interface contact with the electrodes [75,76,77]. Even though, previous studies have reported SSLSBs consisting of sulfide-based SSEs, only a handful of them report the use of ILs to improve the interfacial contacts. Here in this study, the choice of the IL, its optimum viscosity and the volume needed to improve the solid-solid interfacial contacts influencing the interfacial reactions for improved cycle life of this novel QSSLSB were systematically studied.

1.5.3 Super P-Sulfur cathode with High sulfur loading

An increase in the amounts of inactive materials (carbon and binders in sulfur cathode) significantly reduces the weight content of sulfur, resulting in low mass loading. Low mass loading of sulfur notably decreases the energy density of the battery[78]. To achieve the high energy density batteries, active material loading of the cathode has to be increased. However, the porosity of the cathode decreases significantly as the thickness of the cathode increases due to high mass loading of the coating. Since the availability of the SSE amount was limited, the best way to experiment on the mass loading was to test the synthesized cathodes with conventional liquid electrolyte against Li metal chips. Once the optimized combination for the slurry coating was found, those cathodes were used in the QSSLSB.

For high sulfur loading cathodes, two techniques were investigated. First method was a slight modification of the slurry coating technique used for low sulfur loading cathode. Here, thicker coatings were prepared by using the doctor blade technique with different compositions of sulfur, SP carbon and carbon additive such as acetylene black and single walled carbon nano tubes. Various compositions of the cathode were attempted to include as much as sulfur in the cathode. In comparison, low sulfur loading cathode contained 3:2 SP:S ratio whereas 1:3 SP:S was employed in the high sulfur loading cathode. All the parameters and additives including binder were changed for the high sulfur loading cathodes coated by doctor blade technique. Depending on the coatings, the viscosity and the volume of the ionic liquids were also optimized for the best performances.

Another way used to improve the contact at the interface was to press the SSE along with the cathode using a stainless-steel tank under a given pressure. In this technique, pre-mixed SP-S mixture was balled milled with the SSE under Ar atmosphere and pressed together with the SSE to have a blended cathode-SSE interface. Cathode material was mixed with the SSE to increase the ionic conductivity of the cathode as the sulfur utilization suffers as the thickness of the cathode increases. This technique was employed in the rest of the studies as it was successful in high loading QSSLSB with mass loading of 4 mgcm^{-2} with improved cycle stability compared to the slurry coated method. However, the major drawback of this technique was the low initial capacity.

1.6 Dissertation objectives

The main objective of this work was to design a high performing QSSLSB with stable cycle life. Novel SSE synthesized by introducing halogens into argyrodite structure ($Li_6PS_5F_{0.5}Cl_{0.5}$ & $Li_6PS_5F_{0.5}Cl_2$) were used for QSSLSBs assembly. The following were the dissertation objectives in addressing challenges associated with QSSLSB battery technology.

i. Sulfur cathode development: The main challenge of developing sulfur cathode was the poor electronic conductivity of sulfur. Finding the best candidate to enhance electronic conductivity with minimal side reactions and optimizing the correct combination compatible with slurry coating with considerable sulfur loading was another challenge.

ii. Ionic Liquid Optimization: Selection of the ionic liquid was challenging since it should not react with both electrodes and SSE. It was necessary to optimize the properties of the IL including the concentration, volume, solvent diluent etc. to achieve the best results with the SSE and the cathode.

iii. QSSLSBs with high sulfur loading: Again, the cathode had to be optimized to reach the target of 4.0 mgcm^{-2} sulfur loading. With high sulfur loading, both electronic and ionic conductivity were often found to suffer. Different approaches such as incorporation of carbon nano tubes (CNT) and Lithium aluminum titanium phosphate (LATP) SSE were used to improve both conductivities. Mixing the SSE powder with the cathode powder and pressing them together with the SSE pellet

was also used as an alternative approach to reach high sulfur loading QSSLSB with desired conductivities.

The rest of the dissertation is organized as follows. Chapter 2 provides the background of the known high energy density rechargeable batteries and characterization techniques used in this work. Chapter 3 details the experimental procedures implemented for cathode development and electrochemical techniques used for testing cells. Chapter 4 is mainly focused on optimization of ionic liquids. Chapter 5 includes material quality improvements and technical details of assembling a high energy density QSSLSB using cathode coatings. Chapter 6 consists of the details of assembling a high energy density QSSLSB using composite cathode consisting of SSE and cathode powder mixture.

CHAPTER 2

BACKGROUND

2.1 Scope

The focus of this chapter is to summarize the chemistry of Li-ion batteries, Li-Air batteries, and Lithium-sulfur batteries. The chemistry of Li-S battery is explained with a detailed description of polysulfide dissolution mechanism and polysulfide shuttling phenomena generally seen in liquid electrolyte Li-S batteries. A review of solid-state electrolytes used in this project is described next. In addition, a description of material and electrochemical characterization techniques which were applied in this dissertation is summarized at the end of this chapter.

2.2 Chemistry of rechargeable batteries

2.2.1 Li-ion batteries

The concept of Li ion's movement between the cathode and the anode was first proposed by Armon et al. in the early part of 1970's. Then this idea was further developed by Lazzari an Scrosati utilizing a lithiated tungsten dioxide electrode and a titanium disulfide electrode. Still, its voltage was limited to 2.2 V. Then the Goodenough laboratory discovered the reversibility of lithiation and delithiation properties of $NaFeO_2$ structure, and later LiCoO2 was patented as the cathode material of the Sony's first ever commercial Li-ion battery. After that, J.C Hunter from Eveready laboratories discovered the similar

characteristics in MnO2[79,80].

In a conventional Li-ion battery, cathode is a pre-lithiated oxide (Li_xMO_y, M=Fe, Mn or Co etc.) and the anode is mostly graphite. Fig. 2.2.1 shows a schematic of a conventional lithium-ion battery.
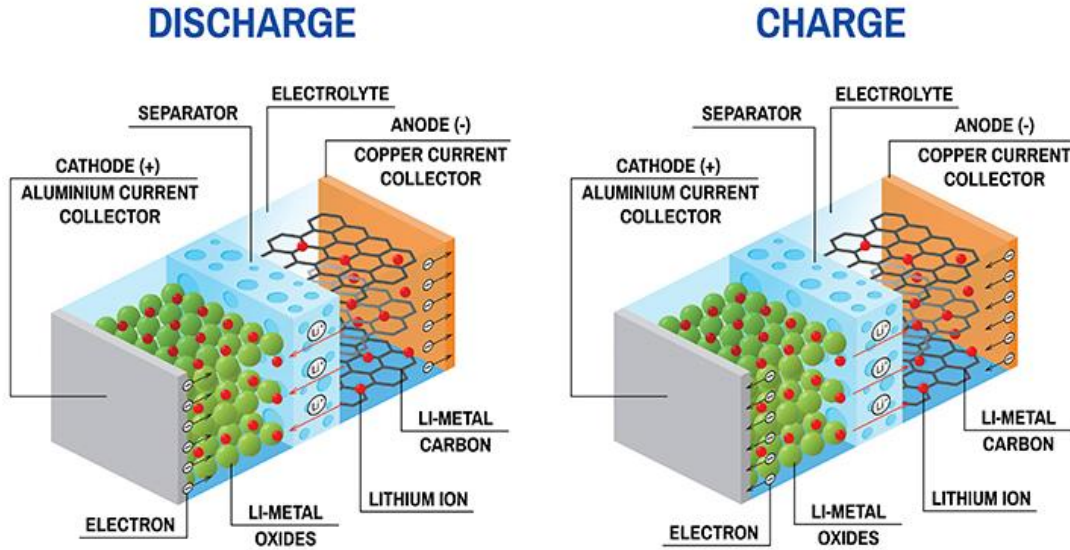
Figure 2.2.1.1: Schematic of the conventional Li-ion battery[81]

The half-cell reactions can be written for the cell chemistry shown in the Fig. 2.2.1.1 as follows.

$$xLi^+ + xe^- + 6C \rightleftharpoons Li_xC_6 \text{ (at the anode)} \tag{2.1}$$

$$LiCoO_2 \rightleftharpoons Li_{1-x}CoO_2 + xLi+ + xe^- \text{(at the cathode)} \tag{2.2}$$
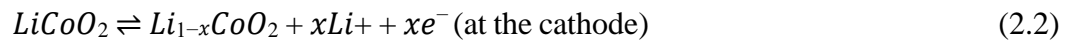
The overall reaction can be written as

$$LiCoO_2 + 6C \rightleftharpoons Li_{1-x}CoO_2 + Li_xC_6 \tag{2.3}$$

In these equations, the forward reaction shows the charging process, while the reverse reactions show the discharging process. The electrolyte used in these batteries are typically consisted of alkyl carbonate with $LiPF_6$ (lithium hexafluorophosphate salt) to provide Li ion conductivity[82].

Most popular Li-ion battery cathodes and their properties are presented in the following table. In table 2.2.1.1 LCO is $LiCoO_2$, LMO is $LiMn_2O_4$, NCA is $LiNi_{0.8}Co_{0.15}O_2$, NMC is $LiNi_xMn_yCo_{1-x-y}O_2$, and LFP is $LiFePO_4$[83].

Table 2.2.1.1: Li-ion battery cathodes and their properties [84]

Cathode material	Midpoint Voltage vs Li (C/20 rate)	Specific Capacity (Ah/kg)	Applications
LCO	3.9	155	Portable electronics
LMO	4.0	100-120	Power tools
NCA	3.7	180	Premium electronic applications
NMC	3.8	160	Portable electronics and electric vehicles
LFP	3.4	160	Power tools

Li-ion batteries with liquid electrolytes present respectable performance; the electrolyte solutions offer high conductivity and excellent wetting of the electrode surfaces. Yet, liquid electrolytes based on highly volatile and flammable organic solvents have given rise to some drawbacks such as low ion selectivity, inadequate stability, and especially the huge issue of safety[85]. On the other hand, the application of all-solid-state lithium batteries

23

(ASSLBs) not only alleviate these difficulties, especially the safety concern and long-term electrochemical and thermal stabilities, but also further advance the energy/power densities and decrease the requirements for packaging and state-of-charge monitoring circuits[86]. Thanks to these benefits, a rapidly expanding trend of assessments on solid-state electrolytes (SSEs) for use in lithium batteries has become apparent in recent years[87].

2.2.2 Li-air Batteries
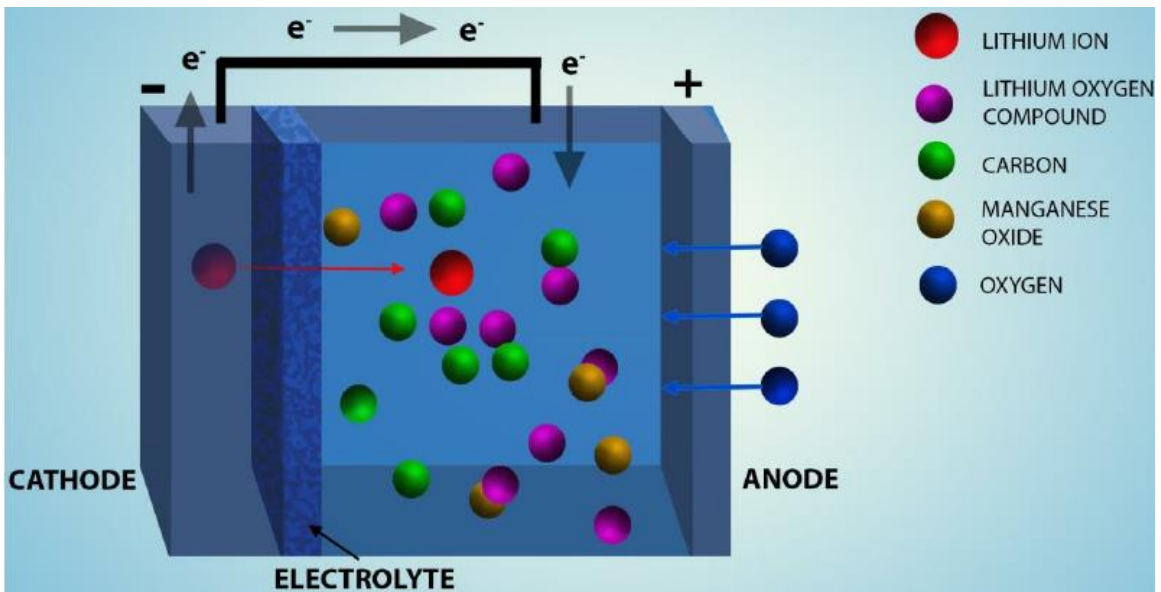
Figure 2.2.2.1: Schematic diagram of Li-air battery [88]

Figure 2.2.2.1 shows and schematic diagram of the Li-air cell. Throughout the discharge of the Li-Air cell, Li is oxidized to Li+ ions at the metallic anode. An electrolyte comprised of Li salt and non-aqueous solvent offers Li+ conductance and reacts with O_2 on the porous cathode composed of carbon and a catalyst[89].

For an aprotic electrolyte which gives a cell potential of 3.0 V equation can be written as,

$$2Li + O_2 \rightarrow Li_2O_2 \qquad\qquad (2.4)$$

In an aqueous electrolyte, the fundamental reactions can be written as,

$$4Li + O_2 + 4H+ \rightarrow 4Li+ + 2H_2O \text{ (acidic media)} \qquad (2.5)$$

$$4Li + O_2 + 2H_2O \rightarrow 4LiOH \text{ (alkaline media)} \qquad (2.6)$$
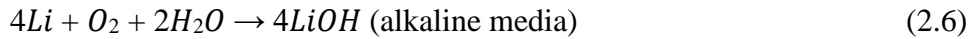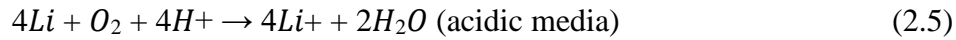
Even though, rechargeable Li-air batteries have a massive theoretical energy density than Li-ion batteries, were failed to become a power source for electric vehicles (EVs). Three types of rechargeable Li-air batteries have been built: non-aqueous, aqueous, and solid. Vast majority of research efforts have been dedicated to the non-aqueous battery in the past two decades. Non-aqueous Li-air batteries still have critical issues to be addressed to accomplish the practical use for EVs, such as a low practical areal capacity, low round-trip energy efficiency, and air purification. The aqueous and solid Li-air systems do not have the critical issues observed in the non-aqueous system; however, they have not indicated considerable capacity for high power density and extended cycling life[90].

2.2.3 Li-sulfur battery

Lithium-Sulfur (Li-S) batteries stands out to be the one of the most promising candidates to meet the energy storage requirement for electric vehicles and portable storage devices, with its natural abundance of materials, high theoretical capacity of 1672 mAhg^{-1}, high energy density of 2600 Whkg^{-1}, low cost and lower impact to the environment[91,92,93,94]. During the discharge process of the Li-S battery Li$^+$ ions produced at the Li anode, migrate through the electrolyte towards cathode and electrons move through the external circuit, producing polysulfides and Li$_2$S at cathode as the final discharge product[95,96].
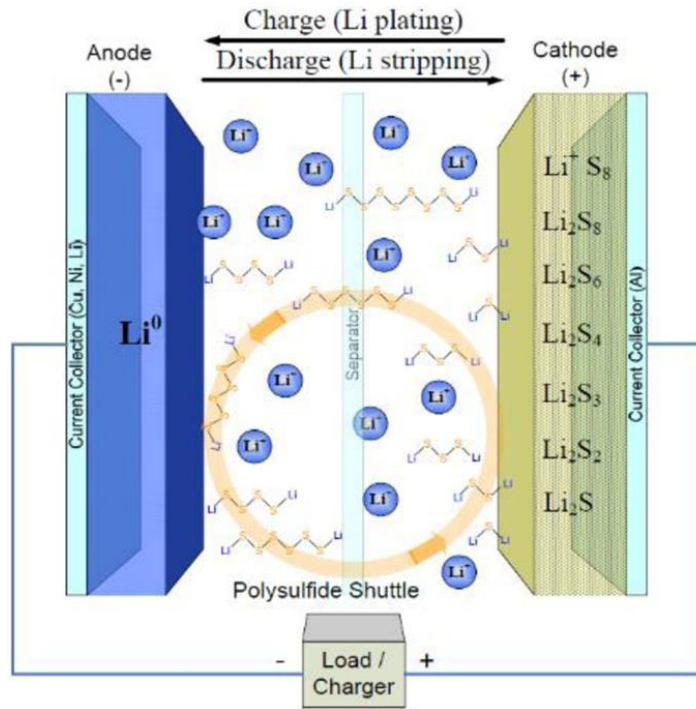
Figure 2.2.3.1: Schematic diagram of liquid electrolyte Li-sulfur battery [97]

With the presence of the liquid electrolyte, in the discharge profile a dual-phase plateau is expected for liquid electrolyte Li-S batteries at the cathode-liquid electrolyte interface (solid-liquid interface). First part of the plateau around 2.3V corresponds to the conversion of S_8 into Li_2S_4, which has an approximate theoretical capacity around 418 mAhg^{-1}.

Equations for the initial discharge reactions can be written as follows,

$$Li \rightarrow Li^+ + e^- \text{ (at anode)} \qquad (2.7)$$

$$S_8 + 2e^- \rightarrow S_8^{2-} \text{ (at cathode)} \qquad (2.8)$$

$$S_8^{2-} + 2e^- \rightarrow 2S_4^{2-} \text{ (at cathode)} \qquad (2.9)$$
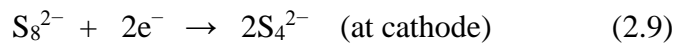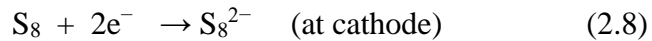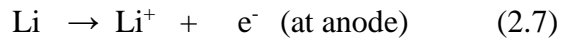
Second phase of the discharge plateau at 2.1V corresponds to the further conversion of Li_2S_4 into the Li_2S and has potential to deliver a theoretical capacity around 1254 mAhg^{-1} [98].

$$Li^+ \;+\; S_4^{2-} \;+\; 4e^- \;\rightarrow\; Li_2S_2 \;+\; Li_2S \qquad\qquad (2.10)$$

$$2Li^+ \;+\; Li_2S_2 \;+\; 2e^- \;\rightarrow\; 2Li_2S \qquad\qquad (2.11)$$
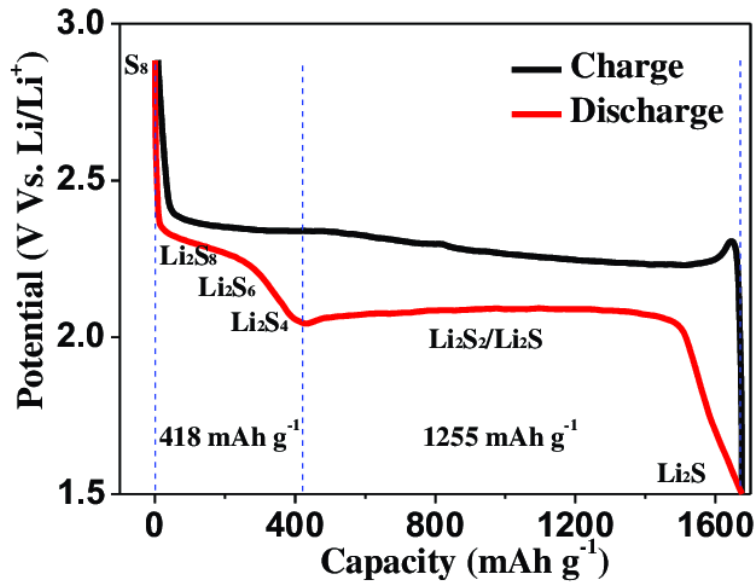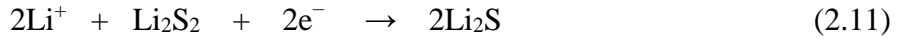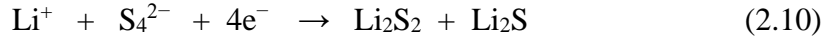
Figure 2.2.3.2: Charge discharge curve for liquid electrolyte Li-S battery [99]

In the absence of the liquid electrolyte, which becomes the solvent for polysulfides, ASSLSB shows different reaction route that involves direct conversion between S_8 and Li_2S without polysulfide formation at the cathode-SSE interface (solid-solid interface). This solid phase reaction shows the discharge plateau around 2.0V.
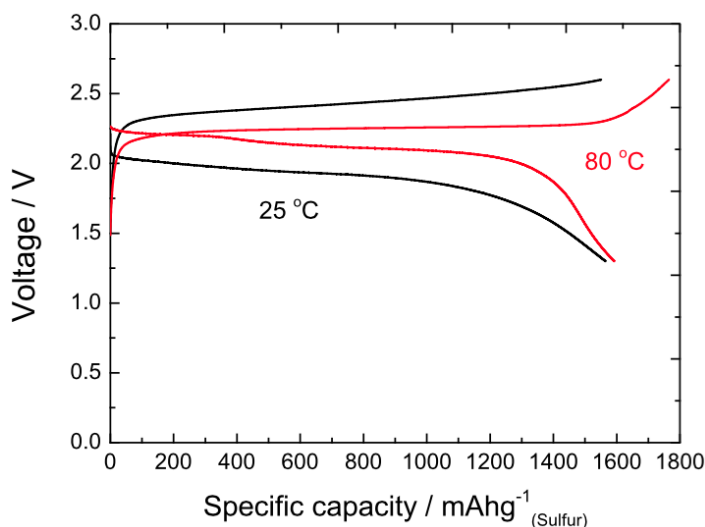
Figure 2.2.3.3: Charge discharge curves for solid-state Li-S battery [100]

When both SSE and small amount of ionic liquid is present simultaneously both solid-liquid and solid-solid reactions take place. As a result of this, mixed discharge profile can be observed with multi-phase discharge plateaus. This kind of batteries with quasi-solid phase reaction are known as the quasi-solid-state Li-S batteries (QSSLSB)[101].

2.3 Proposed solid-state electrolytes and challenges associated with them

Out of various SSEs for Li-S solid state batteries, sulfide based solid electrolytes get higher attention due to their higher ionic conductivity, compatible interface with sulfur-based cathodes, and lower grain boundary resistance [102,103]. Halogen-doped argyrodite solid electrolyte materials such as Li_6PS_5Cl have been extensively studied, but poor compatibility between SSE and Li anode has hampered many efforts to use it in all solid-state batteries [104]. Using a solvent-based process, $Li_6PS_5F_{0.5}Cl_{0.5}$ SSE was synthesized via the introduction of LiF into the argyrodite crystal structure, which affects both the ionic conductivity and interface-stabilizing properties of the SSE.

28
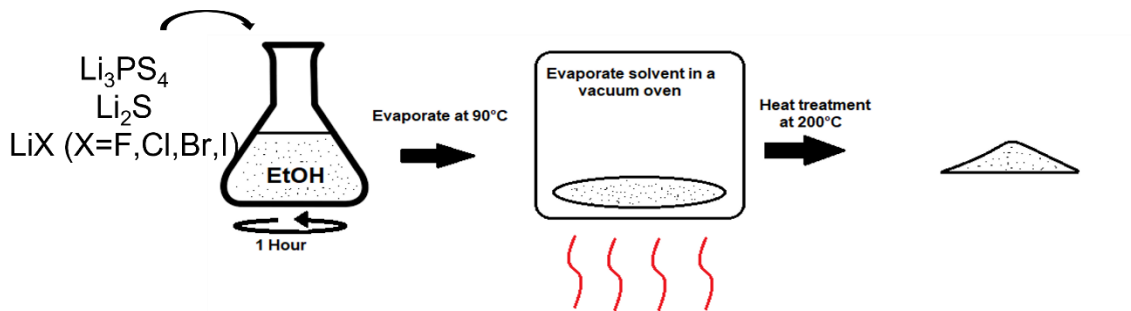
Figure 2.3.1.1: Synthesis process of sulfide-based solid-state electrolytes

Excess LiF from this halogen doping technique creates an LiF-rich SEI layer which stabilizes the SSE/anode interface and effectively prevents Li dendrite formation [105]. The stabilizing influence of $Li_6PS_5F_{0.5}Cl_{0.5}$ & $Li_6PS_5F_{0.5}Cl_2$ combined with their impressive ionic conductivities (table 2.3.1) make them excellent candidates for use in a Li-S battery. In spite of that, there are still some challenges impeding them from practical application. Firstly, sulfide electrolytes are not stable in an ambient environment. They will react with moisture and generate poisonous gas H_2S [106]. So, all the experiments related with the sulfide-based SSEs had to be conducted inside the glove box. Transferring these materials for characterizations (XPS, XRD etc.) also had several challenges due to formation of oxides at the surface.

Table 2.3.1: Solid-state electrolytes tested in this work and their ionic conductivities,

Solid-State electrolyte	Ionic Conductivity ($\times 10^{-4}$ S/cm)
Li_6PS_5F	2.24
$Li_6PS_5F_{0.5}Cl_{0.5}$	3.51
$Li_6PS_5F_{0.5}Br_{0.5}$	3.19
$Li_6PS_5F_{0.5}I_{0.5}$	2.58
$Li_6PS_5F_{0.5}Cl_2$	5.30

2.4 Proposed ionic liquids

Ionic liquid (IL) based electrolytes are taken into consideration to wet the SSE-electrode interface due to their high viscosity thereby reducing the solubility of sulfur and lithium polysulfides, thus reducing the polysulfide shuttling effect.
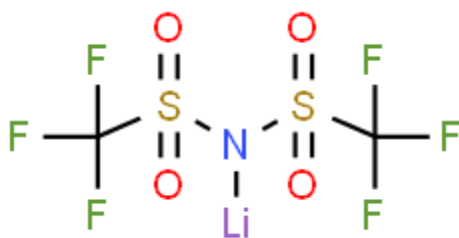
Figure 2.4.1: Structure of LiTFSI molecule

In the literature there are number of reports on ILs containing pyrrolidinium (PYR) as the cation and bis(trifluoromethyl sulfonyl)imide (TFSI) as the anion[107,108,109].
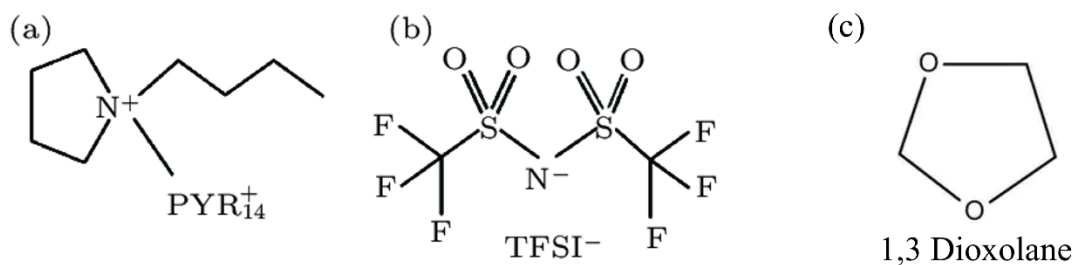
Figure 2.4.2: Structure of (a) PYR14+ molecule, (b) TFSI molecule & (c) 1,3 Dioxolane molecule.

Major drawback of this IL is its low ionic conductivity and high viscosity with the higher TFSI concentration. To improve the conductivity and lower the viscosity, co-solvents are introduced. In this work 1,3-dioxolane (DOL) was used as the co-solvent to prepare the IL and effect of co-solvent has been studied systematically to optimize [110] the performance.

2.5 Challenges associated with high performance sulfur cathodes

Different types of sulfur cathodes have been developed for Li-S liquid electrolyte batteries whereas carbon-sulfur composite cathode stands out with the most effective outcomes due to their higher electronic conductivity[111]. Mixing of sulfur with the carbon powder has to be homogeneous to obtain uniform conductivity. For that Sulfur and carbon powders were Ball-milled at high speeds for long times. The mixtures were then sealed in a Pyrex test tube and heated at 120 °C for 3 hours under vacuum for melt diffusion of Sulfur in the carbon support. Since sulfur has a melting point at 115 °C it was believed that the mixture become homogeneous after this step.

Various carbon black powders such as KETGEN black, Graphite, Carbon nano tubes (CNT), Carbon Super P (SP), etc. were tested in the early stage of this work with the PVDF/NMP binder. When the loading is increased more than 0.1 mgcm^{-2} coatings had tendency to flake out. Before testing with solid electrolyte, these coatings were tested with conventional liquid electrolyte (LE) and Super P and Carbon nano tube coatings have shown promising results. However, for SSE, Sulfur cathode with only super P was successful.

Super P conductive carbon black (SP) was used as the conductive carbon additive for sulfur cathode in this research work. It has average pore volume of 0.14 cm^{3}g^{-1} and surface area

of 62 m^2g^{-1} [112]. To address the issue with the flaking off of the coating, different binders were employed. Water based carboxymethyl cellulose (CMC) solution combined with premixed styrene butadiene rubber (SBR) was found to be successful due to the flexibility of SBR. Due to toxicity of NMP, compared to PVDF/NMP binder CMC/SBR was much safer and easy to handle. Coatings with CMC/SBR were uniform and flexible on the Al foils. On the other hand, this water-based binder came with drawbacks like poor electronic conductivity due to insulating rubber and SSE could not be mixed into the cathode due to the moisture sensitive nature of the SSE. Mixing at high speeds plays an important role, because slurry coating made by using doctor blade technique requires fine particle size and if any larger clusters remaining in the slurry would deteriorate the coatings.

In this study cathode consisting of sulfur as the active material, Super P conductive carbon black, acetylene carbon black (AB) as the conductive carbon additive, and water based carboxymethyl cellulose (CMC) solution combined with premixed styrene butadiene rubber (SBR) as the binder was developed. After the coatings were made, they were dried at 60 °C due to the low melting point of the sulfur. If the annealing temperature was significantly high, the amount of sulfur taken into loading calculation will be less and final loading will have a significant error. So, the drying was carried out at a lower temperature for excessive time. All the experimental steps of cathode coating will be explained in detail in the next chapter.

Other than the challenges associated with coating, electronic and ionic conductivities remain a major concern in the cathode design. Numerous experiments had to be conducted to optimize the electronic conductivity by varying CNT and AB content in the cathode.

Porosity of the cathode is also a significant parameter to pay a special attention while coating. This becomes vital when the loading is increased higher than 2 mgcm^{-2}. Because of heavy mass load, coatings become less porous and wetting at the interface becomes less effective giving rise to poor performance. Incorporation of SSE into the cathode was an alternative way to improve the performance at higher loadings. This became quite challenging because SSE used in this work were moisture sensitive. This will be discussed in detail in the chapters 5 and 6.

2.6 Instruments of material characterization

2.6.1 Scanning electron microscope (SEM)

A scanning electron microscope (SEM) is a type of microscope that uses a focused beam of electrons to create high-resolution images of the surface of a sample. Unlike conventional optical microscopes, which use visible light, SEMs use a beam of electrons that is scanned across the surface of the sample to create an image.

In an SEM, electrons are emitted from an electron source, usually a tungsten filament or field emission source. The electrons are accelerated by a series of lenses and focused into a fine beam that is directed onto the sample. Upon interaction with the material, these incident electrons can undergo different processes. Some electrons can be reflected, or absorbed by the material, while some electrons can excite the material to release secondary electrons. By detecting the backscattered or secondary electrons, a computer-processed image can be produced to visualize the surface topography of the material.

Target materials may also radiate x-ray photons upon interacting with the incident electron beam. Detection of these x-ray photons can be used to probe the elemental composition of

a sample. Therefore, some scanning electron microscopes are also equipped with an x-ray detector. This technique is referred to as energy dispersive x-ray spectroscopy (EDAX or EDS). From such SEM systems, users can not only image the surface topography of the sample, but its constituent elements can also be identified.
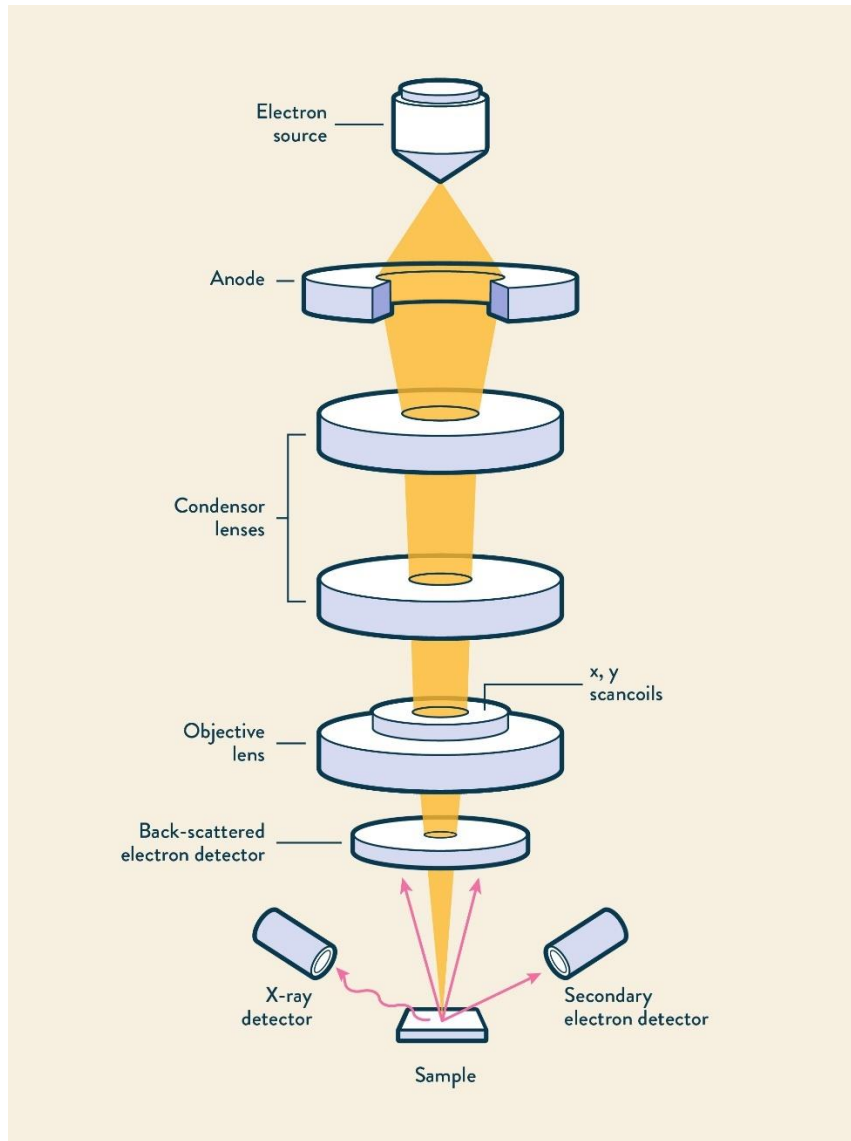
Figure 2.6.1.1: Diagram of Scanning electron microscope with EDS detector [113]

In this work Nova 600 field emission scanning microscope (FESEM) was used for high resolution imaging of the surface and cross-section which was used to estimate the thickness of coatings. TESCAN VEGA 3 thermionic emission scanning microscope was used to image the surface of sulfur cathode and surface of SSE after disassembly of the battery (post cycling experiments). Same instrument was used for mapping the material composition of SSE surface using X-ray dispersive spectroscopy (EDAX).

Figure 2.6.1.2: FESEM and TESCAN SEM systems

2.6.2 X-ray photoelectron spectroscopy (XPS)

XPS is a characterization technique specifically used to investigate the surface chemistry of a material. Often the surface of a material is different from the bulk, especially for nanomaterials. As the size of the material decreases, a larger percentage of atoms can be found at the surface. Therefore, properties of the nanomaterials are dominated by surface properties. Thus, understanding surface chemistry is important. In XPS, the "surface" can be defined as the top 10 nanometers of a sample. The basic idea is that the material of interest is being hit by high energy x-ray photons (with energy hv) which knock inner shell electrons out of the sample. This phenomenon is known as the photoelectric effect and the

ejected electrons are referred to as photoelectrons. Then the kinetic energy (KE) of these photoelectrons is measured by a detector so that the binding energy (BE) can be calculated as shown in equation 2.6.2

$$BE = h\upsilon - KE - \phi \qquad\qquad (2.12)$$

Upon scanning a sample, a spectrum demonstrating the number of electrons emitted at each binding energy is created. The binding energy data can be used to identify elements and their electronic states as each element has specific binding energy corresponding to each atomic orbital. XPS can identify binding energies of all elements except hydrogen and helium. XPS experiments take place in ultra-high vacuum chambers, where pressures are typically in the 10^{-9} Torr range. Most common x-ray sources used in XPS have an energy of about 1.5 keV.

Figure 2.6.2.1: VG Scientific MultiLab 3000 XPS system

In this work, X-ray photoelectron spectroscopy (XPS) (VG scientific-MultiLab 3000) was employed to detect the chemical composition at the cathode-SSE interface after cycling the

batteries. Prior to careful analysis, all the spectra were calibrated with respect to the C-C (sp^2) binding energy (284.8 eV) of the C1s peak.

2.6.3 Thermo gravimetric analysis (TGA)

Thermogravimetric analysis (TGA) is a technique used to study the thermal stability and decomposition behavior of materials. In TGA, a sample is heated at a constant rate while its weight is continuously measured. As the sample is heated, any weight loss or gain is recorded as a function of temperature or time.
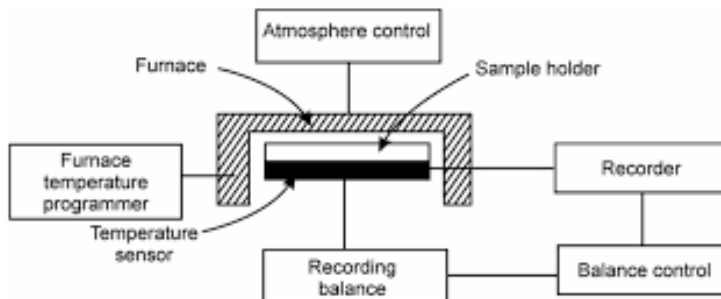
Figure 2.6.3.1: Cross section of a TGA system

The TGA instrument typically consists of a furnace, a balance, a thermocouple to measure temperature, and a computer to record and analyze the data. The sample is placed on the balance, which is located inside the furnace. The furnace is then heated at a constant rate, usually between 5-20 °C per minute, depending on the material being studied.
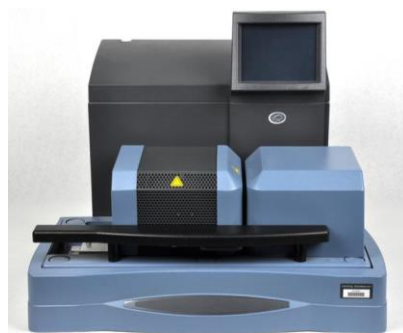
Figure 2.6.3.2: SDT Q600 TGA System

During heating, the sample may undergo various chemical or physical transformations that result in weight loss or gain. For example, organic materials may decompose or volatilize, while inorganic materials may undergo phase changes or decomposition reactions. The weight loss or gain is recorded by the balance and plotted as a function of temperature or time. TGA can provide valuable information about the thermal stability, composition, and behavior of materials.

Thermo gravimetric analysis (TGA) studies of the cathode were done by the thermo gravimetric analyzer SDT Q600 under N_2 gas flow of 100 ml/min by heating the sample up to 800 °C. Sulfur has the melting point at 112.8 °C and boiling point at 444.6 °C and mass loss measured by TGA is due to moisture and loss of sulfur. From that sulfur mass loading of cathode was measured, and predicted calculations were confirmed using this instrument.

2.7 Instruments of electrochemical characterization

2.7.1 Potentiostatic electrochemical characterization

Potentiostat is one of the key instruments used in electrochemical analysis. In a potentiostat, voltage is the controlled variable, while current is the measured variable. In this work, biologic SP200 Potentiostats was used to perform cyclic voltammetry (CV).

CV is a powerful tool for studying the redox behavior of materials, as it can provide information about the electron transfer kinetics, thermodynamics, and reaction mechanisms of a system. In CV, the voltage is typically scanned at a fixed rate, known as the scan rate. The scan rate can be adjusted to study the electrochemical behavior of a sample over a range of timescales. During this work, cyclic voltammetry was performed in the range of 2.8 V- 1.0 V for the cathodes to identify the reaction pathways they follow during the discharge process.

2.7.2 Electrochemical impedance spectroscopy (EIS)

Electrochemical Impedance Spectroscopy (EIS) is an extremely sensitive characterization technique used to establish the electrical response of chemical systems in a nondestructive manner. EIS systems characterize the time response of chemical systems using low amplitude alternating current (AC) voltages over a range of frequencies. Using an electrode setup consisting of a working, reference, and counter electrodes a known voltage is passed from the working electrode through an electrolytic solution and into the counter electrode. Quantitative measurements are produced by the EIS and enable the evaluation of small-scale chemical mechanisms like interfacial reactions at the electrode interface and within

the electrolytic solution. Therefore, EIS is useful in determining a wide range of dielectric and electrical properties of components in research fields studying batteries, corrosion, etc.

In this dissertation work, BioLogic SP 200 system with frequency modulation was employed to conduct the EIS measurements of coin cells. All the spectra were measured in the frequency range of 1 MHz to 50 mHz with an excitation voltage of 5 mV.
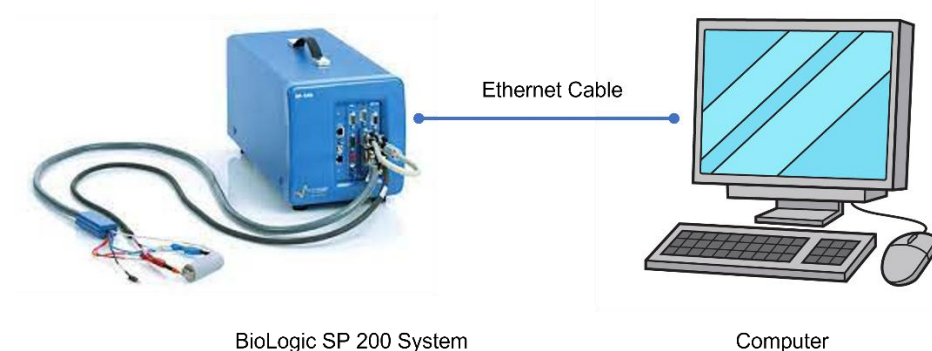
Figure 2.7.2.1: BioLogic SP 200 System used for CV and EIS

2.7.3 Galvanostatic electrochemical characterization

In galvanostatic electrochemical analysis, the voltage is measured while keeping the current constant. Typically, cell capacity is measured using galvanostats. In this work, Arbin 16 channel and 8 channel battery testers were used for capacity measurements, C-rate measurements and cell cycling. The Arbin 16 or 8 Channel Galvanostat is a research-grade instrument designed for battery testing and electrochemical characterization of materials. One of the key features of the Arbin 16 Channel Galvanostat is its ability to test up to 16 cells simultaneously, which makes it an ideal tool for high throughput testing of batteries or other electrochemical systems. The instrument is also equipped with a range of safety features, including overcurrent and overvoltage protection, to ensure safe and

reliable operation. It is programmable for the different voltage and current requirements within 5 V and 10 A limits.

Figure 2.7.3.1: Battery testing system with temperature control used for this work,

The Arbin multi-Channel Galvanostats are controlled via a software, which allows users to set up and run experiments, monitor data in real-time, and analyze results. The software also includes a variety of features for data visualization and analysis, making it easy to extract meaningful insights from complex electrochemical datasets. Experiments of ASSLSB and QSSLSB were carried out at 30 ˚C and 60 ˚C with the help of incubating ovens in the potential range 1.0 – 2.8 V depending on the applied current for the required C rate.

CHAPTER 3

LOW SULFUR LOADING CARBON-SULFUR CATHODE

3.1 Scope

This chapter is focused on the cathode fabrication. Material preparation for the cathode formulation is initially discussed in connection with the slurry coating technique (doctor blading). Then the coin cell assembly will be discussed with the SSE pellet preparation. All-solid-state Li-S battery assembly and the use of ionic liquid to improve the performances of the QSSLSBs will also be discussed in this chapter. Later, cathode and electrochemical characterization results will be presented.

3.2 Introduction

Different cathode preparation methods have been discussed in literature. In this work, doctor blading technique was used to coat the Li-S battery cathode since it is known to produce uniform, porous and efficient cathodes. Scale up capability and modifications which can speed up the production using roll-to-roll techniques etc., gave additional motivation for the use of the doctor blading technique.

Cathode was prepared using a water based carboxymethyl cellulose (CMC) solution and Styrene butadiene rubber (SBR) as the binder while $Li_6PS_5F_{0.5}Cl_{0.5}$ SSE was synthesized using a solvent-based process, via the introduction of LiF into the argyrodite crystal

structure, which enhances both the ionic conductivity and interface-stabilizing properties of the SSE. The SSEs used in the ASSLSBs and QSSLSBs were provided throughout this work by William Arnold and Sharmin Akter in Prof. Hui Wang's group.

ASSLSBs assembled without any ionic liquids were not successful and small amounts of ionic liquids were needed to introduce at the interfaces to improve the electrode-SSE contacts. LiTFSI was used as the ionic salt and the solvents were varied for the ionic liquids.

3.3 Carbon Super P as conducting carbon material and cathode preparation

During the discharge process of the LE Li-S battery Li^+ ions produced at the anode, migrate through the electrolyte towards cathode and electrons move through the external circuit, producing polysulfides and Li_2S at cathode as the final discharge product[114,115]. Sulfur itself, Li_2S_2 and Li_2S are insulators which reduce the active material utilization and electronic conductivity of the cathode affecting the battery performance[116]. Combining different carbon materials such as graphene, mesoporous carbon, carbon nanotubes etc. with the sulfur in the cathode electrode is developed aiming to overcome the conductivity reduction due to insulating sulfur as well as to address the polysulfide volume compensation[117,118,119,120,121].

Super P conductive carbon black (SP) was used as the conductive carbon additive for sulfur cathode in this research work. As the initial step Super P powder (99% MTI) and sulfur powder (99% Thermo scientific) were weighed according to the mass ratios decided. For low sulfur loading batteries SP:S (3:2) was found to be the optimum mass ratio for cathode

coating. Then the powder mixture was ball-milled for 6 hours at 700 rpm at room temperature.

Figure 3.3.1: Ball milling setup used in the cathode coating process.

Then the mixture was transferred into a Pyrex tube and sealed tightly using an Al foil. Then the sample was transferred into a tube furnace and heated at 120 °C for 3 hours under vacuum. This step was necessary during the cathode preparation process to increase the uniformity of the mixture.
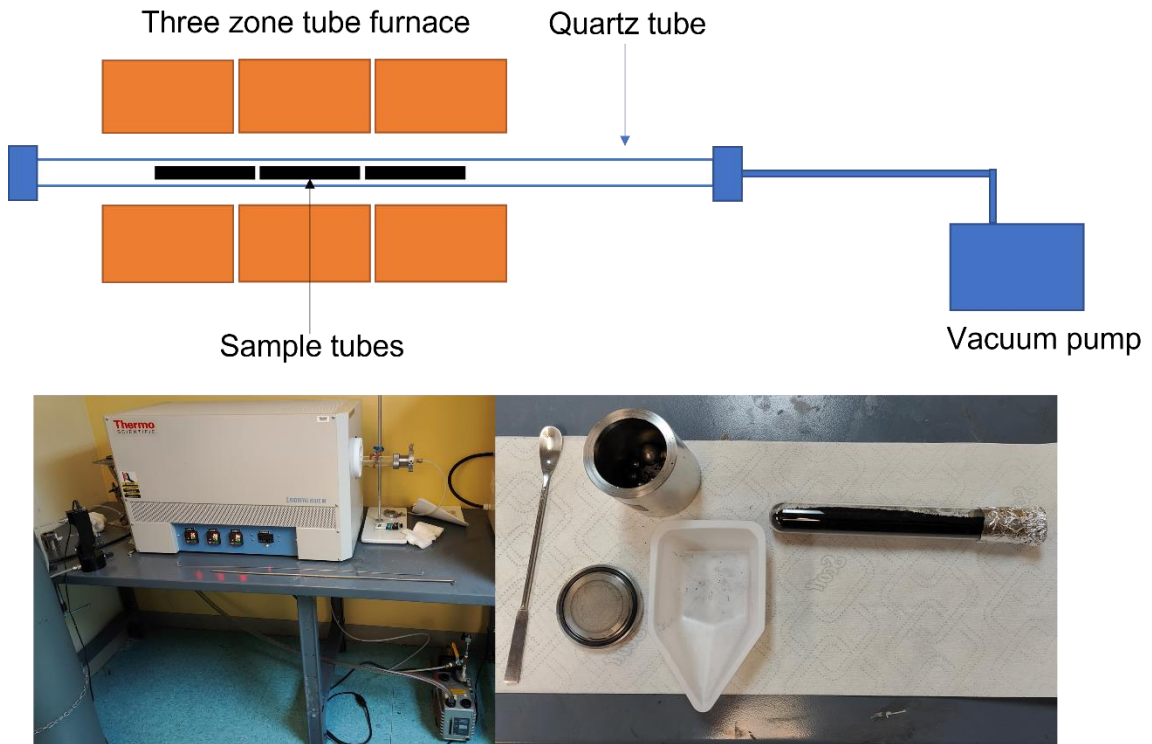
Figure 3.3.2: Experimental setup used to melt-diffusion of sulfur with carbon.

After mixture cooled down to the room temperature, Thermo gravimetric analysis (TGA) was carried out to estimate the carbon-sulfur ratio after heating the mixture.

At the same time , CMC powder was weighed and dissolved in Deionized (DI) water. For low sulfur loading batteries 2.5 w% CMC solution was found to be optimum and it was prepared by mixing 2.5 g of CMC in 97.5 g of DI water. Since CMC solution is more like

45

a gel, it had to be stirred at 550 rpm at 70 °C for 24 hours and the container has to be covered to avoid evaporation of water.
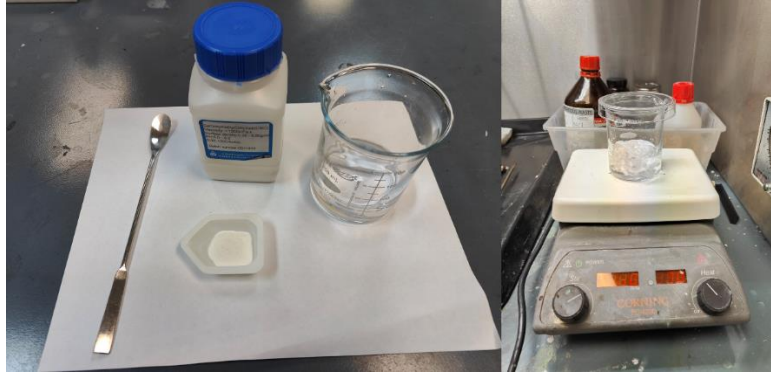
Figure 3.3.3: Preparation CMC solution

Once both the SP:S and CMC were ready, the slurry mixture was prepared by mixing of Super P-Sulfur, acetylene black (AB), 2.5 % CMC dissolved in DI water and premixed SBR (40% in DI water MTI-XTL) in the weight ratio of 90:2:4:4 to formulate the slurry. Slurry mixture was also mixed using the ball-milling machine at the speed of 600 rpm for 3 hours.

Figure 3.3.4: Slurry mixture and its texture before coating

After the mixing was complete, the slurry was doctor bladed at desired wet thickness (90 μm) onto the Aluminum foil of thickness 15 μm. Then the coating was dried inside an oven at 60 °C for 1 hour. To evaporate water, temperature was set at 60 °C due to the low melting point of sulfur (115 °C).

Figure 3.3.5: Doctor blading the coating and drying

After drying, the coating was passed through a rolling system to calendar it into a uniform thickness.

Figure 3.3.6: Calendaring and electrode punching

Then the coating was punched into 2.0 cm² disks and mass was measured to calculate the Sulfur loading using following equation.

$$S_{mass} = (M_e - M_{Al}) \times W\%_{C\text{-}S \text{ Slurry}} \times W\%_{S \text{ SP:S}} \tag{3.1}$$

Here, S_{mass} is the total sulfur mass in the 2.0 cm² disk, M_e is the mass of the electrode, M_{Al} is the mass of the Al foil, $W\%_{C\text{-}S \text{ Slurry}}$ is the weight percentage of SP:S mixture in slurry and $W\%_{S \text{ SP:S}}$ is the Sulfur percentage in SP:S mixture. Final mass loading is defined as Sulfur mass per unit area.

$$\text{Sulfur loading} = \frac{S_{mass}}{Area} \tag{3.2}$$

For low loading cathodes, sulfur loading was calculated to be 0.7 mgcm⁻².

Mixing Super P Sulfur SP:S (3:2) → Ball milling 700 RPM 6 hours → Melt Diffusion 120 °C 3 hours → Cool Down →

Mixing 2.5 w% CMC In DI water → Stir at 70 °C 550 RPM 24 hours →

Add AB 2 W%

SP:S 90 w% AB 2 w% SBR 4 w% CMC 4w% Slurry mixture ← Add Pre-mixed SBR 4 W%

Ball Milling 600 RPM 3 hours →

Doctor Blading on Al Foil ← Wet coating (90 µm) ← Oven drying at 60 °C 1 hour ← Calendaring ← **Cathode Coating**
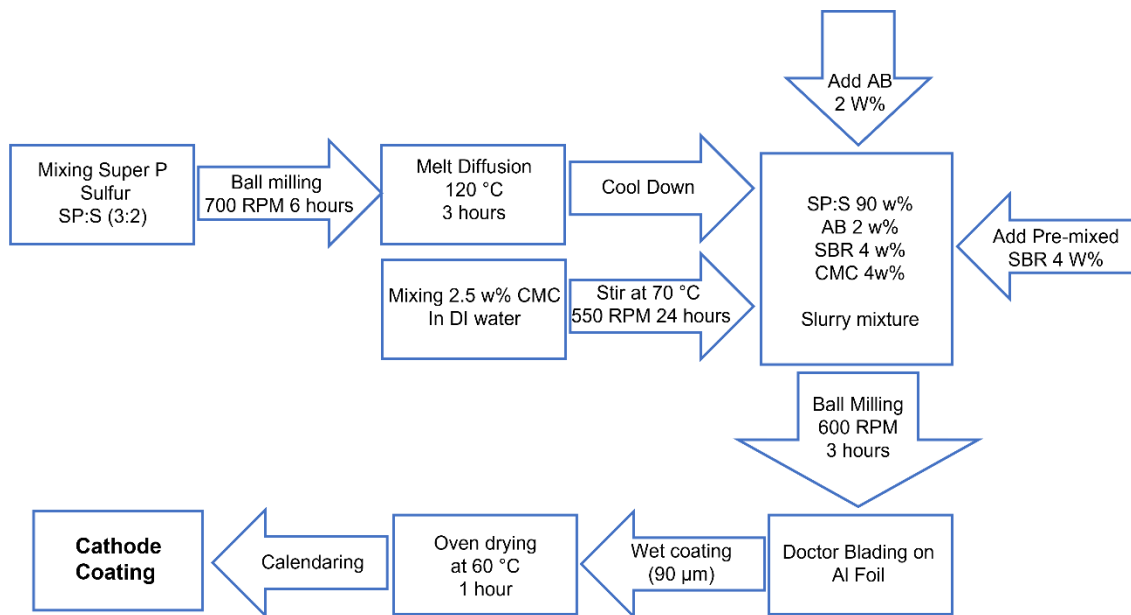
Figure 3.3.7: Schematic of cathode fabrication process

3.4 All solid-state Li-S coin cell assembly

$Li_6PS_5F_{0.5}Cl_{0.5}$ solid electrolyte was synthesized via the stoichiometric mixing of lithium sulfide (Li_2S, Alfa Aesar), lithium chloride (LiCl, Alfa Aesar), lithium fluoride (LiF, Alfa Aesar), and β-Li_3PS_4 precursor in ethanol solvent and stirred for 1 h at room temperature inside a glovebox under argon atmosphere. The solution was heated to evaporate the solvent before a subsequent heat treatment for 1 h at 200℃. The resultant powder was collected and ground using mortar and pestle.

For all of the SSE batteries, electrolyte powder was pressed into 150 mg pellets using stainless-steel pallet die system, inside the glove box. All other components of the battery have to be dried under vacuum before transferring into the glove box.

Coin cell cases, punched cathodes, wave springs and current collectors which were prepared prior to the assembly were dried at 60 °C under vacuum inside a tube furnace for 6 hours to remove the moisture and oxygen.

Figure 3.4.1: Drying cathodes, coin cell cases and current collectors.

Finally, everything was transferred inside the glove box. All solid-state Li-S coin cells were assembled as shown in Fig. 3.4.2.
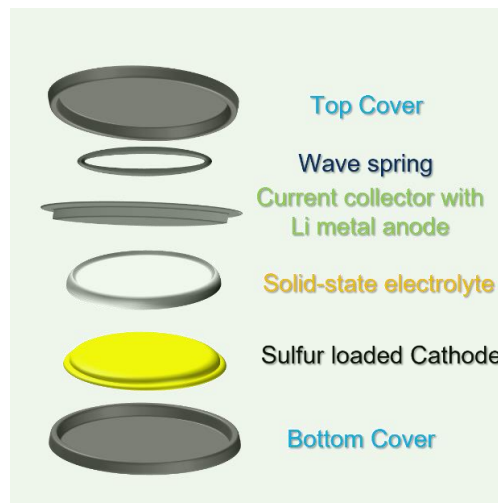
Figure 3.4.2: ASSLSB coin cell parts and assembly

Since initial cells failed, new strategies were attempted to improve the electrode-SSE interfaces. One approach was to press the cathode along with the SSE inside the glove box using stainless steel tank as shown in Fig. 3.4.4. This technique was successful, but the capacity obtained was found to be too low.
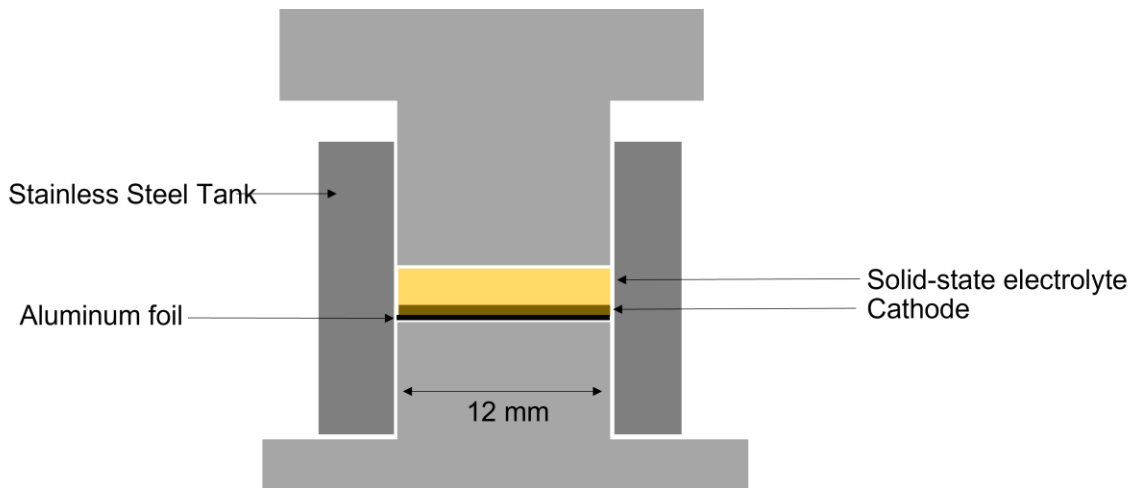
Figure 3.4.4: Cross section of 12 mm Stainless steel tank used to press cathode onto SSE.

Another approach used to enhance the interfacial contact was by heating the interface using intense pulsed light (IPL) after pressing the cathode onto the SSE. Since the SSE is moisture sensitive, the pellet was placed inside a vacuum sealed container (assembled inside the glove box) and then the sample was exposed to the IPL through a transparent window. The IPL constituted of 2100 J energy for 2 ms durations with 1 s delay time. This experiment showed little improvement but did not result in, a significant improvement of the capacity.
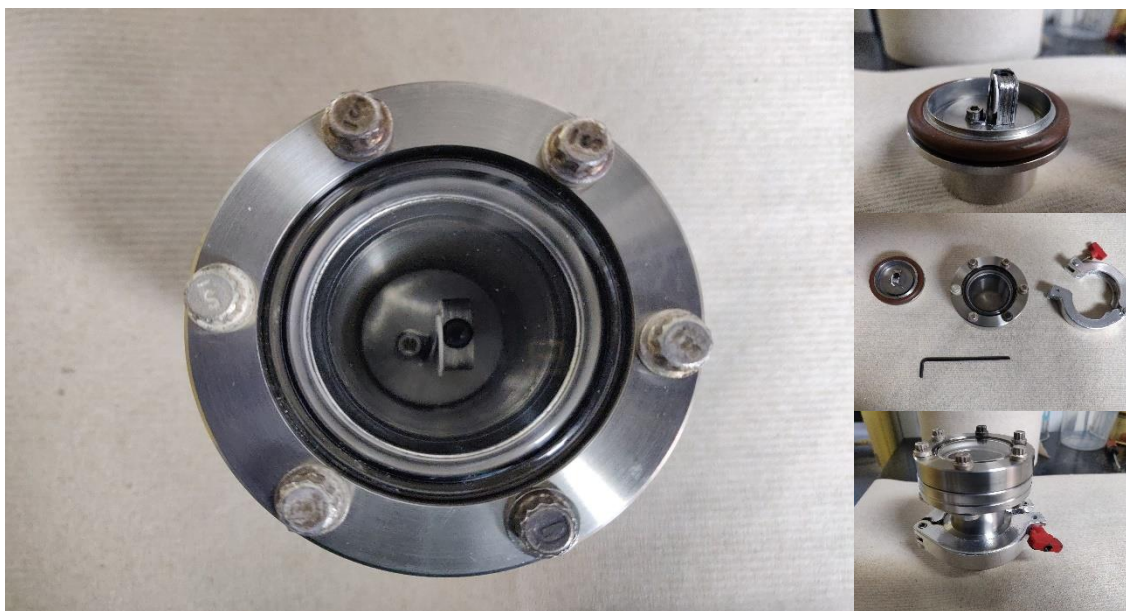
Figure 3.4.5: Experimental setup used for IPL treatment

3.5 Introduction of ionic liquids into the battery (Making QSSLSBs)

Due to the failures of the all-solid-state Li-S batteries tested, next approach to improve the SSE-electrode interface was to introduce some liquid electrolyte at the interfaces to improve the contact. LiTFSI dissolved in 1,3 Dioxolane and 1,2 Dimethoxymethane (DOL:DME) was known as the optimized liquid electrolyte for the liquid electrolyte (LE) Li-S batteries. This liquid electrolyte was tested with the SSE in a coin cell with Li anode and SP:S cathode. Liquid electrolyte composition was 1M LiTFSI in DOL:DME (1:1) and 40 μL of it was added in between each SSE-electrode interface. As expected, the battery showed an improved discharge capacity of 1340 mAh/g but failed to charge. More experiments were also conducted to confirm the results and the final outcome was the same.

Ionic liquid (IL) based electrolytes were taken into consideration due to their high viscosity decreasing the solubility of sulfur and lithium polysulfides, thus reduce the polysulfide

shuttling effect. In the literature there are number of reports on ILs containing pyrrolidinium (PYR) as the cation and bis(trifluoromethyl sulfonyl)imide (TFSI) as the anion[122]. Major drawback of this IL is low ionic conductivity and high viscosity with the higher TFSI concentration. To improve the conductivity and lower the viscosity, co-solvents like DOL were introduced. Effect of co-solvent has been studied and explained in the Chapter 4.

3.6 Material and electrochemical analysis

Thermo gravimetric analysis (TGA) studies of the cathode were done by the thermo gravimetric analyzer SDT Q600 under N_2 gas flow of 100 ml/min. Cathode electrode surface morphology was characterized using the Field emission gun scanning electron microscope (FESEM), TESCAN scanning electron microscope with energy dispersive X-ray spectroscopy (EDAX).

Electrochemical impedance spectroscopy (EIS) measurements of coin cells were carried out using a SP-200 electrochemical system, (BioLogic Science Instruments). Each spectrum was collected in the frequency range of 1 MHz to 50 mHz with an excitation voltage of 5 mV. All the batteries were cycled at 30 °C between 1.0 V and 2.8 V using a 16 channel Arbin battery testing system.

3.7 Results and discussion

After completely drying the cathode coating was scratched and TGA study of the cathode material powder was done by the thermo gravimetric analyzer SDT Q600. Temperature was ramped at 10 °C/min from room temperature to 800 °C under Nitrogen flow of 100 ml/min.
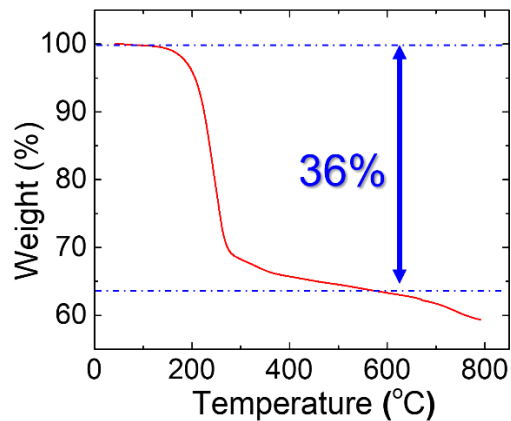
Figure 3.7.1: TGA analysis of cathode coating powder.

Cathode consisting of SP-S(3:2) 90 w% should have approximately 36% sulfur as confirmed from mass loss of 36% of the TGA analysis shown in Fig. 3.7.1, that loading calculation based on the weight ratio was precise.
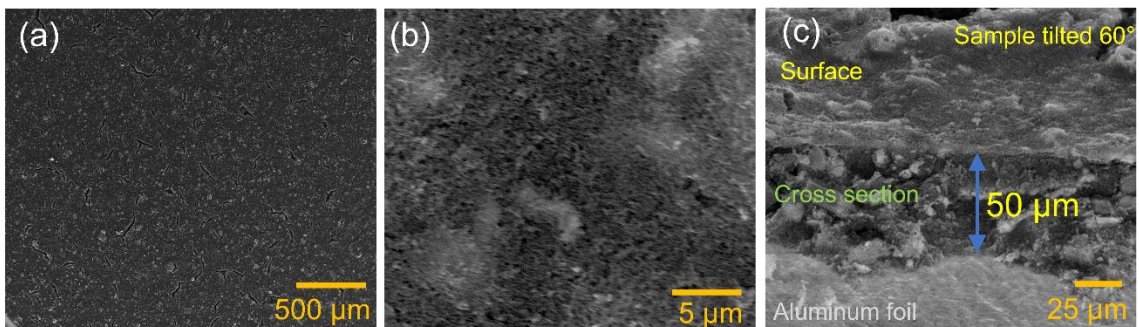
Figure 3.7.2: SEM images obtained from the FESEM

Fig.3.7.2 (a) and (b) show the FESEM images obtained from the surface with magnifications 100 and 10000 respectively. Surface porosity which led to high capacity and cyclability was clearly observable at higher magnification SEM images (Fig. 3.7.2 (b)). Fig. 3.7.2(c) shows the cross-sectional SEM image obtained with 60° tilt angle with 2000 magnification in which the SP:S cathode coating has a thickness of ~50 μm.
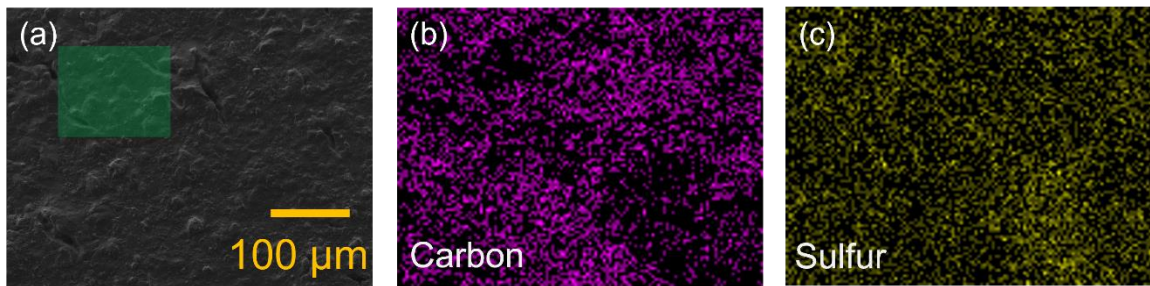
Figure 3.7.3: EDS analysis of cathode powder obtained from the TESCAN SEM

Fig. 3.7.3 shows the EDAX mapping obtained using TESCAN SEM on the cathode surface before cell assembly. Uniform spread of carbon and sulfur in Fig. 3.7.3 (b) & (c) confirmed the homogeneous distribution of sulfur in carbon via melt diffusion method used in this cathode fabrication process. This homogeneous distribution of sulfur in the cathode should have led to the higher active material utilization.
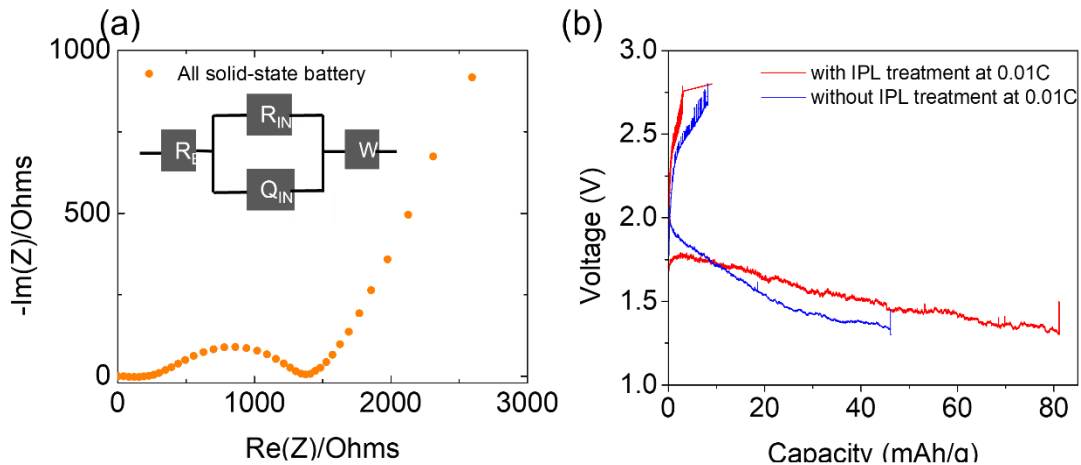
Figure 3.7.4: Electrochemical testing of ASSLSBs ;(a) Electrochemical impedance spectra and (b) charge-discharge curves of ASSLSBs treated with and without IPL treatment.

Fig. 3.7.4 (a) show the electrochemical impedance spectra of a ASSLSB before introducing ionic liquid. Compared to the reported conventional liquid electrolyte Li-S battery,

electrolyte resistance and interfacial resistance were found to be significantly higher verifying the poor interfacial contact. Fig. 3.7.4 (b) shows the charge discharge curve of ASSLSBs for initial cycle, treated with and without IPL treatment tested with 0.01 C rate at room temperature. In comparison with conventional LE Li-S battery as shown in Fig.3.7.5, ASSLSBs had shown really poor performance due to poor interfacial contact even though IPL treatment has improved the initial discharge capacity.
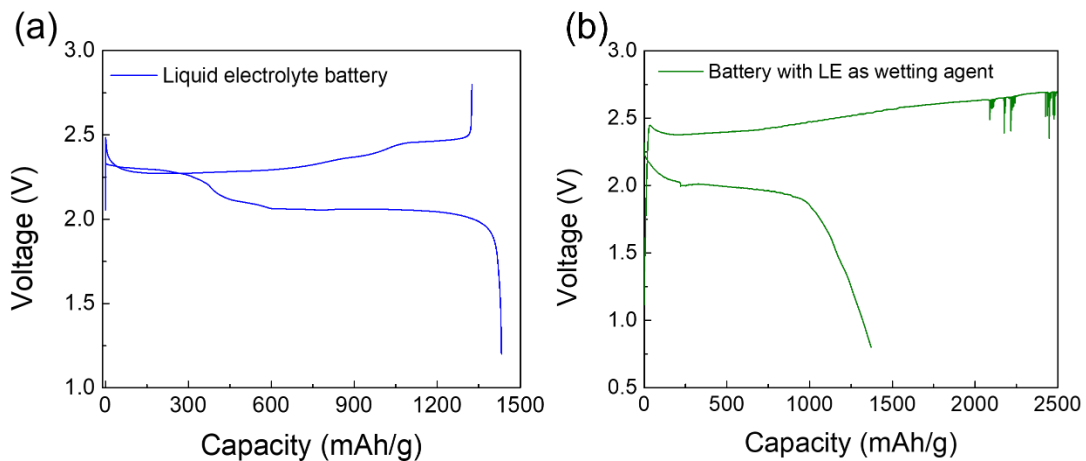
Figure 3.7.5: Charge-discharge curve of (a) conventional liquid electrolyte battery and (b) quasi-solid-state battery with LE as wetting agent at the interfaces .

Figure 3.7.5 (a) shows the charge-discharge curve of conventional liquid electrolyte battery consist of SP-S (3:2) cathode and LiTFSI (0.6M) LiNO$_3$ (0.4M) dissolved in DOL:DME(1:1). Discharge curve clearly demonstrated the dual phase plateau corresponds to the different polysulfide reactions. From this result it was confirmed that the poor performance of ASSLSBs was not limited by the cathode.

Based on the results of ASSLSBs, experiments were designed to introduce ionic liquid at the interface. Initially, liquid electrolyte used in the conventional Li-S battery was used as

the wetting agent during the coin cell assembly. 40 µl of LiTFSI (0.6M) with $LiNO_3$ (0.4M)

dissolved in DOL:DME was added to the cathode-SSE and SSE-anode interfaces. Couple

of these batteries were tested and all of them have shown promising initial capacities but

failing to charge back at the first cycle as shown in Fig 3.7.5 (b). The reason for the inability

to cycle the battery was found to be the dissolution of SSE in DME thereby non stabilizing

the interface as revealed by the AIMD simulation studies carried out by Varun Shreyas in

Prof Narayanan's group.
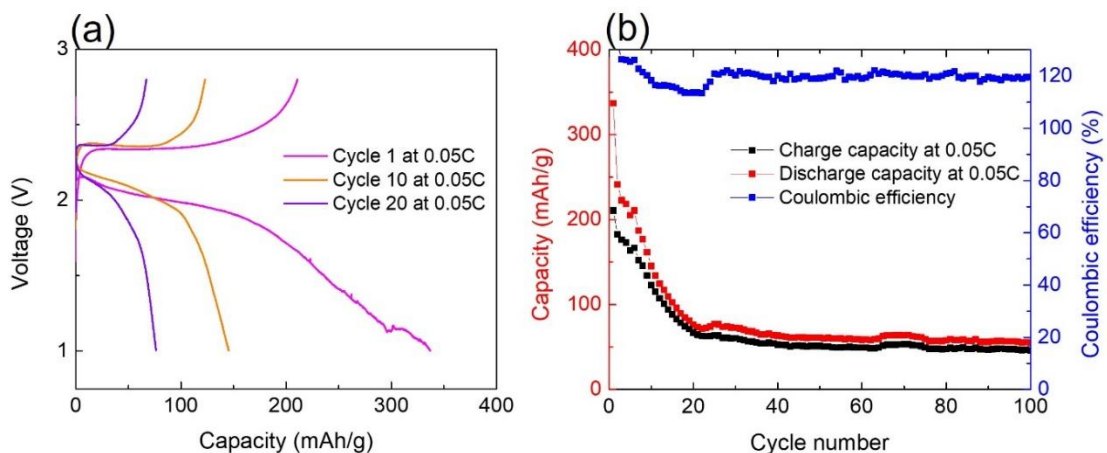
Figure 3.7.6: Performance of QSSLSB with ionic liquid LiTFSI(1M) in PYR

Next, 40 µL of IL consisting of LiTFSI(1M) dissolved in PYR was introduced at both solid-

solid interfaces to assemble the QSSLSB. Assembled QSSLSB was cycled at room

temperature at C/20 (80 mA/g) current rate between 1.0V and 2.8 V. Fig. 3.7.6 (a) shows

the charge-discharge curves of QSSLSB with LiTFSI(1M) dissolved in PYR for cycle

number 1,10 and 20. Fig. 3.7.6 (b) left axis (Red) show the capacity as a function of the

number of cycles while right axis (Blue) represents the coulombic efficiency with the

number of cycles. QSSLSB with LiTFSI(1M) dissolved in PYR IL showed an initial

discharge capacity of 337 mAh/g while capacity decreased and stabilized around 50 mAh/g after 100 cycles as shown in Fig. 3.7.6 (b). A discharge voltage plateau has been observed around 2.1 V corresponds to the conversion of polysulfides (Li_2S_n, $2 < n < 8$) into solid lithium sulfides (Li_2S_2 and Li_2S).

This was the first successful battery which could be cycled for 100 cycles with significant initial capacity and tested at significant C rate. Reason for poor coulombic efficiency and cycle stability was due to the higher viscosity of solvent PYR and the decomposition of SSE and IL as revealed by the AIMD simulation studies. In order to enhance the performance of QSSLSBs, the viscosity of the ionic liquid has to be reduced and a diluent was required to obtain a lower viscosity. Effect of diluent and how it enhanced the performance is discussed in chapter 4.

3.8 Conclusion

Super P-Sulfur based cathode was successfully developed to be used in SSLSBs with a binder based on CMC and SBR. ASSLSBs were successfully assembled without any wetting agent at the interface, but the capacities and performance were poor. After introducing a minute amount of ionic liquids, initial capacity and performance of QSSLSBs were significantly improved and poor contact issue of ASSLSB was diminished with the initiation ionic liquids.

CHAPTER 4

OPTIMIZATION OF IONIC LIQUIDS

4.1 Scope

After identifying LiTFSI dissolved in PYR as the ionic liquid to be used in the QSSLSBs, battery performance optimization experiments were carried out. First part of this chapter covers such optimization experiments. Then the cathode was further optimized by drop casting the SSE on to the surface of the cathode. Middle part of this chapter covers the effect of SSE in the cathode. Latter part of this chapter covers the post cycling analysis which were carried out to understand the interfacial reactions taking place during cycling.

4.2 Introduction

Ionic liquid (IL) based electrolytes were taken into consideration due to their high viscosity limiting the solubility of sulfur and lithium polysulfides, thereby reducing the polysulfide shuttling effect. In the literature, there are number of reports on ILs containing pyrrolidinium (PYR) as the cation and bis(trifluoromethyl sulfonyl)imide (TFSI) as the anion[123]. Major drawback of this IL is its low ionic conductivity and high viscosity with the higher TFSI concentration. To improve the conductivity and lower the viscosity, co-solvents are introduced. Effect of co-solvent has been studied and optimized in previous reports. In this work 1,3-dioxolane (DOL) was used as the co-solvent to prepare the IL[124].

4.3 Effect of Diluent, Concertation and Volume of ionic liquids

All the ionic liquids were prepared inside the Argon filled glove box and stored at room temperature. Relevant masses to prepare LiTFSI solutions (2M and 4M) were weighed and mixed with premixed PYR-TFSI and DOL (1:1 and 3:1) solvent for 48h.

For the assembly of QSSLSB, SP-S cathode with 0.70 mgcm^{-2} sulfur loading was punched into disks of 2.0 cm^2.SSE was pressed into 150 mg pellets using a stainless-steel tank. During the assembly, SSE was wetted with the relevant amounts of IL from both ends using a micropipette. Cathode, SSE and Li metal anode were then assembled into 2032 type coin cell (Fig. 4.3.1).
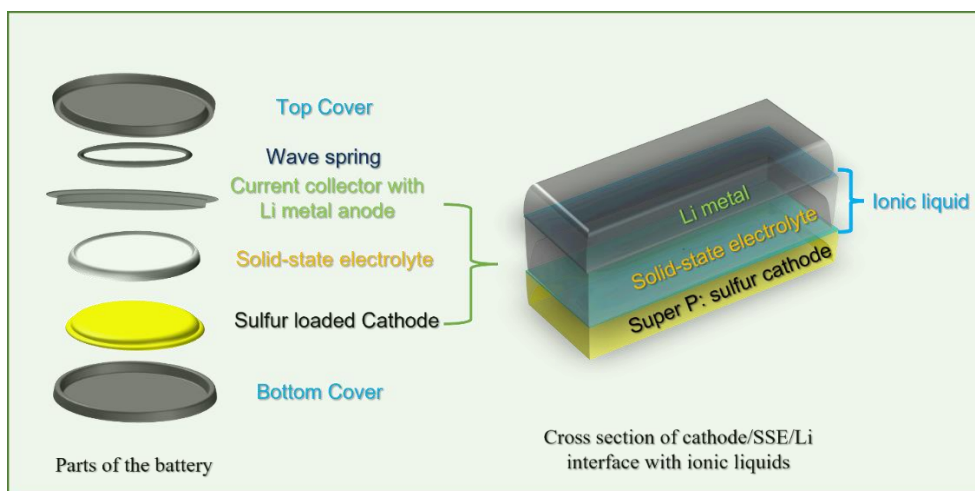
Figure 4.3.1: QSSLSB assembly with ionic liquids.

4.4 Effect of SSE in the cathode

In order to optimize the capacity retention, a pre-determined amount of SSE was incorporated during the SP-S cathode formulation, to enhance the ionic conductivity of the cathode. Specifically, $Li_6PS_5F_{0.5}Cl_{0.5}$ was dissolved in anhydrous ethanol (1 w%) and

drop casted onto the C-S cathode. Then the QSSLSB coin cell were assembled using the SSE and Li as anode with optimized ionic liquid.

4.5 Electrochemical characterizations and Post-cycling characterizations of QSSLSBs

Electrochemical impedance spectroscopy (EIS) measurements of coin cells were carried out using the SP-200 electrochemical system, (BioLogic Science Instruments). Each spectrum was collected in the frequency range of 1 MHz to 50 mHz with an excitation voltage of 5 mV. Cyclic voltammetry measurements were also carried out using same instrument at scan rate of 3 mV/min. All the batteries were cycled at 30 °C between 1.0 V and 2.8 V using a 16 channel Arbin battery testing system.

After cycling, all the cells were reopened inside the glove box. Cathode was separated carefully from the solid electrolyte surface of the SSE was sealed on to a glass slide to transfer into XPS chamber using captain tape. X-ray photoelectron spectroscopy (XPS) (VG scientific-MultiLab 3000) was employed to detect the chemical composition at the cathode-SSE interface after cycling. Prior to careful analysis, all the spectra were calibrated with respect to the C-C (sp^2) binding energy (284.8 eV) of the C1s peak.

4.6 Results and Discussion

Before discharging the cells, electrochemical impedance spectroscopy study of a Li-S battery with and without IL functionalization were carried out. Fig. 4.6.1 (a) shows the Nyquist plots of the electrochemical impedance spectra of batteries consisting of SP-S cathode, $Li_6PS_5F_{0.5}Cl_{0.5}$ SSE and Li anode (i) without any ionic liquid (orange filled circles) (ii) with 40 µL of LiTFSI (1M) dissolved in PYR (Dark blue filled triangles) and (iii) with

40 μL of LiTFSI (2M) dissolved in PYR:DOL (1:1) (Green filled squares). As expected, the electrode-electrolyte interfacial resistance was seen to decrease significantly due to the introduction of the ionic liquid as evidenced by the decrease of the charge transfer resistance and the electrolyte resistance. The first cycle discharge curves of all three cells presented in Fig. 4.6.1 (b) showed a dramatic improvement of the discharge capacities with the addition of ionic liquid diluted with DOL.
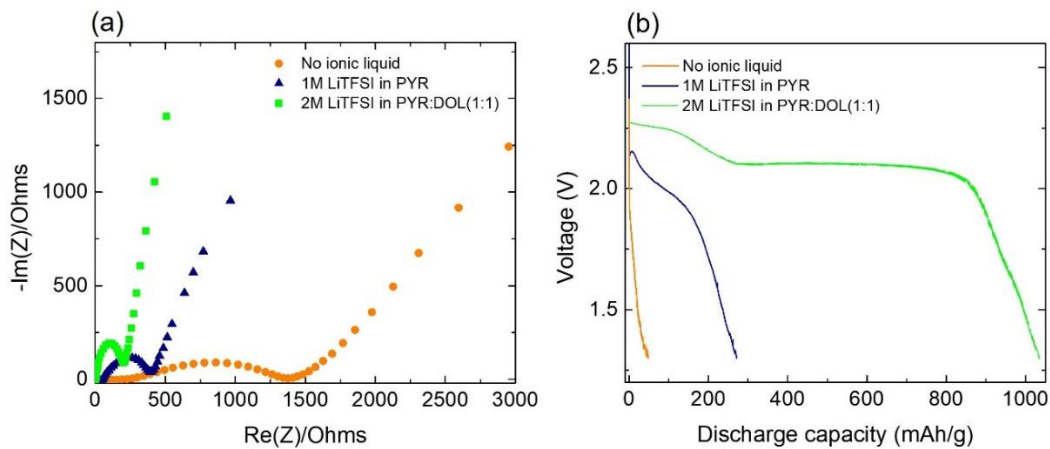
Figure 4.6.1: Electrochemical testing ;(a) electrochemical impedance spectra and (b) Discharge curves at 0.05C rate for batteries with and without ionic liquids

Due to the low initial discharge capacity of the Li-S batteries consisting of SP-S/ SSE/Li, the highly viscous IL (LiTFSI in PYR) was diluted with 1,3-dioxolane (DOL) and LiTFSI content was increased up to 2M (from 1M). Fig. 4.6.2 (a) and (b) panels compare the battery performances with and without DOL in IL. Both batteries were tested at C/20 rate with IL volume of 40 μl at room temperature. The battery without the diluent and LiTFSI concentration of 0.6 M in PYR (best performance battery without diluent) showed initial discharge capacity of ~ 600 mAh/g and fades to a value below 200 mAh/g after 100 cycles

(Fig. 4.6.2 (a)). The battery with PYR:DOL (1:1) with 2M concentration of LiTFSI showed vastly improved initial discharge capacity of ~ 1100 mAh/g, fading below 400 mAh/g after 100 cycles (Fig. 4.6.2(b)).
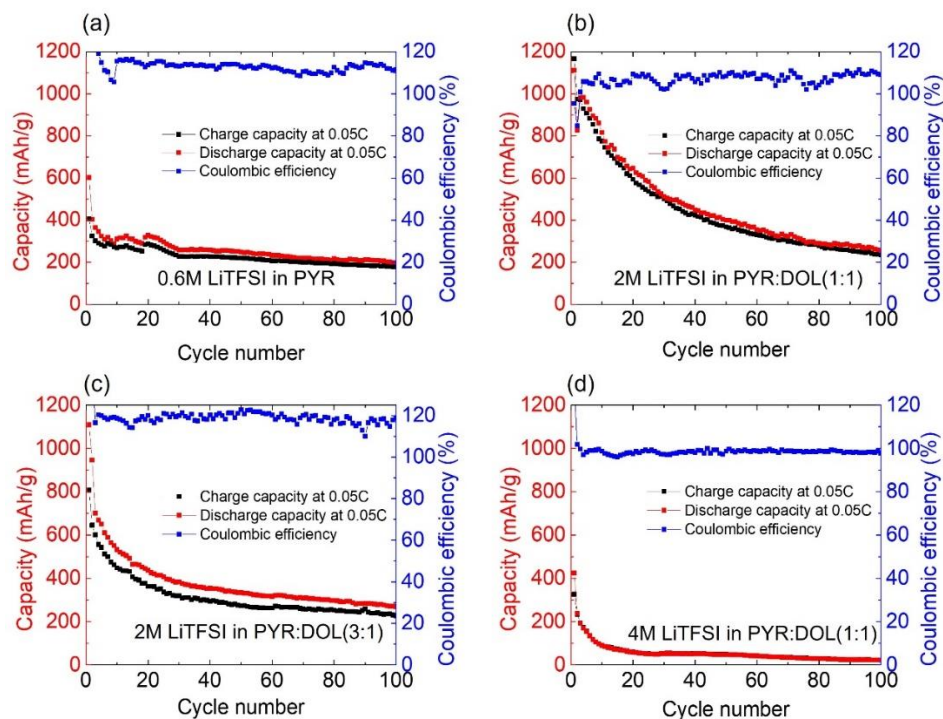
Figure 4.6.2: Performance of batteries consist of SP-S/SSE/Li with ILs (a) 0.6M LiTFSI dissolved in PYR, (b) 2M LiTFSI dissolved in PYR:DOL(1:1), (c) 2M LiTFSI dissolved in PYR:DOL(3:1) and (d) 4M LiTFSI dissolved in PYR:DOL(1:1)

Next, the battery performances at C/20 rate for varying diluent (PYR:DOL) ratios were tested as shown in Fig. 4.6.2 (b) and (c). Cyclability performance of the battery with 40 mL IL of 2M LiTFSI in PYR:DOL ratio 1:1 is shown in Fig. 4.6.2 (b). Fig. 4.6.2 (c) shows the results for PYR:DOL ratio of 3:1. They both showed initial discharge capacity ~ 1100 mAh/g, still faded below 400 mAh/g after 100 cycles. However, the battery with 1:1 ratio

of PYR:DOL showed better coulombic efficiency at the tested C rate. As a result of that, in the rest of the lower loading work, PYR:DOL ratio 1:1 was maintained.

When considering the LiTFSI concentration dependance of batteries at C/20 rate with PYR:DOL ratio of 1:1 and IL volume of 40 mL, for the battery with 2M LiTFSI outperformed (Fig. 4.6.2 (b)) the battery with 4M LiTFSI (Fig. 4.6.2 (d)) concentration which had the initial discharge capacity of ~ 400 mAh/g and degraded very rapidly. This result confirmed again that the high viscosity of IL reduces the battery performance since 4M LiTFSI IL was found to be highly viscous (130 mPa s^{-1}) similar to IL without diluent (140 mPa s^{-1}) compared to the 2M LiTFSI IL (24 mPa s^{-1}).

It was found that 2M LiTFSI concentration in a dilution of PYR with DOL at 1:1 ratio gave the optimum performance. In order to find the optimum volume of the IL required, a volume dependent battery performance study was conducted at C/20 rate as shown in Fig. 4.6.3 for the volumes of (a) 10 ml (b) 20 ml and (c) 40 ml. Both batteries with 40 ml and 20 ml (Fig. 4.6.3(b) and 4.6.3(c)) ionic liquid volumes showed initial discharge capacities ~ 1100 mAh/g with retaining capacity ~300 mAh/g after 100 cycles. The battery with 40 ml IL volume however showed better coulombic efficiency. In contrast, the battery with 10 ml IL volume (Fig. 4.6.3(a)) showed low initial discharge capacity of ~ 800 mAh/g with a rapid degradation over the cycling.
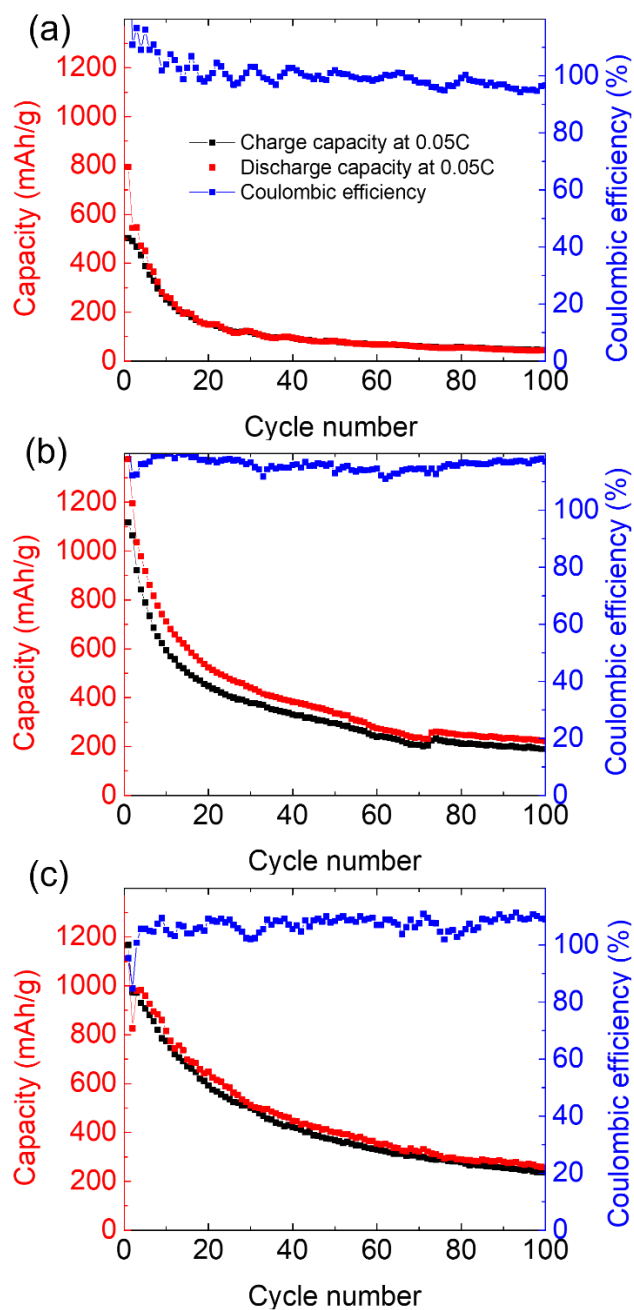
Figure 4.6.3: Performance of batteries consist of SP-S/SSE/Li with 2M LiTFSI PYR:DOL(1:1) with different volumes (a) 10 µL, (b) 20 µL and (c) 40 µL

From all these studies, it was found that the functionalization of the SSE/cathode interface with an IL of 2M LiTFSI in a diluted solution of PYR with DOL at 1:1 ratio and the optimized volume of 40 μL gave the optimum performance.

Thereafter, the C-rate dependance of the battery under optimized conditions were tested for C/20, C/10 and C/5 rates. All three batteries consist of SP-S/$Li_6PS_5F_{0.5}Cl_{0.5}$ SSE/Li with added ionic liquid of 2M LiTFSI in 1:1 ratio of PYR:DOL with total volume of 40 μL. Fig. 4.6.4 shows the C rate performance results. Among all the QSSLSBs tested at optimum conditions, battery tested at C/5 stands out with its significant performance at higher current rate. This result confirmed that the improved cathode, IL and SSE together was capable of handling higher currents with stable coulombic efficiency and capacity.
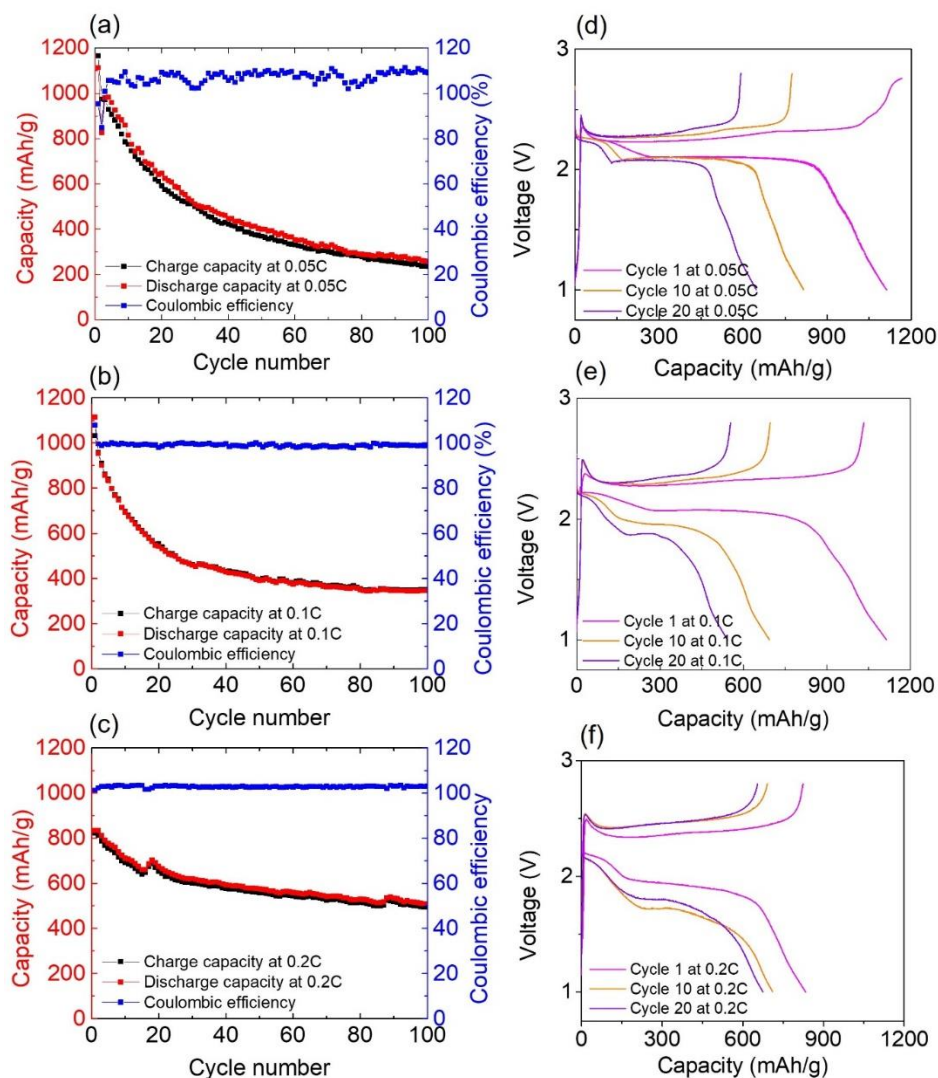
Figure 4.6.4: C rate dependent cyclic performance at (a) C/20, (b) C/10, (c) C/5 rates and charge discharge curves at (d) C/20, (e) C/10, (f) C/5 for batteries consist of SP-S/SSE/Li with 40 μL of IL LiTFSI(2M) PYR:DOL(1:1)

Next, in order to optimize the capacity retention, during the SP-S cathode formulation, a pre-determined amount of SSE was incorporated to enhance the ionic conductivity of the cathode. Specifically, $Li_6PS_5F_{0.5}Cl_{0.5}$ was dissolved in anhydrous ethanol (1 wt%) and drop

casted onto the C-S cathode. Then IL volume dependent study was carried out with 10, 20 and 40 µL volumes of IL and C/10 current rate.
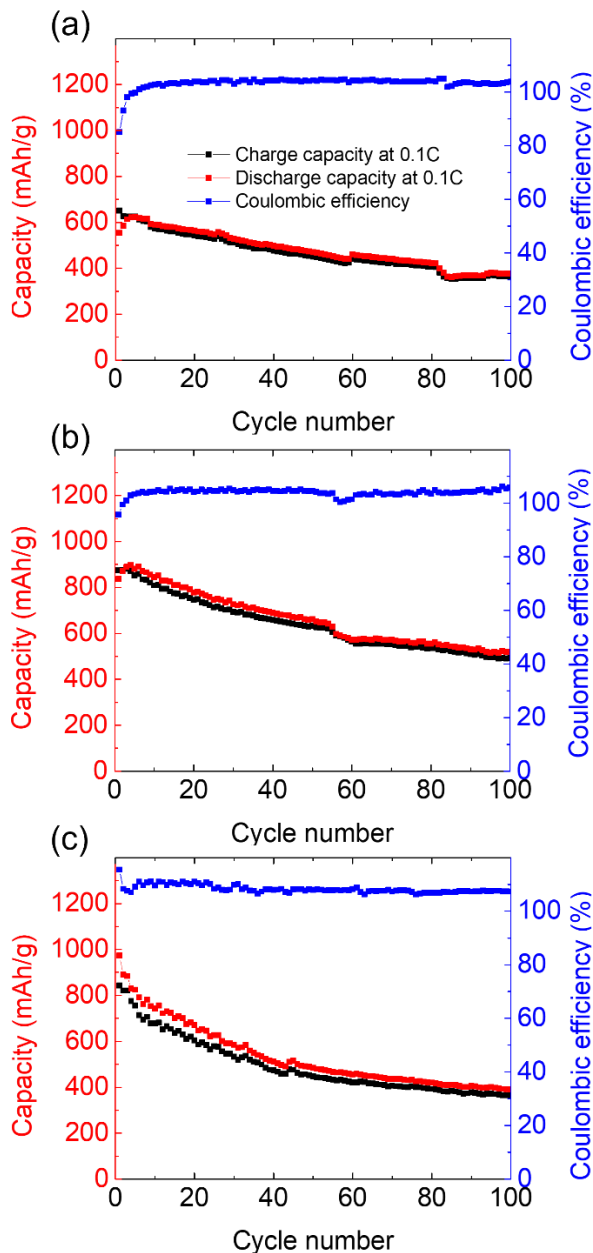
Fig. 4.6.5 (a),(b) and (c) shows the battery performances with SSE in the SP-S cathode at C/10 rate. As shown in Fig. 4.6.3 (a),(b) and (c), the batteries without the SSE in the SP-S cathode showed the higher initial discharge capacity of with lower retention after 100 cycles

However, after the incorporation of $Li_6PS_5F_{0.5}Cl_{0.5}$ in the C-S cathode, the initial capacities were slightly lower but showed an improved capacity retentions of (a) 65%, (b) 58% and (c) 45% after 100 cycles with stabilized coulombic efficiency even at C/10 current rate.
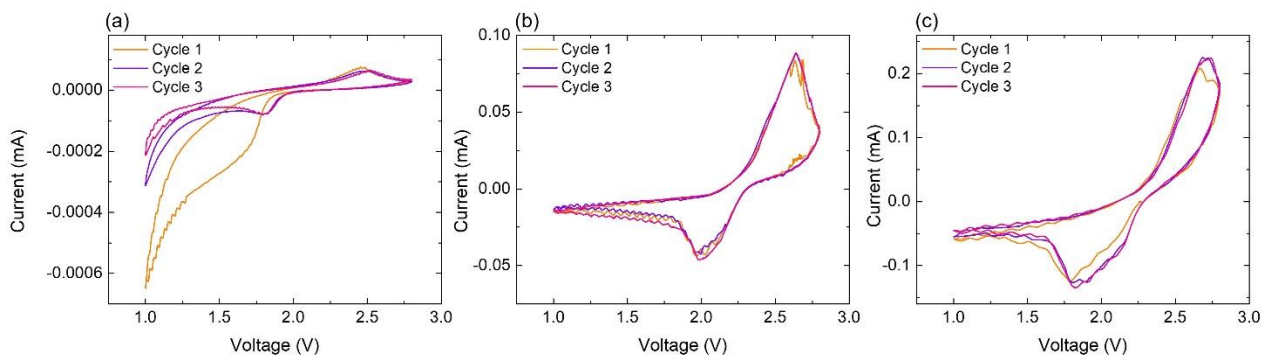
Figure 4.6.6: Cyclic voltammogram of the batteries consist of SP-S cathode, Li anode and SSE (a) with no ionic liquid (b) with IL LiTFSI (1M) dissolved in PYR and (c)with IL LiTFSI (2M) dissolved in PYR:DOL(1:1)

Next, cyclic voltammograms were recorded for batteries consisting of SP-S cathode, Li anode and SSE (a) with no ionic liquid (b) with IL LiTFSI (1M) dissolved in PYR and (c) with IL LiTFSI (2M) dissolved in PYR:DOL(1:1)at scan rates of 3.0 mV/min as shown in Fig. 4.6.6. Generally, in the cathodic scan, the reduction of sulfur in liquid electrolyte Li-S batteries happens in two steps based on the type of electrolyte utilized, The first phase is the reduction of elemental sulfur to lithium polysulfides (Li_2S_n, $2 < n < 8$) in the range of 2.4–2.1 V vs Li/Li+ and the second represents further reduction of polysulfides to solid lithium sulfides (Li_2S_2 and Li_2S) at around 2.1–1.8 V [125,126]. In ASSLSB it is supposed to have a direct conversion of elemental sulfur into solid lithium sulfides (Li_2S_2 and Li_2S). In

69

the battery tested without any ionic liquid has proved that by displaying only single peak implying to direct conversion in the cathodic scan around 1.8V as expected (Fig. 4.6.6 (a)). In comparison, QSSLSBs have also shown combined peak in the range of 2.3-1.8 V verifying the fact that QSSLSB follow more of a direct conversion route while discharging as in ASSLSB, even with the presence of ionic liquid (Fig. 4.6.6 (b) & (c)). Supti Das et.al. has previously reported similar cyclic voltammogram where dual cathodic peaks were seen to combine to a single reduction peak in all-solid-state Li-S battery [127]. According to their work, the difference in the areas under curve in cathodic and anodic scans in ASSLSB was believed to be due to the higher scan rates employed. In contrast they have used much lower currents to test the battery while using higher sweeping rate for the CV measurements compared to this work. During the anodic scan oxidation peak which attributed to conversion of lithium sulfides to elemental sulfur and lithium was observed at 2.5 V and 2.7 V respectively which show a shift from 2.4 V in liquid electrolyte Li-S battery [128]. The reduction and oxidation peaks did not vary significantly during cycling, confirming that a stable cathode-electrolyte interface (CEI) is formed.

Fig. 4.6.7 shows the XPS S2p low binding energy (BE) peak of the cathode-SSE interface of 3 batteries: (a) without any ionic liquid, (b) with the ionic liquid LiTFSI(1M) dissolved in PYR, and (c) & (d) with the ionic liquid LiTFSI(2M) dissolved in PYR:DOL(1:1). All batteries were characterized after complete discharge to 1.0 V. Battery in Fig. 7 (a) lasted only for single cycle (see Fig. 2 (b)) due to its poor interfacial contact and displayed only the characteristic peaks corresponding to PS_4^{3-} and P_2S_5 species of the SSE. Battery in Fig. 7 (b) which consisted of highly viscous IL LiTFSI(1M) dissolved in PYR, charged/discharged for 100 cycles with incredibly low capacity showed an additional

doublet corresponding to terminal/bridging sulfur from long chain Li-polysulfides. However, due to the low material utilization along with poor discharge capacity, peaks correspond to final discharge product of Li_2S were not detected in both these batteries.
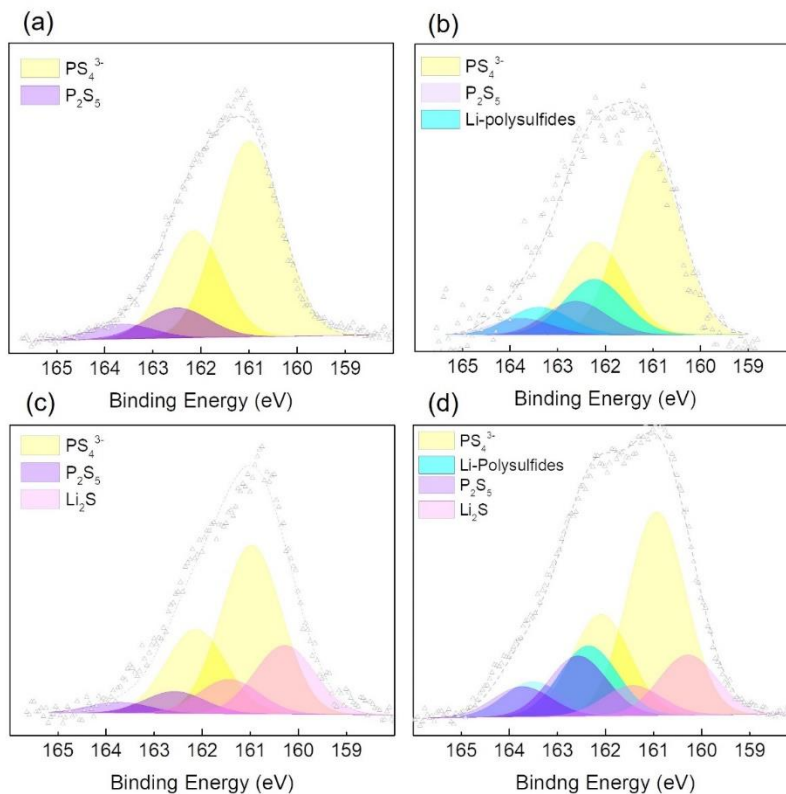
Figure 4.6.7: XPS S2p low binding energy peak of the cathode-SSE interface of (a) no ionic liquid, (b) with LiTFSI (1M) dissolved in PYR and (c)&(d) with LiTFSI (2M) dissolved in PYR:DOL(1:1)

Fig. 4.6.7 (c) & (d) show XPS plots correspond to the batteries with DOL diluted ionic liquid after (c) single cycle and (d) 100 cycles. In both cases characteristic peaks for SSE (PS_4^{3-} and P_2S_5) were detected with the Li_2S peaks. Both batteries have shown significantly high initial discharge capacities confirming the presence of Li_2S peak as the final discharge product. After 100 cycles XPS peaks related to terminal/bridging sulfur from long chain

polysulfides were also detected in the battery. With the presence of SSE, reaction path has less long chain polysulfides hence existence of polysulfides is expected to result mostly from liquid electrolyte reaction path resulting from ionic liquid. After prolonged cycling, part of the polysulfides formed in the cathode, could have dissolved into ionic liquid and deposited at the SSE/cathode interface degrading the cyclability and lowering the capacity. Failure of LiTFSI(1M) in PYR only battery whilst the success of LiTFSI (2M) in PYR:DOL(1:1) battery, even though both of them showed polysulfide peaks in XPS, could be due to lower polysulfide dissolution in diluted ionic liquid. In prior research work by Meisner Q.J. et.al [129] has shown improved capacity retention of ionic liquid-based liquid electrolyte batteries consist of LiTFSI-PYR diluted with DOL due to their lower polysulfide dissolution.
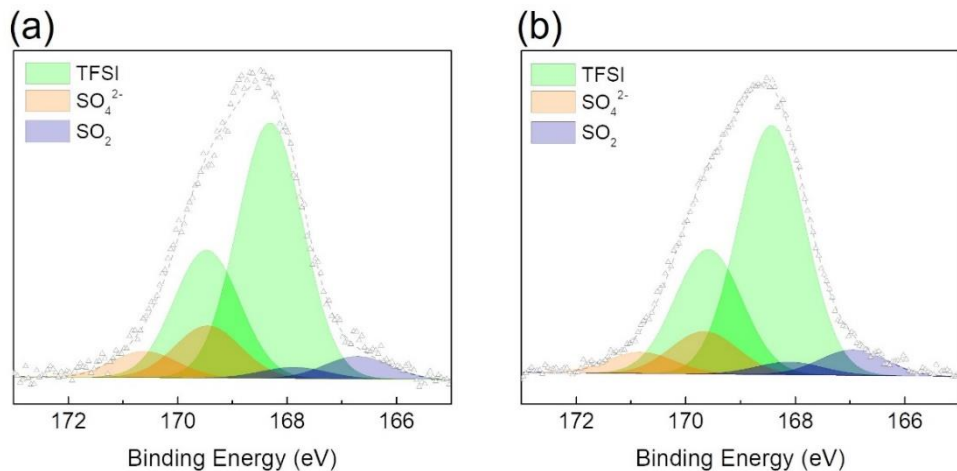
Figure 4.6.8: XPS S2p high BE peak of the cathode-SSE interface of 2 batteries containing (a) LiTFSI(1M) in PYR and (b) LiTFSI(2M) in PYR:DOL (1:1) after discharge of 100 cycles

The XPS S2p high binding energy peak shown in Figure 4.6.8 shows dominant peaks corresponding to TFSI⁻ anions from LiTFSI (solid) and PYR (liquid) for both batteries [130,131]. Peaks corresponding to SO_2 were detected due to the decomposition of TFSI anions resulting from both LiTFSI and PYR. The additional peaks corresponding to sulfates (SO_4^{2-}) are assumed to be due to the reaction of sulfides with any residual oxygen. AIMD simulation results also show a partial decomposition of PYR in the 1M LiTFSI dissolved in PYR, producing stable SO_2 and -SO_2* radical that could also lead to the formation of SO_4^{2-}. This speculation is further confirmed with the AIMD simulation results showing improved stability in IL consisting of LiTFSI(2M) in PYR:DOL(1:1) over LiTFSI(1M) in PYR. However, there is no clear distinction in the XPS results of SO_2 and SO_4^{2-} between the batteries with and without DOL since SO_2 and SO_4^{2-} can be formed from both LiTFSI and PYR.

4.7 Conclusion

Quasi-solid-state electrolyte Li-S batteries consist of Super P-Sulfur composite cathodes, Li anodes and novel $Li_6PS_5F_{0.5}Cl_{0.5}$ SSE were successfully developed with the ionic liquid LiTFSI (2M) dissolved in PYR:DOL(1:1) used as the wetting agent at both electrode-SSE interfaces. Optimum QSSLSB batteries had initial discharge capacity >1100 mAh/g and discharge capacity >400 mAh/g after 100 cycles at the C rate of C/10 with a significant coulombic efficiency. The volumes of IL used at the SSE-electrolyte interfaces are low enough to warrant our QSSLSBs follow solid-state Li-S reaction pathways rather than liquid electrolyte Li-S reaction routes as confirmed by the cyclic voltammetry studies.

40 μL of LiTFSI (2M) dissolved in PYR:DOL(1:1) ionic liquid was found to be the optimum for high performance QSSLSBs as verified by both theoretically and experimentally.

CHAPTER 5

HIGH SULFUR LOADING IN QSSEBs (COATING-BASED)

5.1 Scope

In this chapter, cathode development using coating-based technique is described with characterizations and battery performance results. Next, techniques implemented to increase the electronic conductivity while maintaining the porosity and initial discharge capacity is studied. Latter part of this chapter describes the QSSLSB assembly using ionic liquids and SSE in the cathode.

5.2 Introduction

The sulfur loading in a Li-S battery refers to the amount of sulfur used in the cathode and a high sulfur loading is essential due to high energy for practical applications. However, increasing the sulfur loading also increases the risk of performance issues such as capacity fading, dendrite formation, and self-discharge[132,133]. Finding the optimal sulfur loading is therefore a trade-off between maximizing the energy density and maintaining good performance and stability. Researchers are working on developing new materials and designs to increase the sulfur loading while minimizing these challenges, and this remains an important area of research in the development of Li-S batteries[134,135].

To achieve high energy density in Li-S batteries, various factors have to be considered, such as the amount of sulfur used, the electrolyte/sulfur ratio, and the use of Li-metal-based

anodes. The properties of sulfur cathodes, including their porosity and wettability, are closely linked to the type of electrolytes used, which can significantly affect energy density. It's important to choose a suitable E/S ratio to achieve meaningful results because excess electrolyte can decrease energy density. Improving the areal sulfur loading in cathodes is the most effective way to increase energy density by reducing the weight fraction of inactive components. For an energy density of 300 Wh kg^{-1} or higher, the sulfur loading in the cathode should be at least 4 mg cm^{-2}. However, higher sulfur loading can cause issues such as electrode fracturing, sluggish reaction kinetics, and a more severe shuttle effect, which need to be addressed to commercialize Li-S batteries[136,137].

5.3 Challenges in high sulfur loading cathode synthesis

One of the main challenges in high sulfur loading cathode synthesis for Li-S batteries is the poor electrical conductivity and low reaction kinetics of sulfur. To overcome this challenge, scientists have been exploring various strategies such as incorporating conductive carbon or metal oxide nanoparticles, using porous carbon frameworks, and developing novel sulfur-based cathode materials[138,139]. For this work, Super P carbon black was used as the conductive carbon additive as used in the lower sulfur loading scenario discussed in the previous Chapter. Based on the results from several experiments, amount of sulfur in SP:S mixture was increased to 75w% from 40w% to have highest amount of sulfur for a given coating thickness.

Moreover, high sulfur loading can also lead to the formation of large sulfur particles, which can cause mechanical instability and lead to the cracking or disintegration of the cathode[140]. To overcome this problem, higher mixing speeds were employed during ball

milling for longer period of time with and without the binder. Melt-diffusion step was also carried out for longer period of time to reduce the sulfur aggregation.

In general, as the thickness of the cathode increases, the overall ionic conductivity of the cathode decreases. This is because thicker cathodes have a greater resistance for ion transport, which can limit the rate at which lithium ions can migrate within the material. However, the specific effects of thickness on ionic conductivity can also depend on the composition and structure of the cathode material[141]. For example, increasing the thickness of a cathode composed of a porous carbon framework with uniformly dispersed sulfur particles may not significantly impact the overall ionic conductivity, as the pores can allow for efficient ion transport through the material. That implement the importance of maintaining significant porosity while developing higher loading cathodes[142].

Additionally, the thickness of the electrolyte layer between the cathode and anode can also affect the overall ionic conductivity of the battery. Thicker electrolyte layers can lead to increased resistance to ion transport, while thinner layers can enhance the overall ionic conductivity. Therefore, optimizing both the thickness and composition of the cathode and electrolyte layers is critical for achieving high-performance Li-S batteries[143].

Mixing a solid-state electrolyte (SSE) with the cathode material in a Li-S battery can have several potential benefits for the overall performance and safety of the battery. One advantage is that the SSE can help to prevent the dissolution and diffusion of polysulfides in the electrolyte, which can lead to capacity loss and decreased cycling stability. By incorporating the SSE into the cathode, it can create a physical barrier that can limit the movement of polysulfides and enhance their electrochemical confinement, leading to

improved cycling stability[144]. Another benefit is that the SSE can enhance the overall ionic conductivity of the cathode and facilitate ion transport between the cathode and the anode. This can be particularly useful in high-power applications where fast charging and discharging are required.

Binders play an important role in high loading cathodes in Li-S batteries, as they are used to hold the active material and conductive additives together, and to maintain the structural integrity of the electrode during cycling. At higher sulfur loadings, the use of conventional binders such as polyvinylidene fluoride (PVDF) can lead to increased viscosity and reduced porosity of the electrode, which can limit the diffusion of lithium ions and polysulfides through the cathode material. This can result in decreased electrochemical performance and cycling stability. Moreover, practically use of PVDF and NMP as the binder crates mechanical instability leading to flaking-out of the coating while drying[145].

To address these issues, scientists have been exploring the use of alternative binders that can better accommodate higher sulfur loadings and maintain the porosity of the electrode. One example is the use of water-soluble binders such as carboxymethyl cellulose (CMC), which can provide good adhesion and cohesion properties while water also being easily removed compared to NMP during electrode fabrication[146]. At low sulfur loading experiments CMC was used with the SBR as a flexible binder. However, SBR also has some potential drawbacks in Li-S batteries, including the possibility of polysulfide diffusion through the rubber matrix, which can lead to capacity loss and decreased cycling stability over time[147]. Owing to these facts, amount of SBR used in the high sulfur loading

cathode fabrication was limited to 0.5w%. To counter this reduction, CMC weight ratio was increased to 3% in the premixed solution.

5.4 Cathode coatings with high sulfur loading

Initially, SP:S mixture used in low sulfur loading studies was used to fabricate the high sulfur loading cathodes. To achieve high sulfur loading, thickness of the wet coating at the doctor blade setups was raised to 300 μm from 90 μm. Due to higher mass loading, coating flaked out during the drying process. At this point, it was decided that the cathodes will be tested with liquid electrolyte prior to employing them in the QSSLSBs. For the optimization, different amounts of AB, CNT and Lithium aluminum titanium phosphate glass ceramic (LATP) were added into the SP:S mixture. AB and CNT were used to improve the electronic conductivity while LATP was used to improve the ionic conductivity. Main goal of this experiments was to develop a high performing SP:S cathode with sulfur loading of 4.0 mgcm^{-2}.
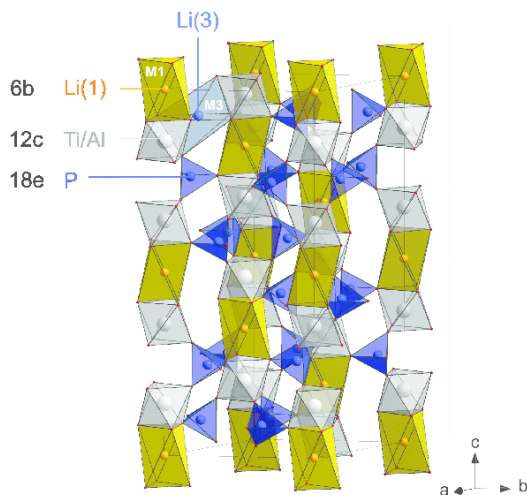
Figure 5.4.1: Crystal structure of LATP[148]

Solid-state electrolytes like LATP are generally less susceptible to degradation from moisture and oxygen than sulfide electrolytes, which can easily react with these substances. LATP, in particular, has a highly crystalline structure that is resistant to water and oxygen. Therefore, the excellent stability of LATP against these substances is a key factor in its suitability for used in cathode formulation with the water-based binder and fabrication process carried out at normal atmospheric conditions[149].

After comprehensive optimization, following recipe was developed to fabricate the cathode. Timcal graphite carbon super P and Sulfur were mixed in the ratio of (1:3) and Sulfur was infused by melt injection under vacuum at 115 °C for 5 hours. Then the mixture of Super P-Sulfur was mixed with acetylene black, Carbon nano tubes, LATP and 3.0 % CMC dissolved in DI water in different weight ratios to formulate the slurry. Next the slurry was coated on aluminum current collector. After excess water is evaporated electrodes were punched into 2.0 cm^2 disks and electrodes had a sulfur loading of 4.0 mgcm^{-2}. These electrodes were further dried under vacuum for 6 hours at 50 °C before the battery assembly.

5.5 Cell assembly and Characterizations

Coatings with different AB,CNT and LATP mixing ratios were fabricated on glass slides to measure the electronic conductivity using the 4-probe method. Thickness required for these calculations were measured by etching off a wedge of the sample and measuring the height of the wedge using FESEM at a tilt angle of 60°. Real thickness of the coatings was mathematically calculated based on the geometry.
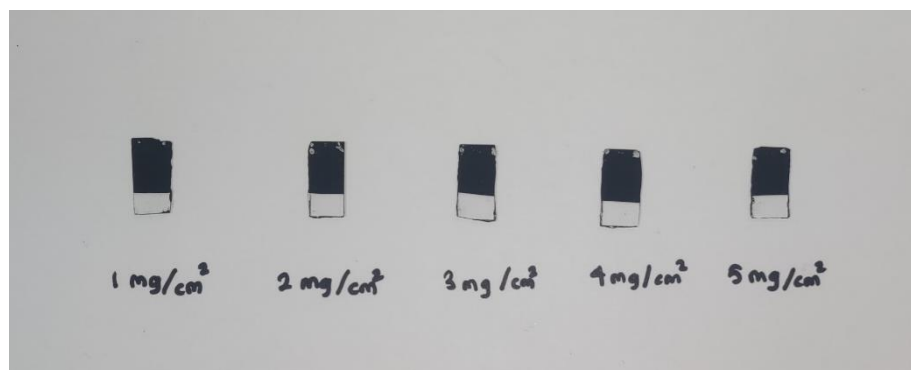
Figure 5.5.1: Photograph of samples coated on glass slide

Prior to the QSSLSB assembly, all the cathodes were tested with the conventional liquid electrolyte after fabrication. LiTFSI (0.4M) and LiNO$_3$ (0.6M) dissolved in DOL:DME (1:1) was the liquid electrolyte employed. Cell guard and Advantec glass fiber separators were combinedly used as the separator. All these coin cells were tested at 30 °C at C/10 C rate using Arbin 8 channel battery testing system between 1.2 V and 2.8 V.

After choosing the cathode, QSSLSBs were assembled with SSEs (Li$_6$PS$_5$F$_{0.5}$Cl$_{0.5}$ & Li$_6$PS$_5$F$_{0.5}$Cl$_2$) with relevant amounts of optimized ionic liquid (LiTFSI (3M) dissolved in PYR:DOL(1:3)). These cells were tested at 30 °C at C/20 C rate using Arbin 8 channel battery testing system between 1.2 V and 2.8 V.

5.6 Results and Discussion

Since the cathodes with high Sulfur loading tested with previously optimized ionic liquids failed to show reasonable initial discharge capacities during preliminary experiments, optimization of the cathode formulation for high loading was necessary.

In the first experiment, the cathode consisted of SP-S(1:3) 84.5w%, CMC 4w%, SBR 0.5w% and AB 2w%. While keeping AB, CMC and SBR contents constant, CNT contents

were changed systematically from 5w%-11w% in the increments of 2 w%. Each battery was tested with an Li anode and the liquid electrolyte LiTFSI (0.4M) and $LiNO_3$ (0.6M) dissolved in DOL:DME (1:1). Glass fiber & Advantec cell guard separators were used in the coin cell configuration. As shown in Fig. 5.6.1, with 4 mg/cm^2 loading addition of CNT and AB to super-P proved to improve the electronic conductivity at high S-loading, and dramatically increased the initial discharge capacity. SP-S(1:3) 84.5w%, AB 2w%, CNT 9w% CMC 4w% and SBR 0.5w% found to be optimum from this preliminary experiment.
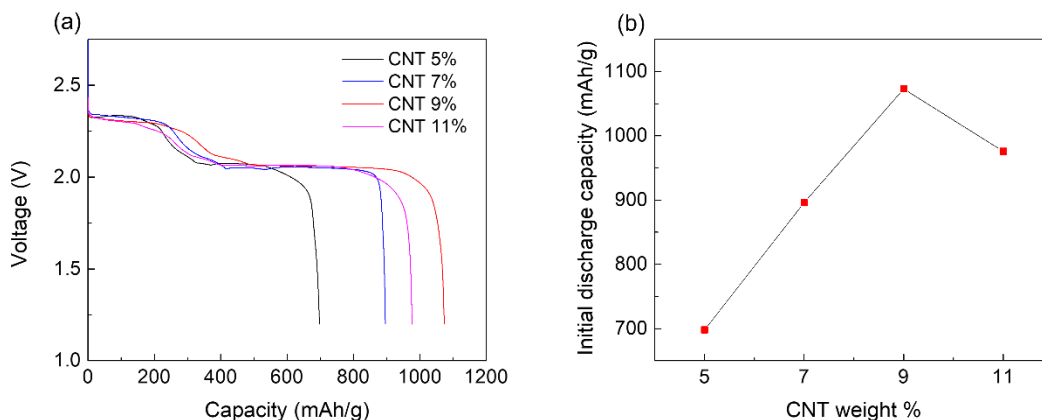
Figure 5.6.1: (a) Initial discharge curves of cathodes with different CNT amounts at C/10 rate and (b) Initial discharge capacity correspond to CNT weight percentage

Similarly, the cathode consisted of SP-S(1:3) 83.5w%, CMC 4w%, SBR 0.5w% and CNT 5w%. while keeping CNT, CMC and SBR contents constant, AB contents were changed systematically from 3w%-9w% in the increments of 2 w%. As shown in Fig. 5.6.2, variation of AB content with constant CNT to super-P ratio also showed improved electronic conductivity at high S-loading, and considerably enhanced the initial discharge

capacity with the best performance achieving for SP-S(1:3) 83.5w%, CNT 5w%, AB 7w%, CMC 4w% and SBR 0.5w%.
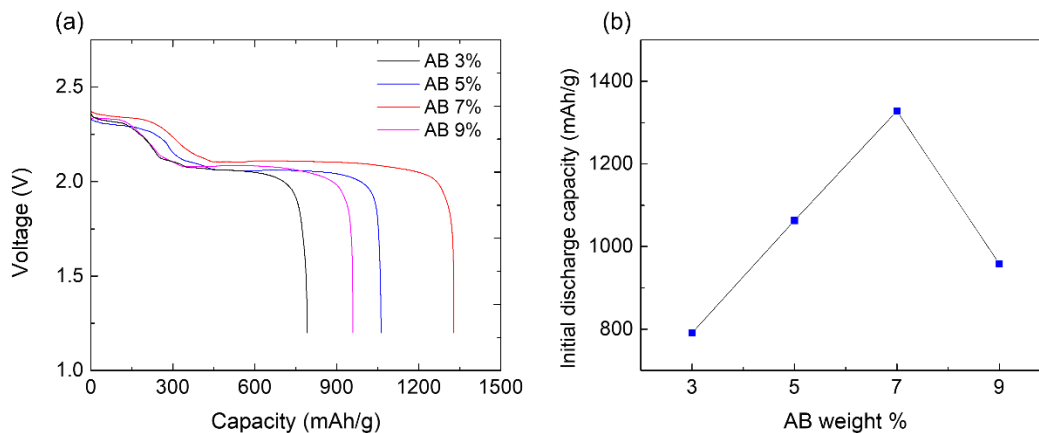
Figure 5.6.2: (a) Initial discharge curves of cathodes with different AB amounts at C/10 rate and (b) Initial discharge capacity correspond to AB weight percentage

Next, the optimized cathodes with 4 mg/cm^2 Sulfur loading were tested using Li$_6$PS$_5$F$_{0.5}$Cl$_{0.5}$ SSE and Li metal anode with 40 μm volume of ionic liquid, 2M LiTFSI in PYR:DOL (1:3) at both the SSE-electrolyte interfaces at 30 °C.
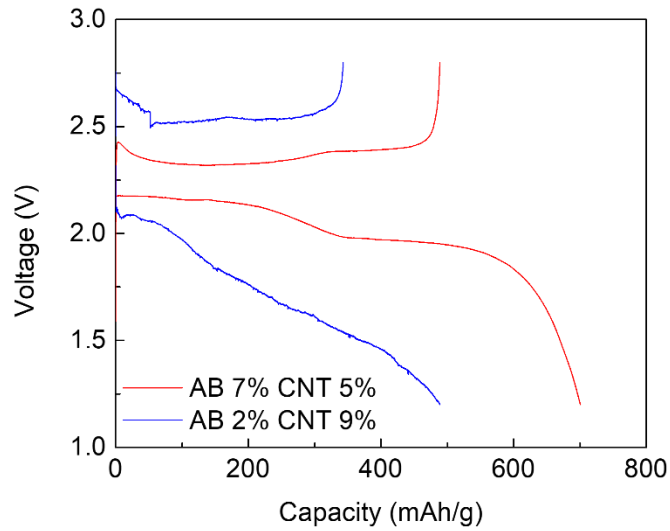
Figure 5.6.3: Charge discharge curves for QSSLSBs with two optimized cathodes at C/20 rate

As sown in Fig. 5.6.3, the cathode with 7 w% AB + 5 w% CNT showed higher initial capacity with the SSE compared to the cathode with 2 w% AB + 9 w% CNT. Still the initial capacity was significantly lower compared to the battery with the same cathode with liquid electrolytes. Based on the performance with solid electrolyte, 7 w% AB + 5 w% CNT cathode was selected for further experiments. Microstructure and conductivity of this cathode with different sulfur loading was studied by coating the samples on glass substrate.
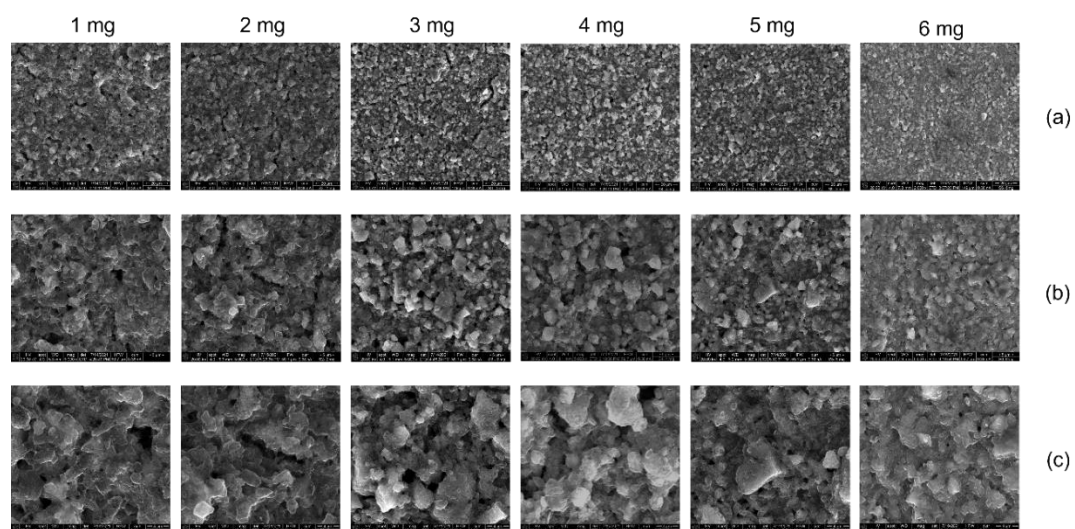
Figure 5.6.4: FESEM images of cathode surface at magnifications of (a) 2000 (b) 5000 and (C) 10000

Fig. 5.6.4 shows FESEM images of SP-S cathodes coated on glass substrates with varying sulfur loadings. These figures show higher porosity for lower loading and gradual decrease of the porosity for higher loading. Next, the samples were tilted 60° and FESEM images were obtained.
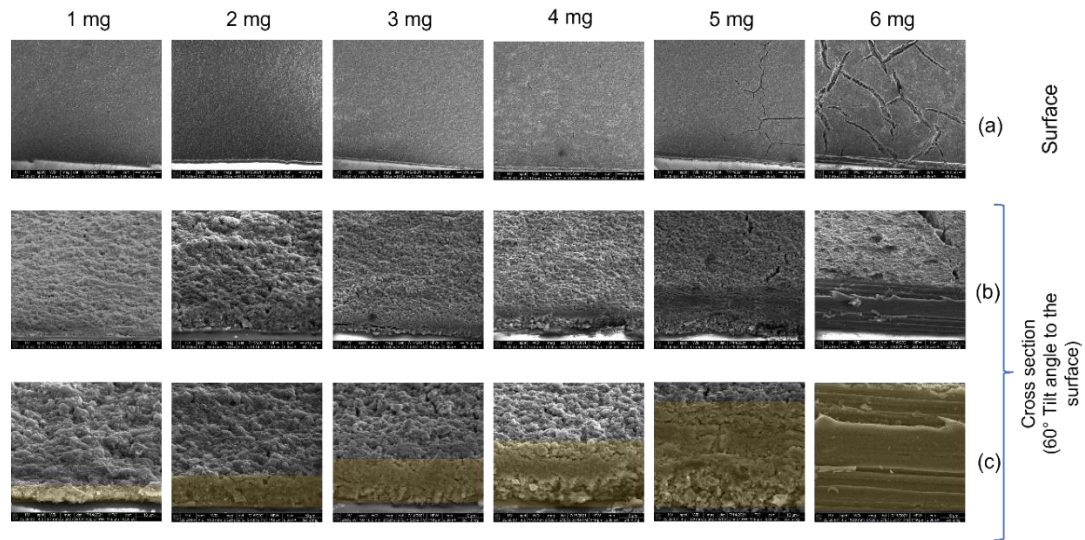
Figure 5.6.5: FESEM images of (a) surface (b),(C) cross section obtained at 60° tilt angle

Fig. 5.6.5 shows SEM images of SP-S cathodes coated on glass substrates with varying sulfur loadings. The rows (a) and (b) show the surface at different magnification ((a)100 & (b)1000) and the bottom row (c) shows the cross-sectional view taken at 60° tilts. Again, the images of the surface showed smooth coating for lower sulfur loading with appearance of cracks for higher loading ($> 5\text{mg/cm}^2$). It also showed higher porosity for lower loading and gradual decrease of the porosity for higher loading. The cross-sectional view again showed systematic increase of the thickness (marked in yellow) for increasing sulfur loading.

In order to obtain the electronic conductivity of coatings, sheet resistance (R_S) of the coatings made on glass slides, was measured after wire bonding them onto a chip carrier. Thickness *(t)* measurements were carried out with the aid of FESM. Conductivity *(σ)* was calculated based on the following equation;

$$\sigma = \frac{1}{R_s t} \qquad (5.1)$$

Table 5.6.1: Electronic conductivity of cathode coatings with different sulfur loading

Loading (mg)	Sheet Resistance (Ohms)	Thickness (um)	Conductivity (S/m)
1	366.03	6.86	398.33
2	213.056	18.83	249.30
3	142.44	28.92	242.72
4	173.94	37.42	153.64
5	174.63	55.07	103.99
6	254.65	78.56	49.99

As expected, conductivity values of the cathode coatings were drastically decreased with increasing sulfur loading as shown in fig 5.6.6. Sheet resistance of the samples has decreased with the increasing sulfur loading up to 5 mg level and significantly increased at 6 mg. This increase assumed to be due to the appearance of cracks at higher sulfur loading.
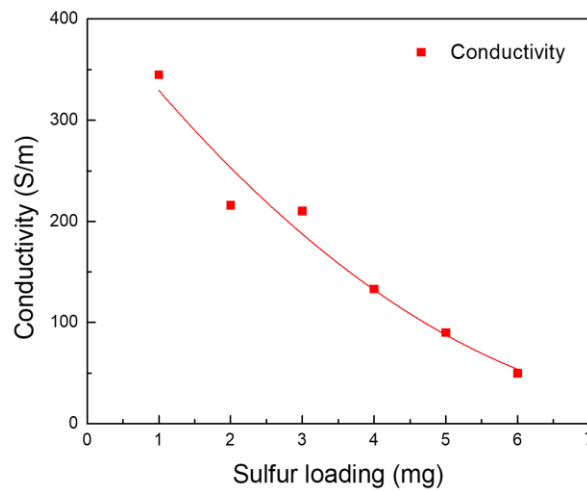
Figure 5.6.6: Electronic conductivity of the cathode with different sulfur loadings
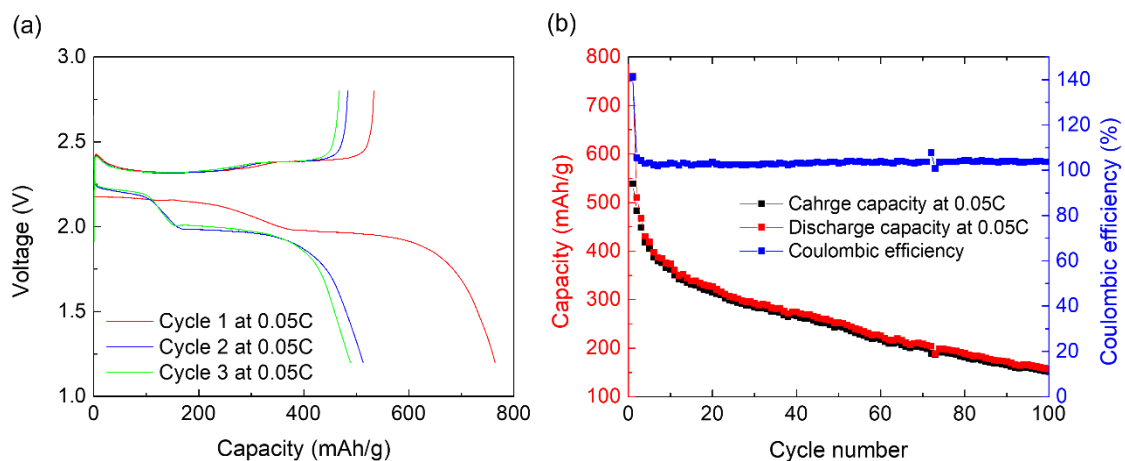
Figure 5.6.7: Performance of the QSSLSB tested with 4 mgcm^{-2} sulfur cathode

Fig. 5.6.7 (a) shows the charge discharge curves of the QSSLSB with 4 mgcm^{-2} sulfur loading cathode(5w% CNT + 7w% AB), Li$_6$PS$_5$F$_{0.5}$Cl$_{0.5}$ SSE and Li metal anode with 40 μL volume of ionic liquid, 2M LiTFSI in PYR:DOL (1:3) at 30 °C. Fig. 5.6.7 (b) shows the overall performance of the battery for 100 cycles. Capacity rapidly dropped below 200 mAh/g by 100 cycles while a significant drop can be seen at the initial cycles. This initial capacity drop was found to be often in the high sulfur loading cathode and believed to be due to lower ionic conductivity of the cathode material after initial cycle reaction products.

With the aim of increasing the Li-ion conductivity of the cathode, Lithium aluminum titanium phosphate glass ceramic (LATP) was added into the optimized Super P-S cathode. The cathodes consisted of SP-S(1:3) 81.5w%, AB 7w%, CNT 5w%, CMC 4w%, SBR 0.5w% and LATP. While keeping CNT, AB, CMC and SBR contents constant, LATP amounts were changed systematically from 0.5w%-2.5w% in the increments of 0.5 w%. One sample with the 5w% LATP was also fabricated to study the conductivity at higher LATP level. All these samples were fabricated in order to have 4 mgcm^{-2} sulfur loading.

Similarly, in the loading study, a comprehensive study on the cathodes associated with LATP was carried out by measuring the electronic conductivity and exploring the microstructure.
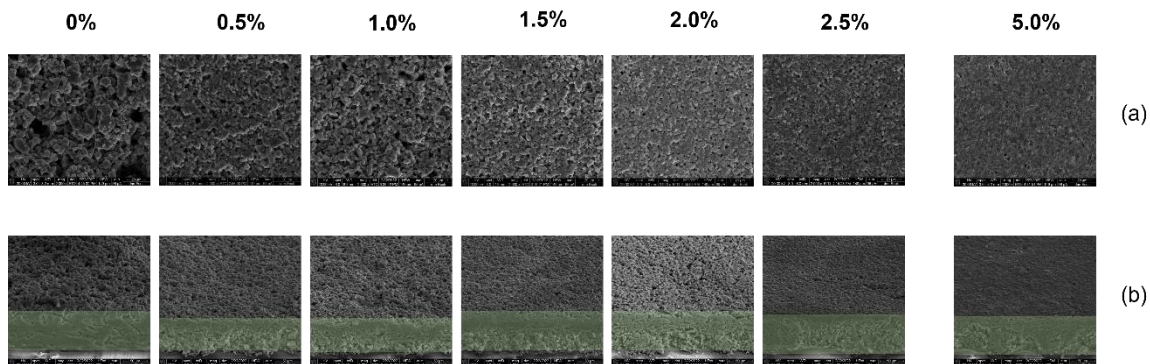
Figure 5.6.8: FESEM images (a) surface at 1000 magnification and (b) cross section obtained at 60° tilt angle for cathodes with different LATP amounts

Fig. 5.6.8 FESEM images of SP-S cathodes with varying amounts of LATP. The row (a) shows the surface at 1000 magnification and the bottom row (b) shows the cross-sectional view taken at 60^0 tilts. Surface images showed decrease in the particle size with the increase of the LATP amount and porosity also decreased with higher associated LATP amounts.

Table 5.6.2: Electronic conductivity of cathode coatings with different LATP amounts

LATP w%	Sheet resistance(Ω)	Thickness(μm)	Conductivity(S/m)
0.5	206	70.32	79.71
1.0	212	72.87	74.75
1.5	216	81.61	65.51
2.0	229	86.36	58.39
2.5	266	82.23	52.79
5.0	412	78.18	35.85

Table 5.6.2 shows the electronic conductivity data for the samples with LATP in the cathode. Fig. 5.6.9 shows the variation of conductivity with LAPT weight percentage in the cathode.
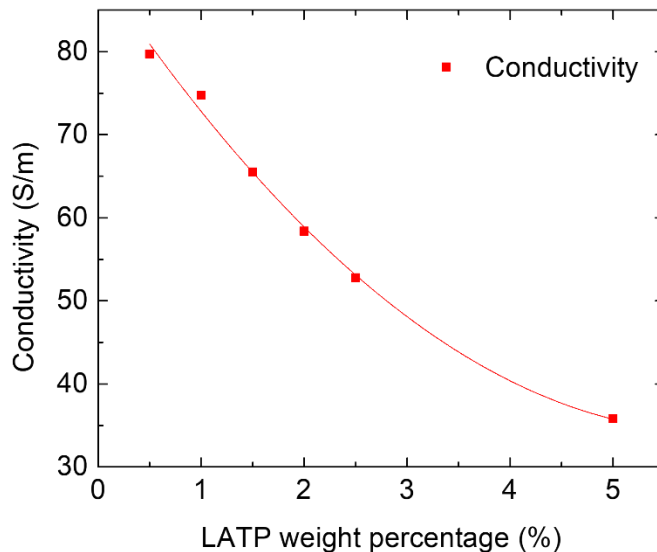
Figure 5.6.9: Variation of conductivity and porosity of cathodes with different LATP amounts

Conductivity of the cathode found to be low compared to the cathodes without LATP due to the low electronic conductivity of LATP. Therefore, the amount of the LATP in cathode was reduced to a value below 3w%. Liquid electrolyte-based batteries were assembled with these cathodes and their initial discharge capacities were studied systematically. The dependence of the initial discharge capacity with the amount of LATP in cathode at C/10 rate is shown in Fig. 5.6.10 (a). The highest capacity was obtained with 2w% LATP in the cathode which was comparatively lower to the cathode without LATP.
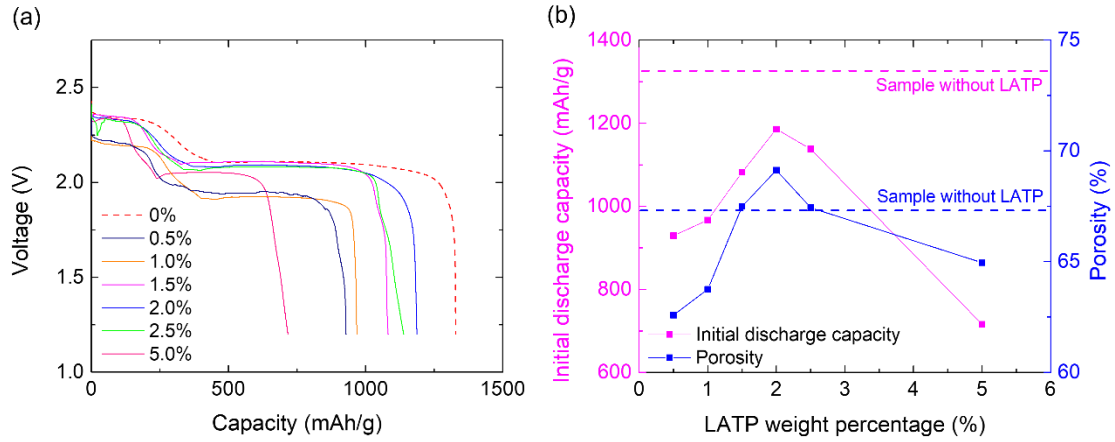
Figure 5.6.10: (a) Initial discharge curves of the liquid electrolyte batteries with different LATP amounts in cathode and (b) Variation of the capacity (left axis) and the porosity (right axis) of cathodes with LATP weight percentage

Fig. 5.6.10 (b) show the variation of capacity and porosity of cathodes with LATP weight percentage, where initial discharge capacity followed similar trend to the porosity below 2.5w% LATP. Porosity values were calculated using the following equations (5.1-5.3);

$$Porosity = \frac{V_{cathode} - (V_S + V_{SP} + V_{CMC} + V_{SBR} + V_{AB} + V_{CNT} + V_{LATP} + V_{Al})}{V_{cathode}} \times 100\% \qquad (5.2)$$

$V_{cathode}$ was calculated from the cathode radius *(r)* and the thickness *(t)* as,

$$V_{cathode} = \pi r^2 t \qquad (5.3)$$

V_S, V_{CMC}, V_{SBR}, V_{SP}, V_{AB}, V_{CNT}, V_{LATP} and V_{Al} were calculated from the S, CMC, SBR, super-P, AB, CNT, LATP and Aluminum masses *(m)* the densities *(ρ)* as,

$$V_x = \frac{m_x}{\rho_x} \qquad (5.4)$$

Sample with 2w% LATP with higher initial capacity with liquid electrolyte, was next assembled into a coin cell with the SSE. Fig. 5.6.11 (a) shows the charge discharge curves of the QSSLSB with 4 mgcm^{-2} sulfur loading cathode(5w% CNT + 7w% AB + 2w% LATP), $Li_6PS_5F_{0.5}Cl_{0.5}$ SSE and Li metal anode with 40 μL volume of ionic liquid, 2M LiTFSI in PYR:DOL (1:3) at 30 °C.
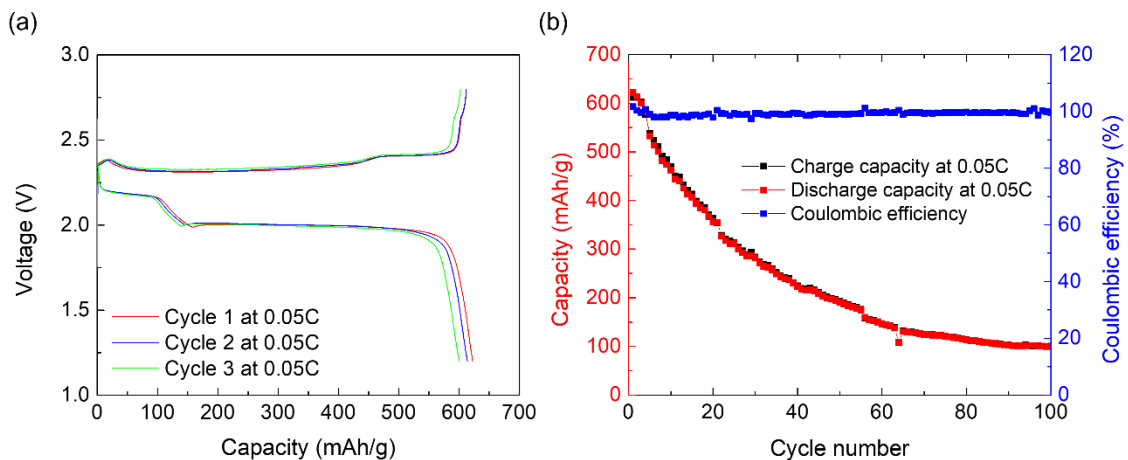
Figure 5.6.11: Performance of the QSSLSB tested with 4 mgcm^{-2} sulfur cathode associated with 2w% LATP at C/20 rate

Even though, the battery has shown stable capacity during the initial cycles, capacity faded down to 100 mAh/g before stabilizing at that value after 100 cycles. However, QSSLSB failed to reach higher initial capacity compared to the liquid electrolyte-based battery. This prompted us to take advantage of some properties of the ionic liquid and appropriate modifications.

Lithium nitrate (LiNO$_3$) is widely used as an additive in LE Li-S batteries due to its well-known ability to form a robust SEI film and suppress the shuttle effect of lithium polysulfides [150]. Different amounts of LiNO$_3$ were added into the ionic liquid and the

performance of the QSSLSBs were studied at C/20 current rate. Volume of the ionic liquid was kept at 40 μL.
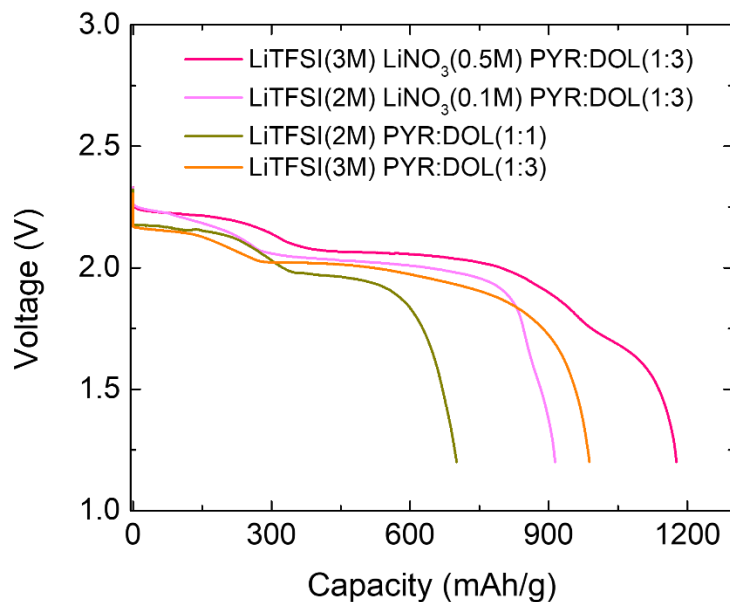
Figure 5.6.12: Initial discharge cycles of QSSLSBs with and without $LiNO_3$ additive

Addition of LiNO3 in the ionic liquid has shown increased initial capacities in the QSSLSBs, yet the cells failed to charge back. Side reaction occurring at the interface was assumed to be the reason behind this poor cycle performance as seen in fig. 5.6.12 (purple and pink lines) where the discharge curve exhibited an extra plateau around 1.7 V. This Ionic liquid composition used in the lower loading studies showed a lower initial capacity. The IL composition yielding highest initial capacity was then re formulated without $LiNO_3$ achieving the initial capacity ~ 1000 mAh/g for 4 mgcm^{-2} loading. Performance of this battery is shown in Fig. 5.6.13.
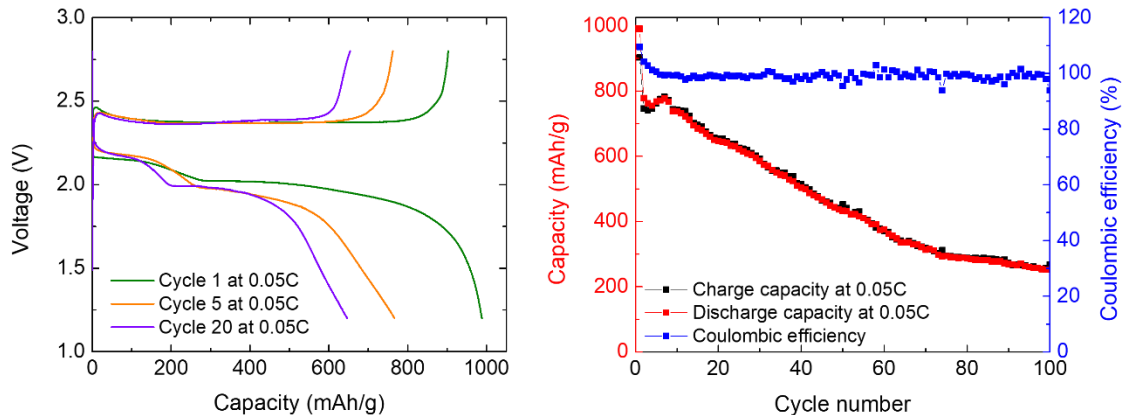
Figure 5.6.13: Performance of the QSSLSB tested with 4 mgcm^{-2} sulfur cathode associated with 2w% LATP and ionic liquid LiTFSI(3M) PYR:DOL(1:3)

Fig. 5.6.13 (a) shows the charge-discharge curves at cycles 1, 5 and 20 (C/20 rate) while Fig. 5.6.13(b) shows capacity versus cycle number (left axis) and coulombic efficiency (right axis) for a battery consisting of SP-S cathode with 4.0 mg/cm^2 loading and 2% LATP, $Li_6PS_5F_{0.5}Cl_{0.5}$ SSE and Li anode with ionic liquid, LiTFSI in PYR:DOL (1:3) at 3M and 40 μL volume at 30 °C at C/20 rate. It showed initial discharge capacity ~ 1000 mA/g which fades gradually reaching ~ 220 mAh/g after 100 cycles.

This lower cycling stability of coating based quasi-solid-state batteries were understood to be due to poor contact at the cathode-SSE interface. In order to enhance the cathode-SSE contact, blending the cathode into the SSE was assumed to be a successful alternative which is discussed in chapter 6.

5.7 Conclusion

Fabrication of high sulfur loading cathode using a coating-based technique with 4.0 mgcm^{-2} was successfully achieved. Addition of CNT and AB into the cathode mixture has significantly improved the electronic conductivity and overall performance of the cathode. Incorporation of LATP into cathode stabilized the performance while improving the ionic conductivity of the cathode. Optimization of the ionic liquid was essential to the successful operation of the battery and LiTFSI (3M) dissolved in PYR:DOL(1:3) found to be the optimum combination.

CHAPTER 6

HIGH SULFUR LOADING QSSEBs

(SOLID-STATE COMPOSITE POWDER-BASED)

6.1 Scope

In this chapter, cathode development using solid composite powder-based technique is discussed with cell assembly and battery performance. Binder-free approach used for the blending of cathode and SSE is described next. Final part of this chapter describes the QSSLSB assembly with lowest possible ionic liquid volumes and SSE incorporation in cathodes.

6.2 Introduction

The traditional way of making thick electrodes by slurry-casting on metal current collectors has some problems, such as fracturing and delamination due to high shrinkage stresses during the drying process [151]. This can cause mechanical instability and poor adhesion between the active material and current collector when the electrode is too thick. Thick electrodes also slow down the transfer of charge (ion and electron) and increase the distance the ions and electrons have to travel[152]. This was proven by the results showed in chapter 5 where microstructures of cathodes were examined.

The binder used in thick electrodes can impede the transport of lithium ions and sulfur species between the cathode and electrolyte, resulting in low sulfur utilization and reduced battery capacity. Only a few studies have looked at ways to make high-loading sulfur cathodes, such as layer-by-layer sulfur cathodes with high sulfur loading, and N, S co-doped graphene sponge with high sulfur loading [153,154,155].

Binders can degrade over time, especially in the presence of the high temperatures and strong acidic conditions that are typical in Li-S batteries, leading to a loss of adhesion between the active material and the current collector[156]. On the other hand, binders can react with the electrolyte to form a SEI layer, which can reduce the transport of lithium ions and sulfur species, leading to decreased battery performance and stability.

As discussed in the chapter 5, degradation of cathode while cycling caused the poor cycle performance of QSSLSBs. It was believed that rigid cathode-SSE interface needed to have improved connection in order operate with smooth Li-ion transfer. Mixing cathode materials with the SSE was the final approach employed in this work.

6.3 Solid-state composite cathodes pressed with SSE

As an alternative approach, SSE ($Li_6PS_5F_{0.5}Cl_2$) was incorporated into the optimized Super P-S cathode mixture and CMC and SBR were removed from the recipe. This technique had its own benefits as well as drawbacks. Even though, mixing SSE with cathode mixture increased the Li-ion conductivity in the cathode side, all the experimental steps had to be carried out under inert atmosphere because SSE was moisture and oxygen sensitive. This required handling of the entire battery assembly process including the cathode formulation inside the glove box. In all cases, cathode containing SSE powder (balled milled together)

was pressed together with the SSE powder in a stainless-steel pellet die inside the glove box.

Experimental procedure started by weighing relevant masses of SP:S(1:3) premixed powder, SSE($Li_6PS_5F_{0.5}Cl_2$), AB and CNT inside the glove box. Then the mixture was transferred into a ball milling container and sealed with the parafilm and insulating tape inside the glove box. Subsequently, ball milling was carried out at 700 RPM for 2 hours. After mixing, the sealed container was transferred into the Ar-filled glove box and powder mixture was collected. Next, a well cleaned and dried stainless-steel 15 mm pallet making tank was transferred into the glove box for the pallet assembly. Then, 200 mg of SSE($Li_6PS_5F_{0.5}Cl_2$) weighed and placed evenly inside the stainless-steel tank. Next, 5 µL of ionic liquid was added onto the SSE using a micropipette. Afterwards, relevant mass of pre-mixed solid composite cathode powder was evenly placed on the SSE powder. As the current collector for the cathode, a stainless-steel mesh with 15 mm diameter was placed on top of the cathode powder. After carefully assembling the pallet-die mold, 80 bar pressure was applied using a hydraulic press for 1 minute. Finally, the pellet with both cathode and SSE was demolded from die set and used in the cell assembly.
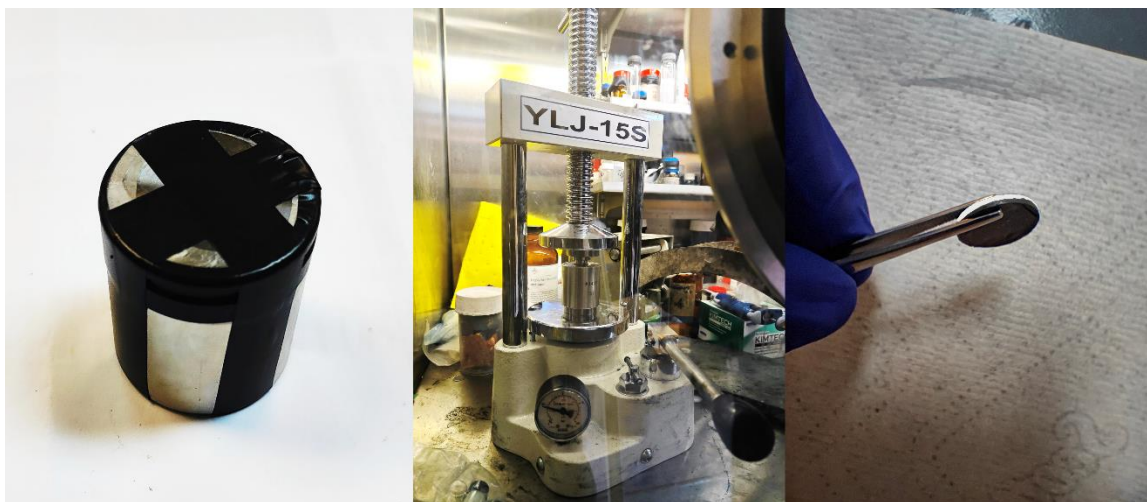
Figure 6.3.1: Solid-state composite cathode with SSE fabrication process

6.4 QSSEB assembly and characterizations

SSE pellet with the cathode powder and current collector pressed together, wetted with relevant amount of IL from anode side using micropipette. Then Li metal attached with current collector was pressed onto the SSE (opposite to the cathode) and assembled into 2032 type coin cell. IL for cathode-SSE interface was added during the cathode-SSE pallet assembly using a micropipette. All the batteries were cycled at 30 °C/60 °C using incubating oven between 1.0 V and 2.8 V using a 16 channel Arbin battery testing system.

After cycling, all the cells were reopened inside the glove box. Cathode separated carefully from the solid electrolyte surface of the SSE, was sealed on to a glass slide to transfer into XPS chamber using captain tape. X-ray photoelectron spectroscopy (XPS) (Al K-alfa monochromator (Thermo scientific)) was employed to detect the chemical composition at the cathode-SSE interface after cycling. Prior to careful analysis, all the spectra were calibrated with respect to the C-C (sp^2) binding energy (284.8 eV) of the C1s peak.

6.5 Results and Discussion

At the beginning, 50 w% SSE was mixed with the cathode composite powder to assemble a QSSLSB without any ionic liquid at the cathode-SSE interface.
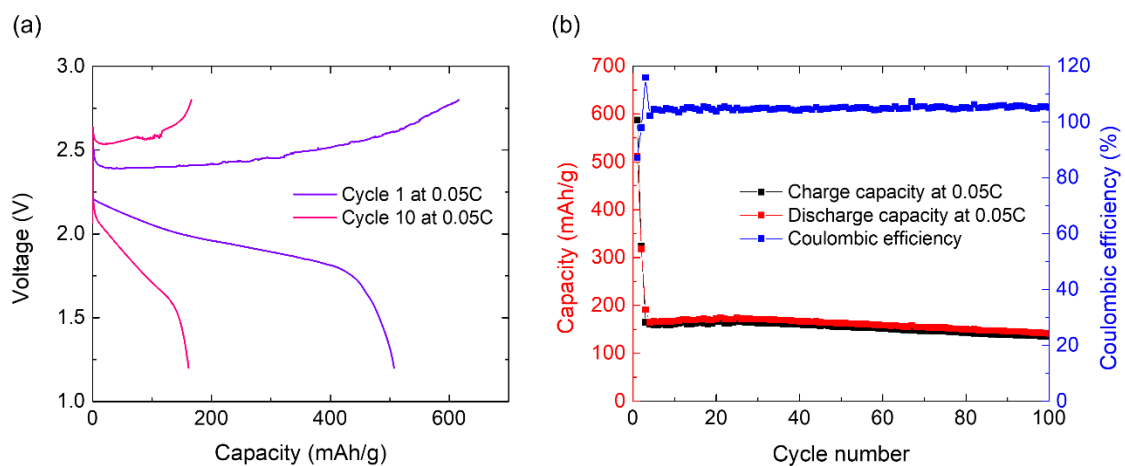
Figure 6.5.1: (a) Charge-discharge curves at 0.05 C at cycle number 1 and 10 (b) Capacity versus cycle number (left axis) and coulombic efficiency (right axis) for a battery consisting of SP-S cathode with 4.0 mgcm^{-2} loading and 50% SSE in cathode

Fig. 6.5.1 (a) shows the Charge-discharge curves at 0.05 C at cycle number 1 and 10 of a battery consisting of SP-S cathode with 4.0 mgcm^{-2} sulfur loading and 50% SSE, $Li_6PS_5F_{0.5}Cl_2$ SSE and Li anode with 20 mL ionic liquid (LiTFSI in PYR:DOL(1:3) at 3M) only at the anode-SSE interface at 30 °C. No IL was used at the cathode-SSE interface. It showed an initial discharge capacity ~600 mAh/g with a sudden drop to < 200 mAh/g within the first 5 cycles as shown in Fig. 6.5.1 (b). This poor performance showed the necessity of the IL at the cathode-SSE interface.
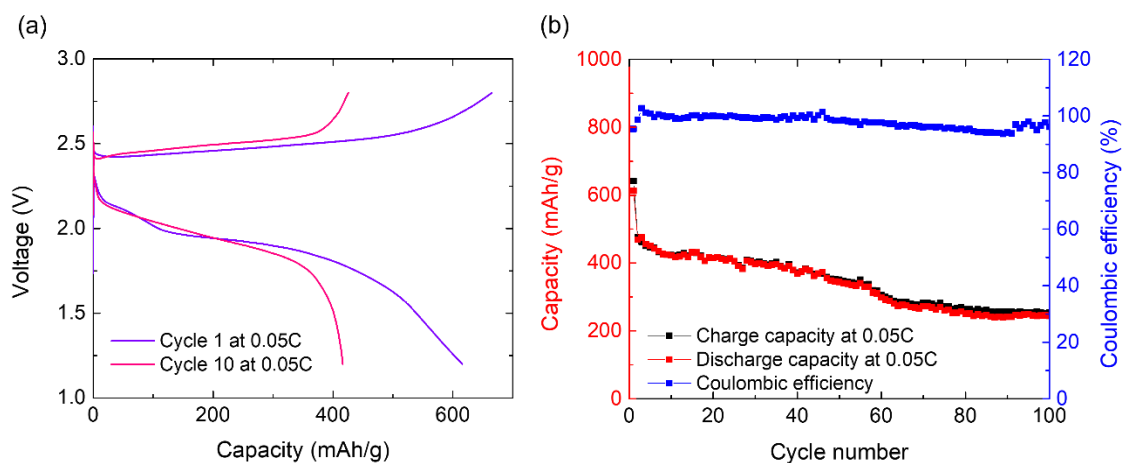
Figure 6.5.2: (a) Charge-discharge curves at 0.05 C at cycle number 1 and 10 (b) Capacity versus cycle number (left axis) and coulombic efficiency (right axis) for a battery consisting of SP-S cathode with 4.0 mg/cm^2 loading and 30% SSE in cathode and 10 μL IL at cathode-SSE interface

Next, a battery consisting of SP-S cathode with 4.0 mg/cm^2 sulfur loading and 30% SSE with $Li_6PS_5F_{0.5}Cl_2$ SSE and Li anode was tested. This time 10 μL IL (LiTFSI in PYR:DOL(1:3) at 3M) at the cathode-SSE interface and 20 μL at the anode-SSE interface at 30 °C. As shown in Fig. 6.5.2 (b) the battery showed an initial discharge capacity ~600 mAh/g and improved cyclability with only a gradual drop of the capacity reaching ~ 200 mAh/g after 100 cycles. Then the IL volume was reduced at the cathode-SSE interface to 5 μL and noticed no appreciable change in the battery performance as shown in Fig 6.5.3.

101
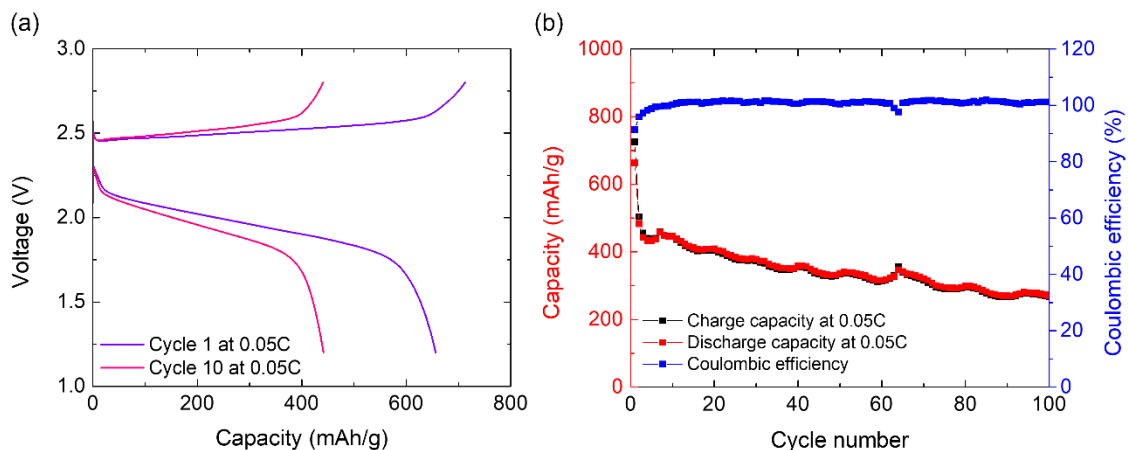
Figure 6.5.3: (a) Charge-discharge curves at 0.05 C at cycle number 1 and 10 (b) Capacity versus cycle number (left axis) and coulombic efficiency (right axis) for a battery consisting of SP-S cathode with 4.0 mg/cm^2 loading and 30% SSE in cathode and 5 μL IL at cathode-SSE interface

Next, the SSE concentration was varied in the optimized Super P-S cathode and tested batteries with 25% and 20% SSE concentrations in the cathode. Fig 6.5.4 (a-c) compares the charge discharge curves of the batteries with different SSE in cathode. Fig. 6.5.4 right panel (d-f) compares the capacity versus cycle number (left axis) and coulombic efficiency (right axis) for batteries consisting of (d) 30% SSE (e) 25% SSE & (f) 20% SSE in the 4.0 mgcm^{-2} SP:S cathode, Li$_6$PS$_5$F$_{0.5}$Cl$_2$ SSE and Li anode with 5 μL ionic liquid (3M LiTFSI in PYR:DOL(1:3)) at the cathode-SSE interface and 20 mL at the anode-SSE interface at 30 °C. The battery with 25% SSE in the cathode showed the best performance retaining its capacity ~ 350 mAh/g after 100 cycles.
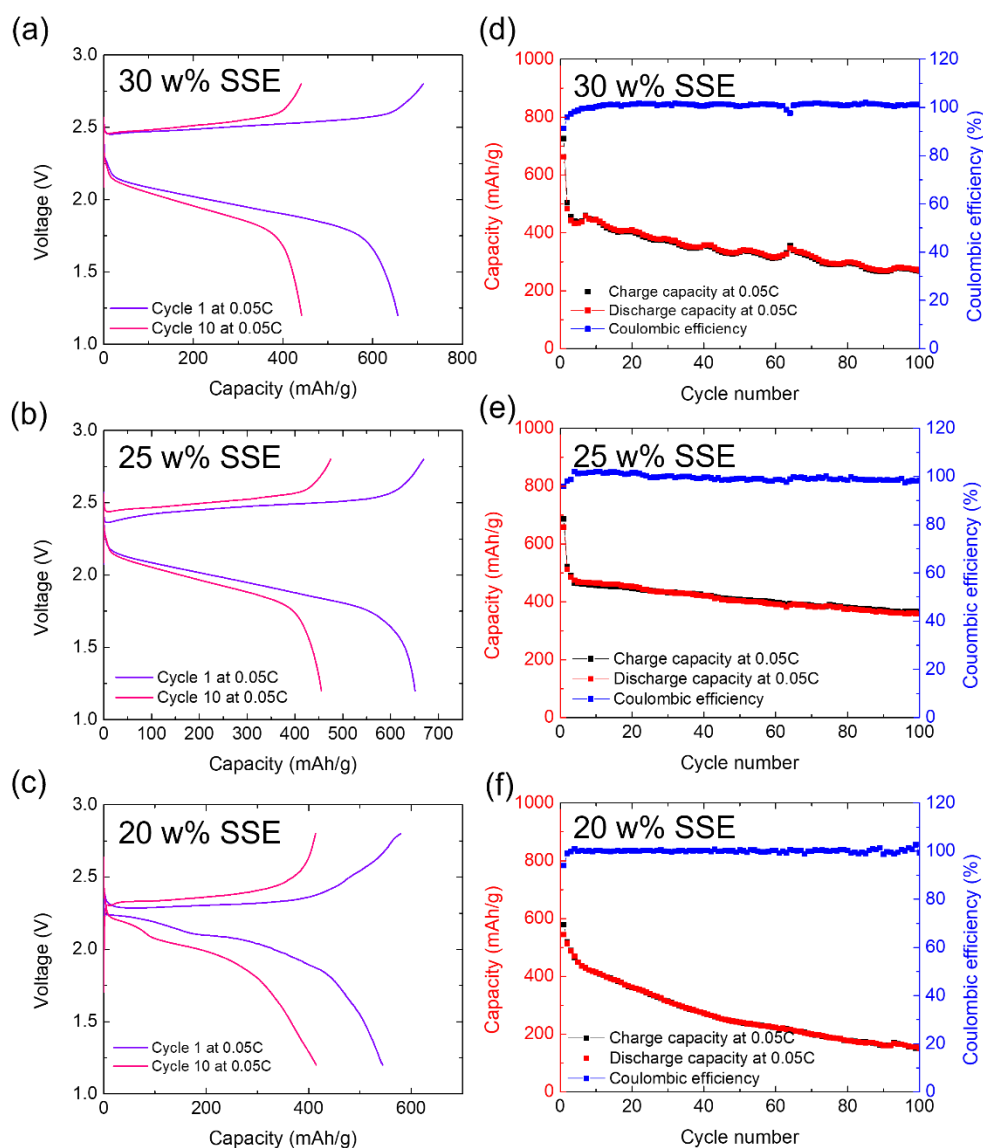
Figure 6.5.4: Performance of QSSLSBs with (a & d)30 w%, (b & e) 25 w% and (c &f) 20 w% SSE in cathode with 5 μL ionic liquid (3M LiTFSI in PYR:DOL(1:3)) at the cathode-SSE interface and 20 mL at the anode-SSE interface at 30 °C

Finally, the battery with 25% SSE in the cathode with 5 μL IL at the cathode-SSE interface and 20 μL at the anode-SSE interface was test at 60 °C. As shown in Fig. 6.5.5, the capacity remained stable by retaining its capacity >400 mAh/g after 100 cycles.
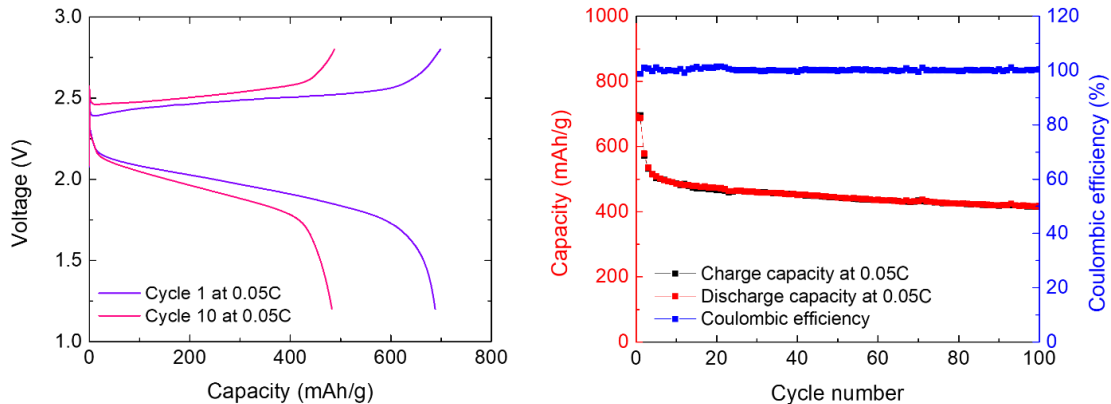
Figure 6.5.5: (a) Charge-discharge curves at 0.05 C at cycle number 1 and 10 (b) Capacity versus cycle number (left axis) and coulombic efficiency (right axis) for a battery consisting of SP-S cathode with 4.0 mg/cm^2 loading and 25% SSE in cathode

In most of the batteries, initial capacity was lower compared to the coating based QSSLSBs and during initial cycles capacity faded by ~ 25%. In order to study the initial capacity drop, two cells were assembled with 25w% SSE in cathode and discharged for 1 and 3 cycles as shown in Fig 6.6.6. First battery (B1) was discharged down to 1.2V (capacity 673 mAh/g) and carefully opened and cathode was separated from the SSE. Second battery (B2) was cycled for two complete cycles then discharged to 1.2V (capacity 515 mAh/g) before disassembling for XPS studies. Both batteries were carefully transferred inside the XPS chamber for the measurements.
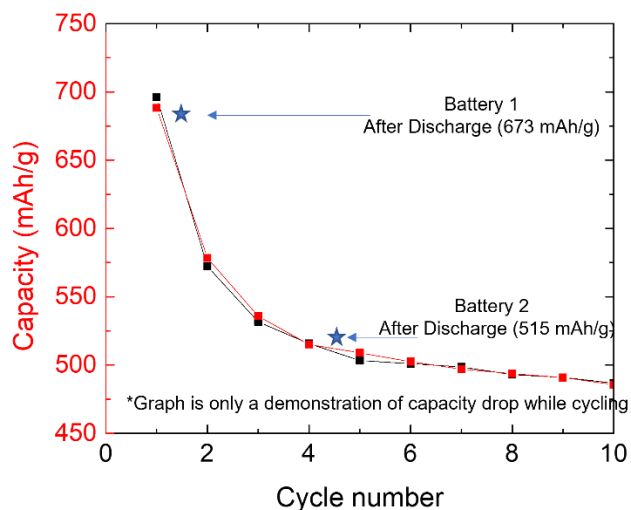
Figure 6.6.6: Initial capacity drop in QSSLSBs. The * indicates where the battery was opened for XPS studies

Figure 6.6.7 shows the S 2P peaks obtained from (a) B1 and (b) B2 using Al K-alfa monochromator (Thermo scientific) XPS system. In both cases, characteristic peaks corresponding to PS_4^{3-} and P_2S_5 species of the SSE were dominating due to plentiful availability of SSE in both SSE and cathode.
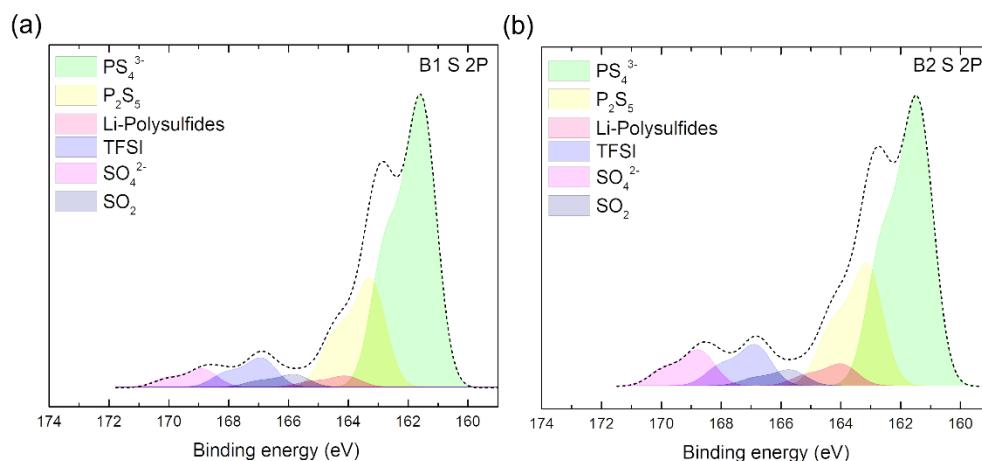
Figure 6.6.7: XPS S2p low binding energy peak of the cathode-SSE interface of (a) after 1 cycle discharge and (b) after 3rd cycle discharge

XPS peaks corresponding to Li_2S were not visible in both cases. This might be due to lower capacity resulting from lower sulfur utilization in the cathode. Another possibility of the absence of the Li_2S peak could be due to physical damage to the interface while attempting to separate the cathode and SSE. Li-polysulfides formed while cycling, was visible even during the first cycle of the battery as shown in Fig. 6.6.7 (a). In most of the cells with solid-composite cathodes pressed on the SSE, discharge curve showed only a single plateau confirming that they undergo solid-state Li-S reaction pathways discussed in chapter 3. Yet there can be polysulfide formed at the cathode-SSE interface due to the presence of IL. Formation of the Li-polysulfides was believed to be the reason for the lower capacity retention because they can impede the ion movement through the cathode-SSE interface under the compact conditions.

6.6 Conclusion

QSSLSB with solid-state cathode composite powder directly pressed on to the SSE pellet was assembled and tested successfully. Even though, the initial capacity was notably lower compared to the coating based QSSLSBs, capacity retention and stability showed a significant improvement. Minute amounts of IL was still necessary even if the interface consisted of a blend of the SSE and cathode powder. However, the amount of IL required to achieve the improved battery performance was significantly lower. Overall understanding of the chemistry of the IL in QSSEBs and the interfacial reactions at the SSE-electrode interfaces will open up new opportunities to develop high-performance, safe and high-energy-density solid-state batteries employing sulfide-based SSEs in the future.

There is a lot to be studied on the SSE-cathode interface for sulfide-based SSE as well as for anode-SSE interface with the presence of ILs in QSSLSBs. Techniques like solid-state composite cathode pressed with SSE will open up new research areas to develop ASSLSBs in future.

REFERENCES

[1]. McCloskey, B. D. (2015). Attainable gravimetric and volumetric energy density of Li–S and Li ion battery cells with solid separator-protected Li metal anodes. The journal of physical chemistry letters, 6(22), 4581-4588.

[2]. Saubanère, M., McCalla, E., Tarascon, J. M., & Doublet, M. L. (2016). The intriguing question of anionic redox in high-energy density cathodes for Li-ion batteries. Energy & Environmental Science, 9(3), 984-991.

[3]. Nitta, N., Wu, F., Lee, J. T., & Yushin, G. (2015). Li-ion battery materials: present and future. Materials today, 18(5), 252-264.

[4]. Petri, R., Giebel, T., Zhang, B., Schünemann, J. H., & Herrmann, C. (2015). Material cost model for innovative li-ion battery cells in electric vehicle applications. International Journal of Precision Engineering and Manufacturing-Green Technology, 2, 263-268.

[5]. Fan, E., Li, L., Wang, Z., Lin, J., Huang, Y., Yao, Y., ... & Wu, F. (2020). Sustainable recycling technology for Li-ion batteries and beyond: challenges and future prospects. Chemical reviews, 120(14), 7020-7063.

[6]. Divakaran, A. M., Hamilton, D., Manjunatha, K. N., & Minakshi, M. (2020). Design, development and thermal analysis of reusable Li-ion battery module for future mobile and stationary applications. Energies, 13(6), 1477.

[7]. Pargoletti, Eleonora, Serena Arnaboldi, Giuseppe Cappelletti, Mariangela Longhi, Daniela Meroni, Alessandro Minguzzi, Patrizia Mussini, Sandra Rondinini, and Alberto Vertova. "Smart interfaces in Li-ion batteries: near-future key challenges." Electrochimica Acta (2022): 140258.

[8]. US Department of Energy, Vehicle and Transportation Office "2021 Batteries annual progress report" (2021)

[9]. Islam, E. S., Ahmed, S., & Rousseau, A. (2021). Future Battery Material Demand Analysis Based on US Department of Energy R&D Targets. World Electric Vehicle Journal, 12(3), 90.

[10]. Rosenman, A., Markevich, E., Salitra, G., Aurbach, D., Garsuch, A., & Chesneau, F. F. (2015). Review on Li-sulfur battery systems: An integral perspective. Advanced Energy Materials, 5(16), 1500212.

[11]. Fang, R., Zhao, S., Sun, Z., Wang, D. W., Cheng, H. M., & Li, F. (2017). More reliable lithium-sulfur batteries: status, solutions and prospects. Advanced materials, 29(48), 1606823.

[12]. Xue, W., Miao, L., Qie, L., Wang, C., Li, S., Wang, J., & Li, J. (2017). Gravimetric and volumetric energy densities of lithium-sulfur batteries. Current Opinion in Electrochemistry, 6(1), 92-99.

[13]. Ji, X., & Nazar, L. F. (2010). Advances in Li–S batteries. Journal of Materials Chemistry, 20(44), 9821-9826.

[14]. Zhang, S. S. (2013). Liquid electrolyte lithium/sulfur battery: Fundamental chemistry, problems, and solutions. Journal of Power Sources, 231, 153-162.

[15]. Park, J. W., Ueno, K., Tachikawa, N., Dokko, K., & Watanabe, M. (2013). Ionic liquid electrolytes for lithium–sulfur batteries. The Journal of physical chemistry C, 117(40), 20531-20541.

[16]. Harks, P. P. R., Robledo, C. B., Verhallen, T. W., Notten, P. H., & Mulder, F. M. (2017). The significance of elemental sulfur dissolution in liquid electrolyte lithium sulfur batteries. Advanced energy materials, 7(3), 1601635.

[17]. Sun, Y. Z., Huang, J. Q., Zhao, C. Z., & Zhang, Q. (2017). A review of solid electrolytes for safe lithium-sulfur batteries. Science China Chemistry, 60, 1508-1526.

[18]. Xiong, S., Xie, K., Diao, Y., & Hong, X. (2014). Characterization of the solid electrolyte interphase on lithium anode for preventing the shuttle mechanism in lithium–sulfur batteries. Journal of power sources, 246, 840-845.

[19]. Xiong, S., Xie, K., Diao, Y., & Hong, X. (2014). Characterization of the solid electrolyte interphase on lithium anode for preventing the shuttle mechanism in lithium–sulfur batteries. Journal of power sources, 246, 840-845.

[20]. Markevich, E., Salitra, G., Rosenman, A., Talyosef, Y., Chesneau, F., & Aurbach, D. (2015). The effect of a solid electrolyte interphase on the mechanism of operation of lithium–sulfur batteries. Journal of Materials Chemistry A, 3(39), 19873-19883.

[21]. Nitta, N., Wu, F., Lee, J. T., & Yushin, G. (2015). Li-ion battery materials: present and future. Materials today, 18(5), 252-264.

[22]. Li, M., Lu, J., Chen, Z., & Amine, K. (2018). 30 years of lithium-ion batteries. Advanced Materials, 30(33), 1800561.

[23]. Li, M., & Lu, J. (2020). Cobalt in lithium-ion batteries. Science, 367(6481), 979-980.

[24]. Botelho Junior, A. B., Stopic, S., Friedrich, B., Tenório, J. A. S., & Espinosa, D. C. R. (2021). Cobalt recovery from Li-ion battery recycling: a critical review. Metals, 11(12), 1999.

[25]. UL research institute (https://ul.org/research/electrochemical-safety/getting-started-electrochemical-safety/what-are-lithium-ion)

[26]. Hausbrand, R., Cherkashinin, G., Ehrenberg, H., Gröting, M., Albe, K., Hess, C., & Jaegermann, W. (2015). Fundamental degradation mechanisms of layered oxide Li-ion battery cathode materials: Methodology, insights and novel approaches. Materials Science and Engineering: B, 192, 3-25.

[27]. Sun, Y. K., Kim, D. H., Yoon, C. S., Myung, S. T., Prakash, J., & Amine, K. (2010). A novel cathode material with a concentration-gradient for high-energy and safe lithium-ion batteries. Advanced Functional Materials, 20(3), 485-491.

[28]. Sharifi-Asl, S., Lu, J., Amine, K., & Shahbazian-Yassar, R. (2019). Oxygen release degradation in Li-ion battery cathode materials: mechanisms and mitigating approaches. Advanced Energy Materials, 9(22), 1900551.

[29]. Ghadbeigi, L., Harada, J. K., Lettiere, B. R., & Sparks, T. D. (2015). Performance and resource considerations of Li-ion battery electrode materials. Energy & Environmental Science, 8(6), 1640-1650.

[30]. Fergus, J. W. (2010). Recent developments in cathode materials for lithium-ion batteries. Journal of power sources, 195(4), 939-954.

[31]. Baccouche, I., Jemmali, S., Manai, B., Nikolian, A., Omar, N., & Essoukri Ben Amara, N. (2022). Li-ion battery modeling and characterization: an experimental overview on NMC battery. International Journal of Energy Research, 46(4), 3843-3859.

[32]. Thapa, A.K., Lavery, B.W., Hona, R.K., Sapkota, N., Kalutara Koralalage, M., Adeniran, A., Ajayi, B.P., Zain, M.A., Wang, H., Druffel, T. and Jasinski, J.B., 2022. Mn-Rich NMC Cathode for Lithium-Ion Batteries at High-Voltage Operation. Energies, 15(22), p.8357.

[33]. Wang, A., Kadam, S., Li, H., Shi, S., & Qi, Y. (2018). Review on modeling of the anode solid electrolyte interphase (SEI) for lithium-ion batteries. npj Computational Materials, 4(1), 15.

[34]. Christensen, J., Albertus, P., Sanchez-Carrera, R.S., Lohmann, T., Kozinsky, B., Liedtke, R., Ahmed, J. and Kojic, A., 2011. A critical review of Li/air batteries. Journal of the Electrochemical Society, 159(2), p.R1.

[35]. Thapa, A. K., & Ishihara, T. (2011). Mesoporous α-MnO2/Pd catalyst air electrode for rechargeable lithium–air battery. Journal of Power Sources, 196(16), 7016-7020.

[36]. SINO Voltaics (https://sinovoltaics.com/learning-center/storage/lithium-air-batteries/)

[37]. Girishkumar, G., McCloskey, B., Luntz, A. C., Swanson, S., & Wilcke, W. (2010). Lithium− air battery: promise and challenges. The Journal of Physical Chemistry Letters, 1(14), 2193-2203.

[38]. Song, M. K., Park, S., Alamgir, F. M., Cho, J., & Liu, M. (2011). Nanostructured electrodes for lithium-ion and lithium-air batteries: the latest developments,

challenges, and perspectives. Materials Science and Engineering: R: Reports, 72(11), 203-252.

[39]. Rosenman, A., Markevich, E., Salitra, G., Aurbach, D., Garsuch, A., & Chesneau, F. F. (2015). Review on Li-sulfur battery systems: An integral perspective. Advanced Energy Materials, 5(16), 1500212.

[40]. Deng, Y., Li, J., Li, T., Gao, X., & Yuan, C. (2017). Life cycle assessment of lithium sulfur battery for electric vehicles. Journal of Power Sources, 343, 284-295.

[41]. Wang, Mingqiang, Ahmet E. Emre, Ji-Young Kim, Yiting Huang, Li Liu, Volkan Cecen, Yudong Huang, and Nicholas A. Kotov. "Multifactorial engineering of biomimetic membranes for batteries with multiple high-performance parameters." Nature communications 13, no. 1 (2022): 1-12.

[42]. Manthiram, A., Fu, Y., & Su, Y. S. (2013). Challenges and prospects of lithium–sulfur batteries. Accounts of chemical research, 46(5), 1125-1134.

[43]. Han, Z., Li, S., Wu, Y., Yu, C., Cheng, S., & Xie, J. (2021). Challenges and key parameters in exploring the cyclability limitation of practical lithium–sulfur batteries. Journal of Materials Chemistry A, 9(43), 24215-24240.

[44]. Zhang, S. S. (2013). Liquid electrolyte lithium/sulfur battery: Fundamental chemistry, problems, and solutions. Journal of Power Sources, 231, 153-162.

[45]. Zhang, S. S. (2013). Liquid electrolyte lithium/sulfur battery: Fundamental chemistry, problems, and solutions. Journal of Power Sources, 231, 153-162.

[46]. Pan, H., Cheng, Z., He, P., & Zhou, H. (2020). A review of solid-state lithium–sulfur battery: ion transport and polysulfide chemistry. Energy & Fuels, 34(10), 11942-11961.

[47]. Famprikis, T., Canepa, P., Dawson, J. A., Islam, M. S., & Masquelier, C. (2019). Fundamentals of inorganic solid-state electrolytes for batteries. Nature materials, 18(12), 1278-1291.

[48]. Armand, M. (1983). Polymer solid electrolytes-an overview. Solid State Ionics, 9, 745-754.

[49]. Cui, Y., Wan, J., Ye, Y., Liu, K., Chou, L. Y., & Cui, Y. (2020). A fireproof, lightweight, polymer–polymer solid-state electrolyte for safe lithium batteries. Nano letters, 20(3), 1686-1692.

[50]. Li, L., Deng, Y., & Chen, G. (2020). Status and prospect of garnet/polymer solid composite electrolytes for all-solid-state lithium batteries. Journal of Energy Chemistry, 50, 154-177.

[51]. Aobing, D. U., Jingchao, C. H. A. I., Jianjun, Z. H. A. N. G., Zhihong, L. I. U., & Guanglei, C. U. I. (2016). All-solid-state lithium-ion batteries based on polymer electrolytes: State of the art, challenges and future trends. Energy Storage Science and Technology, 5(5), 627.

[52]. Yu, X., Bi, Z., Zhao, F., & Manthiram, A. (2016). Polysulfide-shuttle control in lithium-sulfur batteries with a chemically/electrochemically compatible NASICON-type solid electrolyte. Advanced Energy Materials, 6(24), 1601392.

[53]. Arumugam Manthiram, Y. F., Yu-Sheng Su, Challenges and Prospects of Lithium–Sulfur Batteries. Accounts. Chem. Res. 2013, 46, 1125-1134

[54]. Scott Evers, L. F. N., New Approaches for High Energy Density Lithium–Sulfur Battery

Cathodes. Accounts. Chem. Res. 2013, 46, 1135-1143.

[55]. Li, S.; Mou, T.; Ren, G.; Warzywoda, J.; Wang, B.; Fan, Z., Confining Sulfur

Species in Cathodes of Lithium–Sulfur Batteries: Insight into Nonpolar and Polar

Matrix Surfaces. ACS Energy Letters 2016, 1 (2), 481-489

[56]. Ren, G.; Li, S.; Fan, Z.-X.; Warzywoda, J.; Fan, Z., Soybean-derived hierarchical

porous carbon with large sulfur loading and sulfur content for high-performance

lithium–sulfur batteries. Journal of Materials Chemistry A 2016, 4 (42), 16507-

16515

[57]. Hayashi, A.; Ohtomo, T.; Mizuno, F.; Tadanaga, K.; Tatsumisago, M.,

Rechargeable

lithium batteries, using sulfur-based cathode materials and Li2S–P2S5 glass-

ceramic

electrolytes. Electrochimica Acta 2004, 50 (2-3), 893-897

[58]. Hayashi, A.; Ohtomo, T.; Mizuno, F.; Tadanaga, K.; Tatsumisago, M., All-solid

state

Li/S batteries with highly conductive glass–ceramic electrolytes. Electrochemistry

Communications 2003, 5 (8), 701-705

[59]. Machida, N., Electrochemical properties of sulfur as cathode materials in a solid-

state lithium battery with inorganic solid electrolytes. Solid State Ionics 2004, 175

(1-4), 247-250.

[60]. Nagao, M.; Imade, Y.; Narisawa, H.; Kobayashi, T.; Watanabe, R.; Yokoi, T.;

Tatsumi, T.; Kanno, R., All-solid-state Li–sulfur batteries with mesoporous

electrode and thioLISICON solid electrolyte. J Power Sources 2013, 222, 237-242

[61]. Liang, X.; Wen, Z.; Liu, Y.; Zhang, H.; Huang, L.; Jin, J., Highly dispersed sulfur in ordered mesoporous carbon sphere as a composite cathode for rechargeable polymer Li/S battery. J Power Sources 2011, 196 (7), 3655-3658

[62]. Nagao, M.; Imade, Y.; Narisawa, H.; Watanabe, R.; Yokoi, T.; Tatsumi, T.; Kanno, R., Reaction mechanism of all-solid-state lithium–sulfur battery with two-dimensional mesoporous carbon electrodes. J Power Sources 2013, 243, 60-64.

[63]. Yao, X.; Huang, N.; Han, F.; Zhang, Q.; Wan, H.; Mwizerwa, J. P.; Wang, C.; Xu, X., High-Performance All-Solid-State Lithium-Sulfur Batteries Enabled by Amorphous Sulfur- Coated Reduced Graphene Oxide Cathodes. Advanced Energy Materials 2017, 7 (17).

[64]. Hong, X.; Liu, Y.; Li, Y.; Wang, X.; Fu, J.; Wang, X., Application Progress of Polyaniline, Polypyrrole and Polythiophene in Lithium-Sulfur Batteries. Polymers (Basel) 2020, 12 (2).

[65]. Dharmasena, R., Thapa, A. K., Hona, R. K., Jasinski, J., Sunkara, M. K., & Sumanasekera, G. U. (2018). Mesoporous TiO 2 coating on carbon–sulfur cathode for high-capacity Li–sulfur battery. RSC advances, 8(21), 11622-11632.

[66]. Su, Y. S., Fu, Y., & Manthiram, A. (2012). Self-weaving sulfur–carbon composite cathodes for high-rate lithium–sulfur batteries. Physical Chemistry Chemical Physics, 14(42), 14495-14499.

[67]. Singhal, R., Chung, S. H., Manthiram, A., & Kalra, V. (2015). A free-standing carbon nanofiber interlayer for high-performance lithium–sulfur batteries. Journal of Materials Chemistry A, 3(8), 4530-4538.

116

[68]. Ma, L., Zhuang, H. L., Wei, S., Hendrickson, K. E., Kim, M. S., Cohn, G., ... & Archer, L. A. (2016). Enhanced Li–S batteries using amine-functionalized carbon nanotubes in the cathode. ACS nano, 10(1), 1050-1059.

[69]. Li, H., Wang, J., Zhang, Y., Wang, Y., Mentbayeva, A., & Bakenov, Z. (2019). Synthesis of carbon coated Fe3O4 grown on graphene as effective sulfur-host materials for advanced lithium/sulfur battery. Journal of Power Sources, 437, 226901.

[70].Li, T., Bo, H., Cao, H., Lai, Y., Liu, Y., & Huang, Z. (2017). Effects of carbon hosts on electrochemical properties of lithium-sulfur batteries. Int. J. Electrochem. Sci, 12, 5731-5741.

[71].Cho, I., Choi, J., Kim, K., Ryou, M. H., & Lee, Y. M. (2015). A comparative investigation of carbon black (Super-P) and vapor-grown carbon fibers (VGCFs) as conductive additives for lithium-ion battery cathodes. Rsc Advances, 5(115), 95073-95078.

[72]. Jiao, Y., Chen, W., Lei, T., Dai, L., Chen, B., Wu, C., & Xiong, J. (2017). A novel polar copolymer design as a multi-functional binder for strong affinity of polysulfides in lithium-sulfur batteries. Nanoscale Research Letters, 12(1), 1-8.

[73]. Lacey, M. J., Jeschull, F., Edström, K., & Brandell, D. (2013). Why PEO as a binder or polymer coating increases capacity in the Li–S system. Chemical Communications, 49(76), 8531-8533.

[74]. He, M., Yuan, L. X., Zhang, W. X., Hu, X. L., & Huang, Y. H. (2011). Enhanced cyclability for sulfur cathode achieved by a water-soluble binder. The Journal of Physical Chemistry C, 115(31), 15703-15709.

[75]. Yu, X., Bi, Z., Zhao, F., & Manthiram, A. (2015). Hybrid lithium–sulfur batteries with a solid electrolyte membrane and lithium polysulfide catholyte. ACS applied materials & interfaces, 7(30), 16625-16631.

[76]. Busche, M. R., Drossel, T., Leichtweiss, T., Weber, D. A., Falk, M., Schneider, M., ... & Janek, J. (2016). Dynamic formation of a solid-liquid electrolyte interphase and its consequences for hybrid-battery concepts. Nature chemistry, 8(5), 426-434.

[77]. Liang, J., Luo, J., Sun, Q., Yang, X., Li, R., & Sun, X. (2019). Recent progress on solid-state hybrid electrolytes for solid-state lithium batteries. Energy Storage Materials, 21, 308-334.

[78]. Peng, H. J., Huang, J. Q., Cheng, X. B., & Zhang, Q. (2017). Lithium-Sulfur Batteries: Review on High-Loading and High-Energy Lithium–Sulfur Batteries (Adv. Energy Mater. 24/2017). Advanced Energy Materials, 7(24), 1770141.

[79]. Warner, J. T. (2015). The handbook of lithium-ion battery pack design: chemistry, components, types and terminology. Elsevier.

[80]. Nitta, N., Wu, F., Lee, J. T., & Yushin, G. (2015). Li-ion battery materials: present and future. Materials today, 18(5), 252-264.

[81]. https://ruchiragreenearth.com/blog/how-to-choose-the-right-lithium-ion-battery/

[82]. Xu, K. (2021). Li-ion battery electrolytes. Nature Energy, 6(7), 763-763.

[83]. Tran, M. K., DaCosta, A., Mevawalla, A., Panchal, S., & Fowler, M. (2021). Comparative study of equivalent circuit models performance in four common lithium-ion batteries: LFP, NMC, LMO, NCA. Batteries, 7(3), 51.

[84]. Blomgren, G. E. (2016). The development and future of lithium-ion batteries. Journal of The Electrochemical Society, 164(1), A5019.

[85]. Chen, Y., Kang, Y., Zhao, Y., Wang, L., Liu, J., Li, Y., Liang, Z., He, X., Li, X., Tavajohi, N. and Li, B., 2021. A review of lithium-ion battery safety concerns: The issues, strategies, and testing standards. Journal of Energy Chemistry, 59, pp.83-99.

[86]. Huang, W., Feng, X., Han, X., Zhang, W., & Jiang, F. (2021). Questions and answers relating to lithium-ion battery safety issues. Cell Reports Physical Science, 2(1).

[87]. Yu, X., Chen, R., Gan, L., Li, H., & Chen, L. (2022). Battery safety: from lithium-ion to solid-state batteries. Engineering.

[88]. Holmberg, S., Perebikovsky, A., Kulinsky, L., & Madou, M. (2014). 3-D micro and nano technologies for improvements in electrochemical power devices. Micromachines, 5(2), 171-203.

[89]. Christensen, J., Albertus, P., Sanchez-Carrera, R.S., Lohmann, T., Kozinsky, B., Liedtke, R., Ahmed, J. and Kojic, A., 2011. A critical review of Li/air batteries. Journal of the Electrochemical Society, 159(2), p.R1.

[90]. Rahman, M. A., Wang, X., & Wen, C. (2014). A review of high energy density lithium–air battery technology. Journal of Applied Electrochemistry, 44, 5-22.

[91]. Seh, Z. W., Sun, Y., Zhang, Q., & Cui, Y. (2016). Designing high-energy lithium–sulfur batteries. Chemical society reviews, 45(20), 5605-5634.

[92]. Yang, X., Li, X., Adair, K., Zhang, H., & Sun, X. (2018). Structural design of lithium–sulfur batteries: from fundamental research to practical application. Electrochemical Energy Reviews, 1(3), 239-293.

[93]. Zhang, S., Ueno, K., Dokko, K., & Watanabe, M. (2015). Recent advances in electrolytes for lithium–sulfur batteries. Advanced Energy Materials, 5(16), 1500117.

[94]. Manthiram, A., Fu, Y., Chung, S. H., Zu, C., & Su, Y. S. (2014). Rechargeable lithium-sulfur batteries. Chemical reviews, 114(23), 11751-11787.

[95]. Yin, Y. X., Xin, S., Guo, Y. G., & Wan, L. J. (2013). Lithium–sulfur batteries: electrochemistry, materials, and prospects. Angewandte Chemie International Edition, 52(50), 13186-13200.

[96]. Barchasz, C., Molton, F., Duboc, C., Leprêtre, J. C., Patoux, S., & Alloin, F. (2012). Lithium/sulfur cell discharge mechanism: an original approach for intermediate species identification. Analytical chemistry, 84(9), 3973-3980.

[97]. Li, G., Li, Z., Zhang, B., & Lin, Z. (2015). Developments of electrolyte systems for lithium–sulfur batteries: a review. Frontiers in Energy Research, 3, 5.

[98]. Kawase, A., Shirai, S., Yamoto, Y., Arakawa, R., & Takata, T. (2014). Electrochemical reactions of lithium–sulfur batteries: an analytical study using the organic conversion technique. Physical Chemistry Chemical Physics, 16(20), 9344-9350.

[99]. Guo, J., & Liu, J. (2019). A binder-free electrode architecture design for lithium–sulfur batteries: a review. Nanoscale Advances, 1(6), 2104-2122.

[100]. Yamada, Takanobu, Seitaro Ito, Ryo Omoda, Taku Watanabe, Yuichi Aihara, Marco Agostini, Ulderico Ulissi, Jusef Hassoun, and Bruno Scrosati. "All solid-state lithium–sulfur battery using a glass-type P2S5–Li2S electrolyte: benefits on anode kinetics." Journal of The Electrochemical Society 162, no. 4 (2015): A646.

[101]. Yang, X., Luo, J., & Sun, X. (2020). Towards high-performance solid-state Li–S batteries: from fundamental understanding to engineering design. Chemical Society Reviews, 49(7), 2140-2195.

[102]. Zheng, C., Wang, K., Li, L., Huang, H., Liang, C., Gan, Y., ... & Zhang, J. (2021). High-Performance All-Solid-State Lithium–Sulfur Batteries Enabled by Slurry-Coated Li6PS5Cl/S/C Composite Electrodes. Frontiers in Energy Research, 8, 606494.

[103]. Sakuda, A., Hayashi, A., & Tatsumisago, M. (2013). Sulfide solid electrolyte with favorable mechanical property for all-solid-state lithium battery. Scientific reports, 3(1), 1-5.

[104]. Chen, Y., Li, W., Sun, C., Jin, J., Wang, Q., Chen, X., ... & Wen, Z. (2021). Sustained release-driven formation of ultrastable sei between Li6PS5Cl and lithium anode for sulfide-based solid-state batteries. Advanced Energy Materials, 11(4), 2002545.

[105]. Fan, X., Ji, X., Han, F., Yue, J., Chen, J., Chen, L., ... & Wang, C. (2018). Fluorinated solid electrolyte interphase enables highly reversible solid-state Li metal battery. Science advances, 4(12), eaau9245.

[106]. Muramatsu, H., Hayashi, A., Ohtomo, T., Hama, S., & Tatsumisago, M. (2011). Structural change of Li2S–P2S5 sulfide solid electrolytes in the atmosphere. Solid State Ionics, 182(1), 116-119.

[107]. Shin, J. H., & Cairns, E. J. (2008). N-Methyl-(n-butyl) pyrrolidinium bis (trifluoromethanesulfonyl) imide-LiTFSI–poly (ethylene glycol) dimethyl ether mixture as a Li/S cell electrolyte. Journal of power sources, 177(2), 537-545.

[108]. Moreno, M., Simonetti, E., Appetecchi, G.B., Carewska, M., Montanino, M., Kim, G.T., Loeffler, N. and Passerini, S., 2016. Ionic liquid electrolytes for safer lithium batteries. Journal of The Electrochemical Society, 164(1), p.A6026.

[109]. De Giorgio, F., Soavi, F. and Mastragostino, M., 2011. Effect of lithium ions on oxygen reduction in ionic liquid-based electrolytes. Electrochemistry Communications, 13(10), pp.1090-1093.

[110]. Meisner, Q. J., Rojas, T., Glossmann, T., Hintennach, A., Liu, Q., Cao, J., ... & Zhang, Z. (2020). Impact of co-solvent and LiTFSI concentration on ionic liquid-based electrolytes for Li-S battery. Journal of The Electrochemical Society, 167(7), 070528.

[111]. Dharmasena, R., Thapa, A. K., Hona, R. K., Jasinski, J., Sunkara, M. K., & Sumanasekera, G. U. (2018). Mesoporous TiO 2 coating on carbon–sulfur cathode for high-capacity Li–sulfur battery. RSC advances, 8(21), 11622-11632.

[112].Cho, I., Choi, J., Kim, K., Ryou, M. H., & Lee, Y. M. (2015). A comparative investigation of carbon black (Super-P) and vapor-grown carbon fibers (VGCFs) as conductive additives for lithium-ion battery cathodes. Rsc Advances, 5(115), 95073-95078.

[113]. https://www.technologynetworks.com/analysis/articles/sem-vs-tem-331262

[114]. Yin, Y. X., Xin, S., Guo, Y. G., & Wan, L. J. (2013). Lithium–sulfur batteries: electrochemistry, materials, and prospects. Angewandte Chemie International Edition, 52(50), 13186-13200.

[115]. Barchasz, C., Molton, F., Duboc, C., Leprêtre, J. C., Patoux, S., & Alloin, F. (2012). Lithium/sulfur cell discharge mechanism: an original approach for intermediate species identification. Analytical chemistry, 84(9), 3973-3980.

[116]. Mikhaylik, Y. V., & Akridge, J. R. (2004). Polysulfide shuttle study in the Li/S battery system. Journal of the electrochemical society, 151(11), A1969.

[117]. Ai, W., Zhou, W., Du, Z., Chen, Y., Sun, Z., Wu, C., ... & Yu, T. (2017). Nitrogen and phosphorus co-doped hierarchically porous carbon as an efficient sulfur host for Li-S batteries. Energy storage materials, 6, 112-118.

[118]. Jung, D. S., Hwang, T. H., Lee, J. H., Koo, H. Y., Shakoor, R. A., Kahraman, R., ... & Choi, J. W. (2014). Hierarchical porous carbon by ultrasonic spray pyrolysis yields stable cycling in lithium–sulfur battery. Nano letters, 14(8), 4418-4425.

[119]. Gao, X., Sun, Q., Yang, X., Liang, J., Koo, A., Li, W., ... & Sun, X. (2019). Toward a remarkable Li-S battery via 3D printing. Nano energy, 56, 595-603.

[120]. Bauer, I., Thieme, S., Brückner, J., Althues, H., & Kaskel, S. (2014). Reduced polysulfide shuttle in lithium–sulfur batteries using Nafion-based separators. Journal of Power Sources, 251, 417-422.

[121]. Liang, C., Dudney, N. J., & Howe, J. Y. (2009). Hierarchically structured sulfur/carbon nanocomposite material for high-energy lithium battery. Chemistry of Materials, 21(19), 4724-4730.

[122]. Shin, J. H., & Cairns, E. J. (2008). N-Methyl-(n-butyl) pyrrolidinium bis (trifluoromethanesulfonyl) imide-LiTFSI–poly (ethylene glycol) dimethyl ether mixture as a Li/S cell electrolyte. Journal of power sources, 177(2), 537-545.

[123]. Shin, J. H., & Cairns, E. J. (2008). N-Methyl-(n-butyl) pyrrolidinium bis (trifluoromethanesulfonyl) imide-LiTFSI–poly (ethylene glycol) dimethyl ether mixture as a Li/S cell electrolyte. Journal of power sources, 177(2), 537-545.

[124]. Meisner, Q. J., Rojas, T., Glossmann, T., Hintennach, A., Liu, Q., Cao, J., ... & Zhang, Z. (2020). Impact of co-solvent and LiTFSI concentration on ionic liquid-based electrolytes for Li-S battery. Journal of The Electrochemical Society, 167(7), 070528.

[125]. Kumaresan, K., Mikhaylik, Y., & White, R. E. (2008). A mathematical model for a lithium–sulfur cell. Journal of the electrochemical society, 155(8), A576.

[126]. Barchasz, C., Molton, F., Duboc, C., Leprêtre, J. C., Patoux, S., & Alloin, F. (2012). Lithium/sulfur cell discharge mechanism: an original approach for intermediate species identification. Analytical chemistry, 84(9), 3973-3980.

[127]. Das, S., Ngene, P., Norby, P., Vegge, T., de Jongh, P. E., & Blanchard, D. (2016). All-Solid-State Lithium-Sulfur Battery Based on a Nanoconfined LiBH4Electrolyte. Journal of The Electrochemical Society, 163(9), A2029–A2034.

[128]. Dharmasena, R., Thapa, A. K., Hona, R. K., Jasinski, J., Sunkara, M. K., & Sumanasekera, G. U. (2018). Mesoporous TiO 2 coating on carbon–sulfur cathode for high-capacity Li–sulfur battery. RSC advances, 8(21), 11622-11632.

[129]. Meisner, Q. J., Rojas, T., Glossmann, T., Hintennach, A., Liu, Q., Cao, J., ... & Zhang, Z. (2020). Impact of co-solvent and LiTFSI concentration on ionic liquid-based electrolytes for Li-S battery. Journal of The Electrochemical Society, 167(7), 070528

[130]. Shen, Z., Zhong, J., Xie, W., Chen, J., Ke, X., Ma, J., & Shi, Z. (2021). Effect of LiTFSI and LiFSI on cycling performance of lithium metal batteries using thermoplastic polyurethane/halloysite nanotubes solid electrolyte. Acta Metallurgica Sinica (English Letters), 34(3), 359-372.

[131]. Nandasiri, M. I., Camacho-Forero, L. E., Schwarz, A. M., Shutthanandan, V., Thevuthasan, S., Balbuena, P. B., ... & Murugesan, V. (2017). In situ chemical imaging of solid-electrolyte interphase layer evolution in Li–S batteries. Chemistry of Materials, 29(11), 4728-4737.

[132]. Yang, X., Gao, X., Sun, Q., Jand, S.P., Yu, Y., Zhao, Y., Li, X., Adair, K., Kuo, L.Y., Rohrer, J. and Liang, J., (2019). Promoting the transformation of Li2S2 to Li2S: significantly increasing utilization of active materials for high-sulfur-loading Li–S batteries. Advanced materials, 31(25), p.1901220.

[133]. Peng, H.J., Huang, J.Q., Cheng, X.B. and Zhang, Q., (2017). Review on high-loading and high-energy lithium–sulfur batteries. Advanced Energy Materials, 7(24), p.1700260.

[134]. Fang, R., Zhao, S., Hou, P., Cheng, M., Wang, S., Cheng, H.M., Liu, C. and Li, F., (2016). 3D interconnected electrode materials with ultrahigh areal sulfur loading for Li–S batteries. Advanced materials, 28(17), pp.3374-3382.

[135]. Wang, X., Gao, T., Han, F., Ma, Z., Zhang, Z., Li, J., & Wang, C. (2016). Stabilizing high sulfur loading Li–S batteries by chemisorption of polysulfide on three-dimensional current collector. Nano Energy, 30, 700-708.

[136]. Pei, F., Lin, L., Fu, A., Mo, S., Ou, D., Fang, X., & Zheng, N. (2018). A two-dimensional porous carbon-modified separator for high-energy-density Li-S batteries. Joule, 2(2), 323-336.

[137]. Yin, F., Jin, Q., Gao, H., Zhang, X., & Zhang, Z. (2021). A strategy to achieve high loading and high energy density Li-S batteries. Journal of Energy Chemistry, 53, 340-346.

[138]. Liang, J., Sun, Z. H., Li, F., & Cheng, H. M. (2016). Carbon materials for Li–S batteries: Functional evolution and performance improvement. Energy Storage Materials, 2, 76-106.

[139]. Demir-Cakan, R., Morcrette, M., Nouar, F., Davoisne, C., Devic, T., Gonbeau, D., Dominko, R., Serre, C., Férey, G. and Tarascon, J.M., 2011. Cathode composites for Li–S batteries via the use of oxygenated porous architectures. Journal of the American Chemical Society, 133(40), pp.16154-16160.

[140]. Li, S., Leng, D., Li, W., Qie, L., Dong, Z., Cheng, Z., & Fan, Z. (2020). Recent progress in developing Li2S cathodes for Li–S batteries. Energy Storage Materials, 27, 279-296.

[141]. Kim, J.H., Lee, Y.H., Cho, S.J., Gwon, J.G., Cho, H.J., Jang, M., Lee, S.Y. and Lee, S.Y., 2019. Nanomat Li–S batteries based on all-fibrous cathode/separator assemblies and reinforced Li metal anodes: towards ultrahigh energy density and flexibility. Energy & Environmental Science, 12(1), pp.177-186.

[142]. Ye, H., Yin, Y. X., Xin, S., & Guo, Y. G. (2013). Tuning the porous structure of carbon hosts for loading sulfur toward long lifespan cathode materials for Li–S batteries. Journal of Materials Chemistry A, 1(22), 6602-6608.

[143]. Li, C., Zhang, H., Otaegui, L., Singh, G., Armand, M., & Rodriguez-Martinez, L. M. (2016). Estimation of energy density of Li-S batteries with liquid and solid electrolytes. Journal of Power Sources, 326, 1-5.

[144]. Zhao, S., Kang, Y., Liu, M., Wen, B., Fang, Q., Tang, Y., He, S., Ma, X., Liu, M. and Yan, Y., 2021. Modulating the electronic structure of nanomaterials to enhance polysulfides confinement for advanced lithium–sulfur batteries. Journal of Materials Chemistry A, 9(35), pp.18927-18946.

[145]. Guo, Q., & Zheng, Z. (2020). Rational design of binders for stable Li-S and Na-S batteries. Advanced Functional Materials, 30(6), 1907931.

[146]. Liu, J., Zhang, Q., & Sun, Y. K. (2018). Recent progress of advanced binders for Li-S batteries. Journal of power sources, 396, 19-32.

[147]. Yuan, H., Huang, J.Q., Peng, H.J., Titirici, M.M., Xiang, R., Chen, R., Liu, Q. and Zhang, Q., 2018. A review of functional binders in lithium–sulfur batteries. Advanced Energy Materials, 8(31), p.1802107.

[148]. Epp, V., Ma, Q., Hammer, E. M., Tietz, F., & Wilkening, M. (2015). Very fast bulk Li ion diffusivity in crystalline Li 1.5 Al 0.5 Ti 1.5 (PO 4) 3 as seen using NMR relaxometry. Physical Chemistry Chemical Physics, 17(48), 32115-32121.

[149]. Zhao, E., Ma, F., Guo, Y., & Jin, Y. (2016). Stable LATP/LAGP double-layer solid electrolyte prepared via a simple dry-pressing method for solid state lithium-ion batteries. Rsc Advances, 6(95), 92579-92585.

[150]. Liang, X., Wen, Z., Liu, Y., Wu, M., Jin, J., Zhang, H., & Wu, X. (2011). Improved cycling performances of lithium sulfur batteries with LiNO3-modified electrolyte. Journal of Power Sources, 196(22), 9839-9843.

[151]. Zhang, Z., Bao, W., Lu, H., Jia, M., Xie, K., Lai, Y., & Li, J. (2012). Water-soluble polyacrylic acid as a binder for sulfur cathode in lithium-sulfur battery. ECS Electrochemistry Letters, 1(2), A34.

[152]. Lu, Y.Q., Li, J.T., Peng, X.X., Zhang, T., Deng, Y.P., Wu, Z.Y., Deng, L., Huang, L., Zhou, X.D. and Sun, S.G., 2016. Achieving high-capacity retention in lithium-sulfur batteries with an aqueous binder. Electrochemistry communications, 72, pp.79-82.

[153]. Qie, L., & Manthiram, A. (2015). A facile layer-by-layer approach for high-areal-capacity sulfur cathodes. Advanced materials, 27(10), 1694-1700.

[154]. Osada, N., Bucur, C. B., Aso, H., & Muldoon, J. (2016). The design of nanostructured sulfur cathodes using layer by layer assembly. Energy & Environmental Science, 9(5), 1668-1673.

[155]. Zhang, L., Liang, P., Man, X.L., Wang, D., Huang, J., Shu, H.B., Liu, Z.G. and Wang, L., (2019). Fe, N co-doped graphene as a multi-functional anchor material for lithium-sulfur battery. Journal of Physics and Chemistry of Solids, 126, pp.280-286.

[156]. Peled, E., Goor, M., Schektman, I., Mukra, T., Shoval, Y. and Golodnitsky, D., 2016. The effect of binders on the performance and degradation of the lithium/sulfur battery assembled in the discharged state. Journal of the Electrochemical society, 164(1), p.A5001.

CURRICULUM VITAE

Milinda Bharatha Kalutara Koralalage (He/His/Him)

Louisville, KY 40217
milindabharatha@gmail.com
+1 502 654 0680
LinkedIn: www.linkedin.com/in/MilindaBharatha-KalutaraKoralalage

EDUCATION

2020-2023   Doctor of Philosophy (Ph.D.) (Expected Graduation : Spring 2023)

Quasi-Solid-state Lithium sulfur batteries
Department of Physics and Astronomy, University of Louisville – USA
Thesis advisor : Dr. Gamini Sumanasekera

2018-2020   Master of Science (M.Sc.)

Department of Physics and Astronomy, University of Louisville – USA
Thesis advisor : Dr. Gamini Sumanasekera GPA: 4.0

2013-2016   Bachelor of Science (Special degree in Physics) (B.Sc.)

Department of Physics, University of Peradeniya – Sri Lanka
Thesis advisor : Dr. Buddika Dassanayake   GPA: 3.38

WORK EXPERIENCE

Graduate Research Assistant: Department of Physics and Astronomy & Conn Center for Renewable Energy Research, University of Louisville - USA (August 2020-Present)

- Material synthesis for cathodes and anodes of Li batteries and electrode fabrication including slurry preparation and doctor blade coating.
- Liquid electrolyte, solid-state electrolyte and quasi-solid-state electrolyte coin cell assembly. Assisting pouch cell fabrication.
- Electrochemical testing of liquid, solid-state and quasi-solid-state Li batteries: Galvanostatic and Potentiostatic (charge -discharge, Cyclic voltammetry, EIS, etc.)

- Material Characterization using scanning electron microscopy (SEM), Raman, Thermogravimetric analysis, X-ray photoelectron spectroscopy (XPS) and X-ray diffraction (XRD)

Graduate Teaching Assistant: Department of Physics and Astronomy, University of Louisville - USA (August 2018-December 2020)

- Conducted senior level laboratory classes such as Introductory Modern Physics and Atomic and Nuclear Physics.
- Conducted entry level laboratory classes covering topics such as classical mechanics and electromagnetism.
- Graded undergraduate homework assignments and examinations.

Teaching Assistant: Department of Physics, University of Peradeniya – Sri Lanka (January 2017-June 2018)

- Conducted senior level laboratory classes such as Electromagnetism and Advanced modern Physics.
- Graded undergraduate homework assignments and conducted discussion classes such as electric and magnetic fields.

SKILLS

- Capability in Lithium-sulfur/Lithium-ion electrode fabrication (doctor blade), material synthesis, Coin cell assembly and high-capacity pouch cell fabrication.

- Experience in battery testing: capacity (ARBIN battery tester)/impedance (Biologic SP-200)/cyclic voltammetry (Biologic SP-200), Experience in maintaining dry glove boxes and battery assembling machines.

- Extensive hands-on experience in working with plasma enhanced chemical vapor deposition (PECVD) system, multi-zone quartz tube furnaces, vacuum pumps (mechanical, diffusion, turbo)

- In-depth knowledge in material and electrode analysis techniques such as: scanning electron microscope (SEM), X-ray diffraction (XRD), X-ray photoelectron spectroscopy (XPS), Raman spectroscopy, Energy-dispersive X-Ray spectroscopy (EDAX), Thermogravimetric analysis (TGA) and UV-visible spectroscopy.

- Data Analysis and Visualization: Origin Pro, Mathematica, Microsoft Office package

AWARDS AND ACHIEVEMENTS

- Schwartz Award for outstanding graduate performance in Physics (Spring 2023)
- Peoples award – 3 minutes Thesis Competition, University of Louisville (Fall 2022)
- Doctoral Dissertation Completion Award (Spring 2023)

PUBLICATIONS

1. Milinda Kalutara Koralalage, R. Parish, A. M. Bates, S. McNamara, W. F. Paxton, and G. U. Sumanasekera. "The Influence of Absorbate Desorption and Kinetic Isotope Effects on the Surface Conductivity of Diamond." Journal of Electronic Materials 51, no. 6 (2022): 3336-3341.

2. Arnold William, Varun Shreyas, Yang Li, Milinda Kalutara Koralalage, Jacek B. Jasinski, Arjun Thapa, Gamini Sumanasekera, Anh T. Ngo, Badri Narayanan, and Hui Wang. "Synthesis of Fluorine-Doped Lithium Argyrodite Solid Electrolytes for Solid-State Lithium Metal Batteries." ACS Applied Materials & Interfaces 14, no. 9 (2022): 11483-11492.

3. Arnold, William, Varun Shreyas, Sharmin Akter, Yang Li, Selim Halacoglu, Milinda Kalutara Koralalage, Xiaolin Guo et al. "Highly Conductive Iodine and Fluorine Dual Doped Argyrodite Solid Electrolyte for Lithium Metal Batteries." Available at SSRN 4233149.

4. Thapa, Arjun Kumar, Brandon W. Lavery, Ram K. Hona, Nawraj Sapkota, Milinda Kalutara Koralalage, Ayodeji Adeniran, Babajide Patrick Ajayi et al. "Mn-Rich NMC Cathode for Lithium-Ion Batteries at High-Voltage Operation." Energies 15, no. 22 (2022): 8357.

5. Alzahrani, Ali, Milinda Kalutara Koralalage, Jacek Jasinski, and Gamini Sumanasekera. "Direct Fabrication of Vertically Stacked Double Barrier Tunnel Junctions Based on Graphene and h-BN." Electronic Materials Letters 18, no. 3 (2022): 313-320.

6. Alzahrani, Ali, Adel Alruqi, Bhupendra Karki, Milinda Kalutara Koralalage, Jacek Jasinski, and Gamini Sumanasekera. "Direct fabrication and characterization of vertically stacked Graphene/h-BN/Graphene tunnel junctions." Nano Express 2, no. 4 (2021): 040010.

7. Adikaram, K. K. M. B. B, Kumarage, W. G. C., Varga, T., & Dassanayake, B. S. (2019). Improvement of the photo-activity of CdS thin films using TX-100. Journal of Electronic Materials, 48(7), 4424-4431.

8. Milinda Kalutara Koralalage, Varun Shreyas, Arnold, William, Sharmin Akter, Jacek B. Jasinski, Arjun Thapa, Gamini Sumanasekera, Hui Wang , and Badri Narayanan. "Super P

– Sulfur composite cathode and novel solid-state electrolyte for quasi-solid-state Lithium-Sulfur batteries" ACS Applied Materials & Interfaces (Manuscript under review)

9. <u>Milinda Kalutara Koralalage,</u> Varun Shreyas, Arnold, William, Sharmin Akter, Jacek B. Jasinski, Arjun Thapa, Gamini Sumanasekera, Hui Wang , and Badri Narayanan. "Super P – Sulfur composite cathodes for quasi-solid-state Lithium-Sulfur batteries with high energy density" (Manuscript in Preparation)

ORAL AND POSTER PRESENTATIONS

- Oral Presentation: iPURSE 2016 (Peradeniya University International Research Sessions) "Growth and Characterization of TX-100 treated CBD-CdS thin films." Proceedings iPURSE 20, 329

- Poster Presentation: Conn Center LAC Price Event , University of Louisville "Quasi-solid-state Li-S Batteries" April 2022

- Oral Presentation: ECS 242nd conference 2022 Atlanta, GA. "Quasi-Solid-State Lithium-Sulfur Batteries Consist of Super P – Sulfur Composite Cathode" (awaiting decision).